University of Alberta

Characterization of the Winter Regime of an Urban River

by

Joshua Alexander Maxwell

A thesis submitted to the Faculty of Graduate Studies and Research

in partial fulfillment of the requirements for the degree of

Master of Science

in

Water Resources Engineering

Department of Civil and Environmental Engineering

Spring 2012

Edmonton, Alberta

Abstract

In the northern reaches of the globe, cities built along rivers create open leads in the river's seasonal ice cover through warm water effluent discharge. These open leads are known for producing episodic frazil events which can block downstream intakes, causing major problems for recipients of the intake water. The Edmonton reach of the North Saskatchewan River presents an excellent example of such a case.

During the 2010/11 winter, instrumentation was deployed in and along the North Saskatchewan River in Edmonton to document surface ice characteristics and suspended frazil formations. A dataset was compiled consisting of third party information and data collected during this study. Through the analysis of this data, the 2010/11 freeze-up was characterized, open lead formations were documented and suspended and surface ice events in an open lead were categorized. Formation criteria were then developed for suspended frazil events.

Acknowledgements

This research project was funded through grants from the Natural Sciences and Engineering Research Council of Canada; this support is gratefully acknowledged. Assistance provided by EPCOR Utilities Inc., in the form of space, power and security is also highly appreciated. A number of other individuals and agencies provided highly valuable data and assistance which formed parts of this thesis:

- Nadia Kovachis, Alberta Environment
- Igor Jakab, Rick Perron, University of Alberta
- Vincent Corkery, Gary Corlett, Bing Lin, EPCOR Water Services
- Bob Kotchubajda, David Patrick, Environment Canada

The author would like to thank Drs. Faye Hicks and Mark Loewen for all of their assistance and guidance throughout this study. For their assistance in the field and in the office, thanks also to: Perry Fedun, Tadros Ghobrial, Chris Krath and Vincent McFarlane. Thanks to Drs. Faye Hicks, Mark Loewen and Jeff Kavanaugh for sitting on the final oral examination committee.

The author is also thankful for the support of his family and friends through this process. Of special importance is his wife, Anita who provided so much love and understanding throughout this time. The author would also like to acknowledge his newborn daughter, Jasmine for providing motivation to complete this thesis in a timely manner.

Contents

List of Equations

List of Tables

List of Figures

List of Symbols and Abbreviations

α	=the absorption coefficient expressed in dB/m;
β	=the analog to digital scaling factor, 97.4 dB for 16 bit digitization
c	=the speed of sound in water;
$G[R]$	=the receiver gain correction supplied by the instrument manufacturer;
N	=the pre-processed digital counts
OCV	=the transducer receiving response in (dB), referred to as the Open Current Voltage;
R	=the range of the target from the transducer;
S_v	=the volume backscatter strength in decibels (dB) per unit volume
T_a	= the air temperature;
TVR	=the transmit voltage response of the transducer;
τ	=the user specified pulse length;
V_{Tx}	=the actual RMS voltage applied to the transducer as a function of the supply voltage;
ψ	= the transducer beam width
Q_{GBWTP}	= the discharge from the Gold Bar Wastewater Treatment Plant outfall, adjusted for travel time from the outfall to location of ice generation

1. Introduction

Many Canadian cities are located along rivers. In northern latitudes, these rivers develop seasonal winter ice covers. Water is withdrawn from these rivers for both public and private purposes and is commonly discharged back into river as warm water effluent. When this effluent is of sufficient volume or temperature, openings will be created in the ice covers which are referred to as open leads. These open leads are known for episodic suspended frazil ice events (Ghobrial *et al.*, 2010).

Frazil ice are small disc or needle shaped particles which form in turbulent open water that has become super-cooled below 0°C by several hundredths of a degree (Ashton, 1986). These ice crystals are well known for their ability to adhere to almost any material but especially steel and other metals. As a result, frazil is notorious for blocking water intakes by adhering to the intake screens or trash racks (Daly *et al.*, 1992). When an intake is not located in an open lead, the intake operator need only worry about frazil adhesion for the freeze-up season portion of the year. However, when there are multiple intakes and outfalls in line along an open lead, the downstream intakes maybe at risk of frazil ice blockages throughout the entire winter season.

To prevent or mitigate frazil adhesion and blockages, a number of measures have been designed. These mitigation measures have included mechanical removal, warm water back flushing to melt or dislodge frazil, and heating of the intake screen to melt any adhered particles (Daly, 1991). All of these methods are costly

and are less effective when treating well developed frazil blockages as opposed preventing suspended frazil from adhering in the first place. Part of the problem with frazil ice blockage mitigation is that most intake operators only become aware of frazil ice once it has already adhered to the intake screen and restricted or stopped river water supply. As result, operators are faced with a choice between periodically deploying mitigation measures even when frazil is not present or risking lengthy downtime to treat more severe blockages.

The North Saskatchewan River, which flows through the City of Edmonton (Figure 1-1) is an excellent example of a northern river in an urban environment. The Gold Bar Wastewater Treatment Plant (GBWTP) within Edmonton discharges treated sanitary and storm water runoff throughout the year. During the winter it creates an open lead approximately 14 km long. Frazil events are known to occur in this open lead throughout the winter (Ghobrial et al, 2010).

In this study, sonar instruments were deployed in the GBWTP open lead to profile suspended and surface ice features, and automated time lapse cameras were installed along the study reach to document surface ice. Meteorological data were collected by an Environment Canada weather monitoring station located at the Edmonton City Centre Airport and by a monitoring station located at the sonar instrument deployment site. Water temperature and pressure sensors were also installed along the study reach. Bathymetry data were also collected. Using these data, an analysis was conducted with three primary goals:

1. To document the progression of the 2010/11 freeze-up, characterize the formation of the winter ice cover and record mid-winter changes in the ice cover (such as open leads).
2. To record suspended frazil and surface ice events using sonar instruments and to produce code to automate the analysis of this data.
3. To identify meteorological or hydrological parameters that can be used to predict the formation of suspended frazil events in the GBWTP open lead.

The following is a summary of the Chapters presented in this thesis. In Chapter 2, a geomorphological and hydrological description of the study reach is presented along with the data available from third parties. Chapter 3 introduces the instrument and procedures used for data collection during this study and presents some examples of raw data. In Chapter 4, the progression of freeze-up is documented and visible openings in the mid-winter ice cover are identified. In Chapter 5, the sonar data are analyzed and used to examine surface ice conditions; this surface ice is then classified and its source identified. In Chapter 6, the sonar data are used to study suspended ice. Discrete ice events are identified and forecast criteria for both suspended and floating ice are developed. Finally, a summary is presented in Chapter 7, describing the most notable findings of this thesis and making recommendations for future studies.

1.1. Past Studies of River Ice Processes Using Sonars

The Shallow Water Ice Profiling Sonar (SWIPS) was created by ASL Environmental Sciences Inc.(ASL) as an adaptation of ASL's well developed sea ice draft measurement instrument, the Ice Profiling Sonar (IPS) (Marko *et al.*, 2006). The value of the sonar instrument was first demonstrated by Jasek *et al.* (2005), who deployed a low frequency (235kHz) sonar instrument in the Peace River during the 2004/05 winter season. Jasek *et al.* (2005) found that the low frequency sonar instrument could be used to detect both surface ice and suspended frazil particles. However, it was also noted that the low frequency sonar appeared to be insensitive to ice particles smaller than approximately 6 mm. It was recommended by Jasek *et al.* (2005) that an additional higher frequency sonar unit be deployed in future studies for improved suspended frazil profiling capabilities.

During the 2005/06 winter, Morse and Richard (2009) deployed a 420 kHz sonar instrument in the St. Lawrence River. In their study, relative suspended frazil concentrations were estimated in arbitrary units since the relationship between concentration and the acoustic signal was unknown. By comparing hydrological and meteorological conditions against the relative suspended frazil concentrations, they concluded that the frazil ice concentrations were a strong function of local flow conditions and a weak function of meteorological conditions. Morse and Richard (2009) hypothesized that this correlation was a result of locally strong turbulent forces re-entraining frazil particles that had

previously been deposited on the underside of pans further upstream, thus locally increasing the number of frazil particles suspended in the flow.

Also during the 2005/06 winter season, Marko et al. (2006) deployed high (546kHz) frequency and low (235kHz) frequency sonar instruments in the Peace River. They found that the high frequency sonar instrument was much more effective for the detection of suspended frazil than the low frequency sonar instrument. However, the high frequency sonar was prone to saturation of the return signal when measuring slush ice. Saturation occurs when the return signal intensities measured by the sonar are above the sonar's measurable range. Marko *et al.* (2006) concluded that a combination of a high and low frequency sonar instrument for a single installation allowed the monitoring of major ice-related parameters, including vertical distribution of suspended frazil and thickness of the surface ice. It was recommended that further laboratory based studies be conducted to allow for more quantitative estimates of frazil particle concentrations.

In a laboratory investigation, Ghobrial *et al.* (2009 and 2012) deployed high (546kHz) frequency and low (235kHz) frequency sonar instruments in a 0.80m wide, 1.20m long and 1.50m deep frazil generation tank located in a cold room at the University of Alberta. In these studies, frazil particle concentrations and size distributions were measured by sieving and microscope examination, respectively. Relationships between SWIPS return signal intensities and suspended frazil concentrations were determined for a particle size range of 0.25mm and 4.25mm.

This relationship was found to have strong coefficient of determination (R^2) values of 0.96 and 0.93 for the high and low frequency units, respectively. However, the accuracy and validity of these relationships in the field remains uncertain and requires further research (Ghobrial *et al.*, 2012).

1.2. Past Winter Ice Studies of the North Saskatchewan River

Gerard and Andres (1982) conducted a winter ice study at several sites within the City of Edmonton during the 1981/82 winter. The goal of this study was to investigate predictors for the roughness of an ice cover's underside. As part of this study, Gerard and Andres (1982) reported the progression of the 1981/82 freeze-up front through Edmonton. It was observed that the ice cover initiated about 200 km downstream of Edmonton on 30-Nov-81 and progressed upstream. On 4-Dec-81, bridging also occurred at the Dawson Bridge (Figure 1-1) and the ice cover progressed sequentially upstream with a celerity of about 7 km per day. On 10-Dec-81 the ice cover had reached Devon.

Choles (1997) collated all of the data related to ice processes along the North Saskatchewan River, from the Bighorn Dam downstream to the confluence with the Brazeau River 140 kilometers upstream of Edmonton. Choles (1997) observed that although bridging locations were generally consistent between years, bridging times were unpredictable. It was also noted that tight bends in the

river or mid channel features such as islands and bars were common locations for bridging events.

During the 2008 freeze-up season and throughout the 2009/10 winter season Ghobrial *et al.* (2009 and 2010) deployed low and high frequency sonar instruments in the North Saskatchewan at Edmonton. These field studies were complementary to the laboratory studies of Ghobrial *et al.* (2009 and 2012) and compared the suspended frazil SWIPS signals measured in the laboratory against those measured in the field.

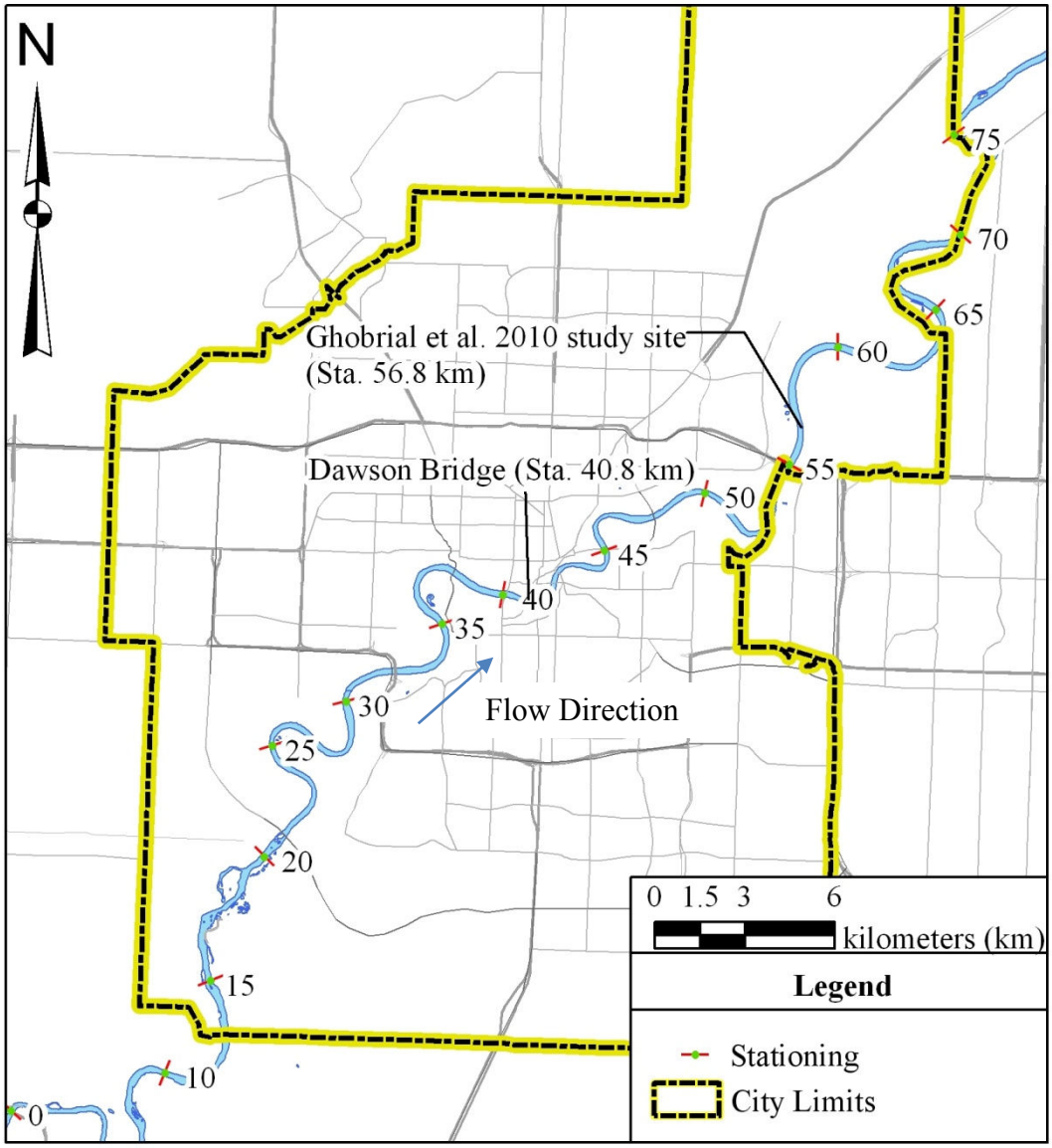

Figure 1-1. Map of study reach, illustrating locations of previous study.

2. Study Reach Description and Third-Party Data

2.1. Description of Study Reach[1]

Figure 2-1 presents a map of the North Saskatchewan River at Edmonton; the stations shown refer to kilometers (km) along the river, in terms of distance downstream of the Highway 60 bridge at Devon. Also shown are the collection locations of third party data, which will be discussed in Section 2.2. The study reach covered in this thesis spans from station 9.2 km to 63.9 km. A major portion of this study's efforts were focused upon the open lead created by the GBWTP outfall (Figure 2-2). A large portion of this thesis is focused on the mid-winter suspended frazil and surface pan events occurring in the GBWTP open lead.

The North Saskatchewan River is a gravel bed river with a mean bed material size of ~3 cm in the Edmonton reach (Kellerhals *et al*., 1972). Using satellite images viewed in Google Earth [Google], the study reach can be broken into two sections based on river geomorphology. Upstream of the Highway 216 (Anthony Henday Drive) bridge, the channel exhibits an irregular meandering pattern with slight anabranching tendencies, with numerous islands and mid-channel bars. The river is partially entrenched within the valley walls (Kellerhals *et al*., 1972). Downstream of the Highway 216 Bridge, the channel continues the irregular meandering pattern but loses its anabranching tendency and contains very few

[1] Portions of this section have been published (Maxwell *et al.*, 2011).

mid-channel bars or islands. The river also becomes slightly more entrenched within the valley walls.

The North Saskatchewan River flow is regulated by the Brazeau and Bighorn Dams. The Brazeau Dam began operation in 1963 and the Bighorn Dam began operation in 1972 (Kellerhals *et al*., 1972). From the beginning of the gauge record in 1911 to 1963, the mean flow at Edmonton for the winter months of November to March was 45 m^3/s (Environment Canada, 2011b). After the Bighorn dam began operation, the mean flows for the winter months from 1972 to 2010 increased to 133 m^3/s; the mean summer flows have decreased from 339 m^3/s to 245 m^3/s.

2.2. Available Data

2.2.1. Bathymetry Data

Cross sectional survey data was available from Alberta Enviroment's flood risk mapping study model of the North Saskatchewan River. This model was initially built in HEC-2 format (Phillips Planning & Engineering Limited, 1994) and was later converted into HEC-RAS format (Northwest Hydraulic Consultants, 2007). The exact stations of the model's cross sections are not known as they were adjusted (but not re-surveyed) when the model was converted to HEC-RAS format (Northwest Hydraulic Consultants, 2007). Despite this, the model's cross sectional data provides the best available bathymetry data for this study reach. The locations of these cross sections were plotted in aerial photographs in the

Northwest Hydraulic Consultants (2007) report. The cross section locations were transferred to Figure 2-3 by visually comparing landmarks in both maps using Geospatial Information System (GIS) software. The station of each cross section was determined from Figure 2-3.

2.2.2. Meteorological Data

The Environment Canada weather monitoring station located at the Edmonton City Centre Airport collected hourly meteorological data throughout the entire 2011/12 season. The data collected from this station included: air temperature, dew point, humidity, wind speed, wind direction, visibility and general weather conditions (e.g. snowing).

2.2.3. Water Temperature Data

Water temperatures were obtained from the operators of the University of Alberta cooling water plant and the GBWTP outfall. Hourly river water temperatures were collected from the cooling water intake. At the University of Alberta (station 39.2 km). Hourly water temperatures and discharges at the GBWTP outfall were supplied by EPCOR Water Services Inc. The GBWTP outfall discharge rate follows a diurnal trend, ranging from a minimum of 1.5 m^3/s in the morning to a maximum of about 3.5 m^3/s in the afternoon.

The GBWTP effluent temperature dropped to ~3°C for several hours on a daily basis as illustrated in the example shown in Figure 2-4(a). This was due to the temperature sensor being installed at too shallow of a depth in the outfall, such

that at low stages the sensor was exposed to cold air[2]. The outfall discharge measurements also contained several drops to 0 m^3/s for one or two hour periods as shown in Figure 2-4(b). These values are known to be erroneous because at no time did the outfall cease discharging effluent.[3]

2.2.4. River Stage Data

Stage measurements were collected every 15 minutes by the Water Survey of Canada (WSC) gauge (ID# 05DF001) located at station 42.8 km. River discharge is also calculated by WSC using their stage measurements. At the time of this analysis these discharge data was not available.

2.2.5. Photographic Data

The Department of Earth and Atmospheric Sciences at the University of Alberta operated two online cameras on the roof of the Tory Building, at river station 39.5 km. One of these was a 2.0 megapixel 223M Network Camera [Axis Communications] (looking upstream), capable of collecting day and night photographs. The other (looking downstream) was a 0.3 megapixels CC640 camera [Campbell Scientific] which took daytime photographs only. Both these cameras collected pictures at 15 minute intervals throughout the entire winter season.

[2] Personal communication with Gary Corlett, Epcor Water Services, Inc., 15-Dec-11
[3] Personal communication with Bing Lin, Epcor Water Services, Inc., 7-Nov-11

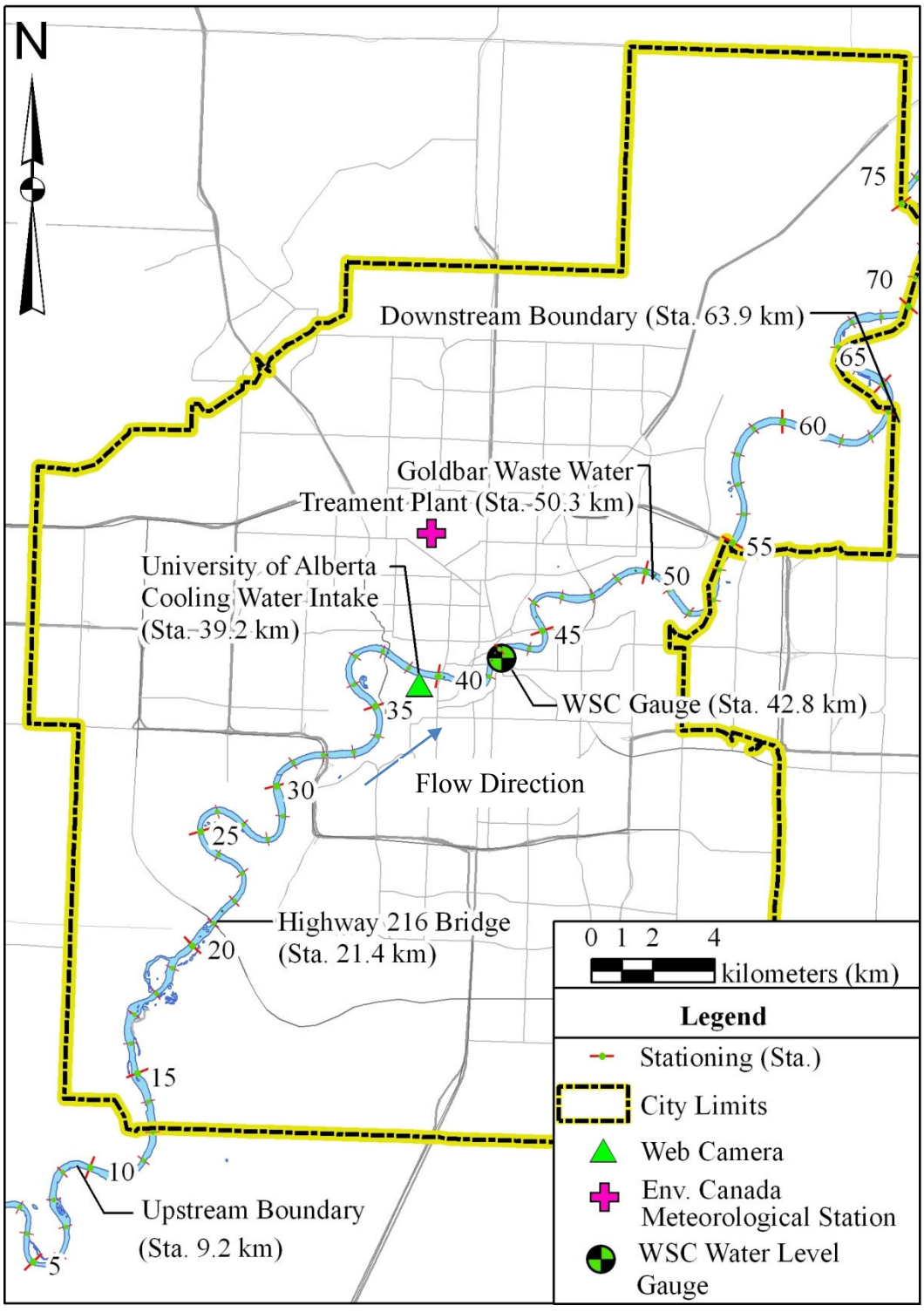

Figure 2-1. Study reach on the North Saskatchewan River and collection locations of available data.

Figure 2-2. Picture of GBWTP outfall and the upstream head of the open lead it creates.

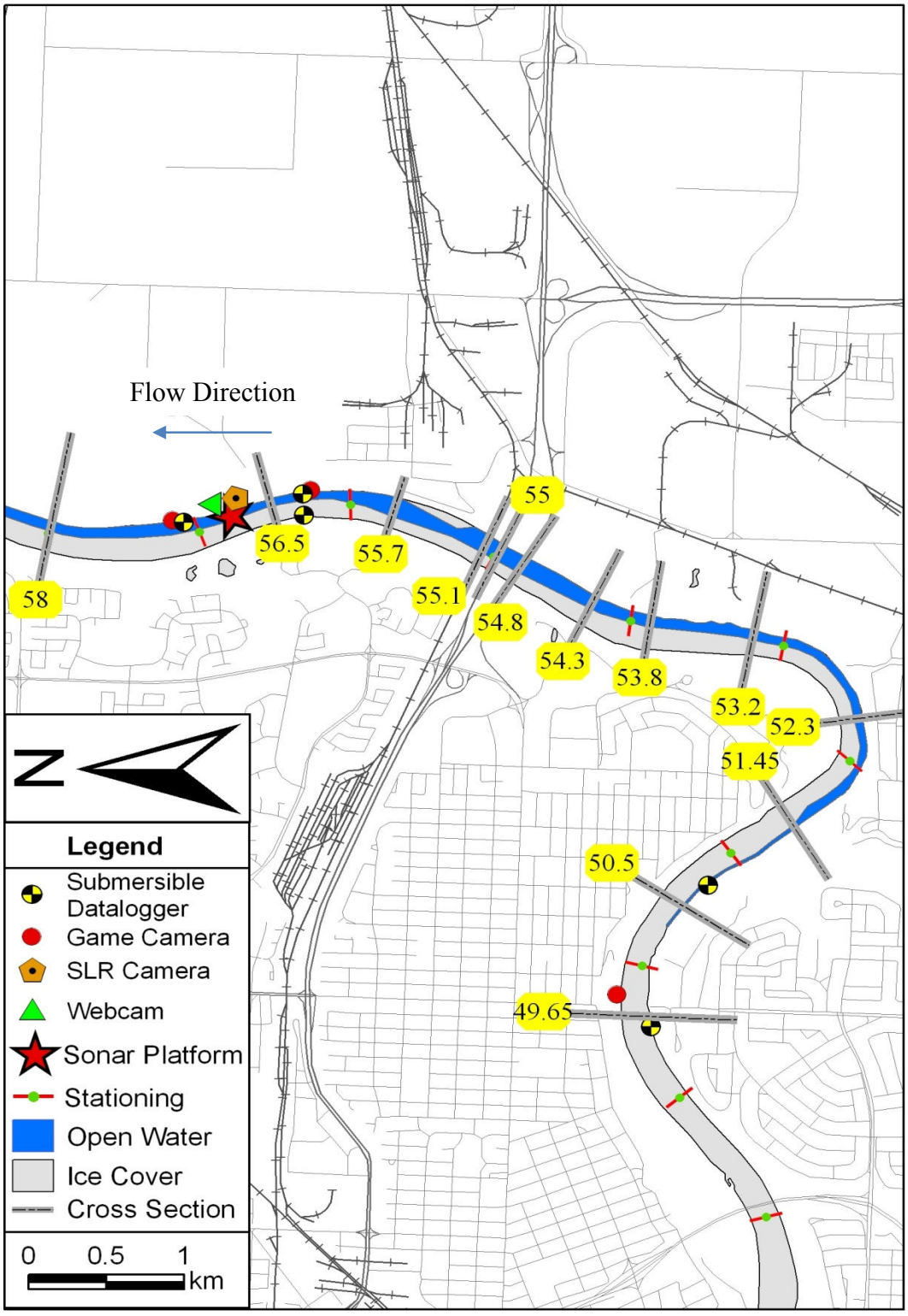

Figure 2-3. Locations of cross sections extracted from HEC-RAS model of North Saskatchewan River provided by Alberta Environment.

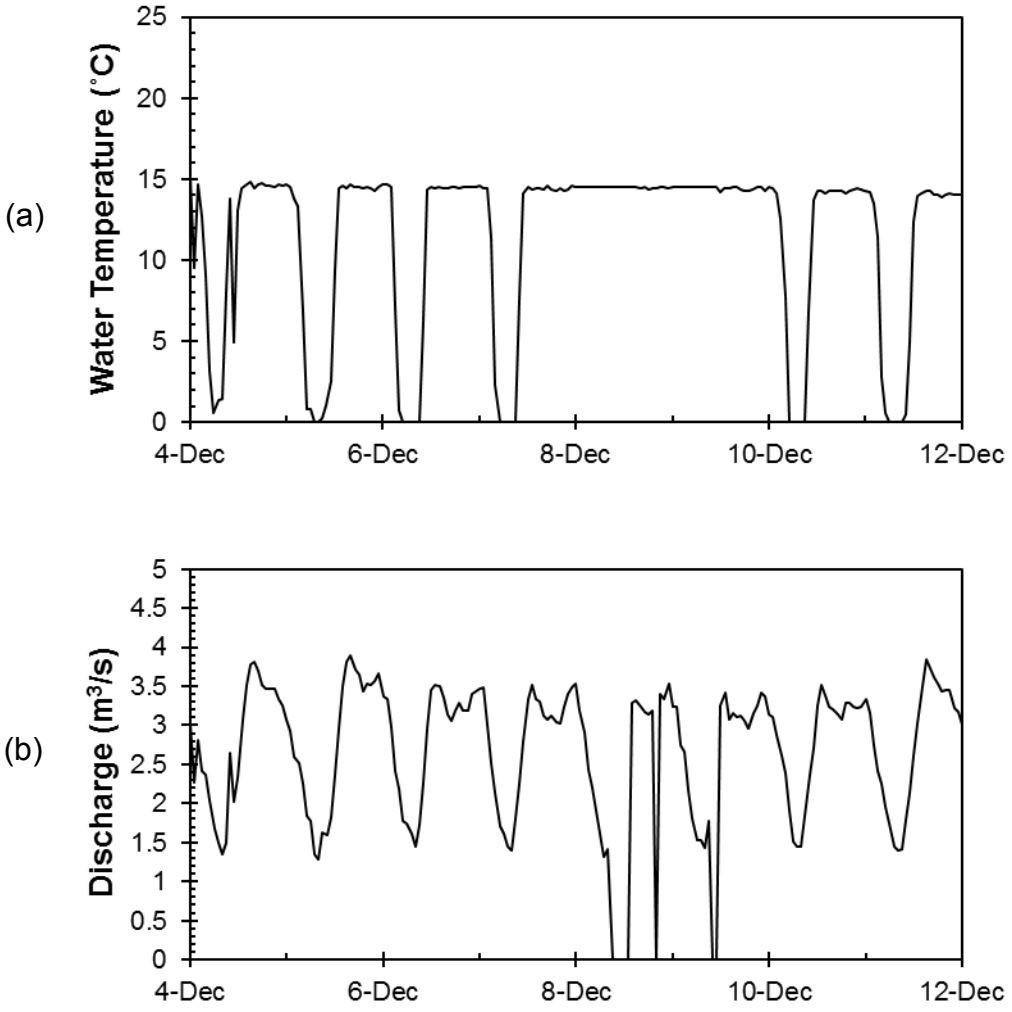

Figure 2-4. Sample plots of effluent (a) temperature and (b) discharge from the Gold Bar Wastewater Treatment Plant from 4-Dec-10 to 12-Dec-10.

3. Field Measurements and Methods

In this chapter the instrumentation and methods used in this thesis are documented. Figure 3-1 illustrates the study reach covered the North Saskatchewan River within the Edmonton city limits (station 9.2 km to 63.9km).

Within the study reach, automated time lapse cameras were installed to document the progression of freeze-up. The cameras downstream of the GBWTP outfall (station 50.3 km) were operated throughout the entire winter to monitor ice pans in the mid-winter open lead created by the GBWTP outfall, which extended from station 50.3 km downstream to approximately station 63.9 km.

A large portion of the research efforts documented in this thesis were focused on the river reach from station 56.3 km to station 57.1 km. A location plan for the instrumentation in this reach is shown in Figure 3-2. At station 56.8 km, a sonar instrument platform containing high and low frequency SWIPS instruments and an Acoustic Doppler Current Profiler (ADCP) was deployed 45 m from the right bank. The sonar instruments were connected to data collection computers located in a site trailer on the right bank of the river (Figure 3-3). Also in this trailer, a SLR camera linked to a floodlight collected day and night photographs of the ice conditions at the instrumentation platform. On the right bank[4], a monitoring station (Figure 3-4) was installed with two remotely accessible cameras, an air temperature sensor and a water temperature sensor. Approximately 500 m

[4] In this context, right bank refers to the bank on right when in the downstream direction.

upstream and downstream from this location submersible dataloggers collected water temperature and pressure data.

3.1. Instrumentation

3.1.1. Depth Sounder

A SonarLite depth sounder [Ohmex Instrumentation] was used for the measurement of depths during the bathymetry surveys. Table 3-1 presents the technical specifications of the instrument. The accuracy of this unit is qualified by the root mean square (RMS) term. RMS indicates the measurement is within the quoted accuracy 68.2% (one standard deviation) of the time. The depth sounder was mounted on the stern of a boat during the surveys. At the beginning and end of each survey, the depth reading of the depth sounder was verified using a direct measurement of the distance from the depth sounder transducer to the river bed.

Table 3-1. Manufacturer specifications for SonarLite Depth Sounder (Ohmex Instrumentation, 2005).

Transducer Frequency	230 kHz
Depth Range	0.30m to 80.00m
Accuracy/Resolution	0.025m RMS/0.01m
Pulse Frequency	0.5Hz

3.1.2. Global Positioning Systems

A GPSMap 76Csx [Garmin Ltd.] handheld global position system (GPS) was used in this study to document the locations of installed equipment and the coordinates of the edge of the ice cover adjacent to the sonar instruments (Figure 3-2). This unit updates its position at a rate of 1 Hz and has horizontal positioning accuracy of 3 to 5m, 95% of the time (Garmin Ltd., 2009).

A Trimble R8 GNSS Real Time Kinetic Global Positioning System (RTK-GPS) [Trimble] was used for accurate horizontal and vertical positioning during bathymetry surveys and water surface elevation measurements. An RTK-GPS collects accurate position measurements through the operation of two separate GPS receivers: the base and the rover. The base receiver is located in a fixed position while the rover is moved between observation points, collecting the actual position measurements. Since it is known that the base receiver is not moving, any inaccuracies seen in the base's GPS position are a result of errors caused by local conditions. The difference between the measured and the actual base receiver location is transmitted via radio link to the rover receiver. The rover receiver applies the base correction to its observations, resulting in measurement accuracies that would be unattainable with a single GPS arrangement.

The manufacturer specifications for the RTK-GPS are shown in Table 3-2. The positioning accuracy of the RTK-GPS has two components: a base accuracy and a parts per million (ppm) accuracy. The base accuracy is the uncertainty in the

rover receiver's position immediately adjacent to the base receiver. The ppm accuracy is the error resulting from the separation between the rover and base receiver. For example, if the rover were 1 km away from the base, the ppm accuracy would be 0.001 m. Every point measured for this study using the RTK-GPS was within 5 km of the base receiver.

Table 3-2. Manufacturer specifications for R8 GNSS Real Time Kinetic Global Positioning System (Trimble, 2012).

Horizontal Positioning Accuracy/Resolution	0.01m + 1ppm RMS/ 0.001m
Vertical Positioning Accuracy/Resolution	0.02m + 1ppm RMS / 0.001m
Max. Sampling Rate	1 Hz
Maximum Range from Base Station	10 km

This instrument required a calibration to ensure accurate position measurements. The calibration consisted of collecting 3 minute (180 sample) measurements on geodetic benchmarks surrounding the intended survey site. The resulting GPS position was then compared against the actual position of each benchmark by the RTK-GPS's internal software. By collecting a minimum of three measurements on geodetic benchmarks the RTK-GPS is able to calculate a correction. If additional benchmark measurements are made, the accuracy of the calibration is improved. Errors in the calibration are quantified by comparing the unknown benchmark location against the calibrated GPS coordinate; the difference between the values is the residual.

For this study, six geodetic benchmarks observations were used for the calibration, the maximum horizontal and vertical residuals observed were 0.028 m

and 0.032 m, respectively. Combining these residuals with the manufacturer's rated accuracy, at a distance of 5 km from the RTK-GPS base station the horizontal and vertical error could be as high as 0.043 m and 0.057 m, respectively.

3.1.1. Monitoring Station

A monitoring station collected air and water temperatures measurements and operated two remotely accessible CC640 cameras. Air temperature measurements were collected using a Model 107 temperature sensor [Campbell Scientific] mounted about 2 m above the ground. The temperature probe was housed in a 31303-5A radiation shield [Campbell Scientific] to prevent solar radiation from affecting the air temperature measurements. The specifications of the Model 107 temperature sensor are shown in Table 3-3. Water temperatures were collected using a Model 107B soil and water temperature probe [Campbell Scientific], refered to as the near shore water temperature sensor at station 56.8 km. The specifications of the Model 107B temperature sensor are shown in Table 3-3. The air and water temperature sensors were polled using a CR1000 datalogger [Campbell Scientific] mounted inside the monitoring station.

Table 3-3. Manufacturer's specifications for Model 107 air temperature probe (Campbell Scientific, 2010).

Temperature Range	-35°C to 50°C
Accuracy	±0.4°C

Table 3-4. Manufacturer's specifications for Model 107B water temperature probe (Campbell Scientific, 2003).

Temperature Range	-35°C to 50°C
Accuracy	±0.5°C

3.1.2. Time Lapse Cameras

3.1.2.1. Game Cameras

Three models of game cameras were used in this study. Game cameras are intended for the documentation of wild game behavior, but those used in this study also included a time lapse feature. These game cameras were installed on trees using either screws or zip-ties. The manufacturer's specifications for each game camera are shown in Table 3-5. Those cameras with a built in flash can be used to acquire night time images but their range is limited to approximately 15 m. An example of an installed Moultrie I65 Gamespy camera [Moultrie] is shown in Figure 3-5.

Table 3-5. Game camera manufacturer specifications (Moultrie 2010, Reconyx 2009, Treebark Cameras 2011).

Camera Model	Manufacturer	Image Resolution (Megapixels)	Maximum Frame Rate	Image Storage Method	Built In Flash
I65 Game spy (I65)	Moultrie	6.0	1 per hour	SD Flash Card	Yes
Rapid Fire Professional PC 85 (PC85)	Reconyx	3.1	1 per minute	Compact Flash Card	Optional
Mini P41 (P41)	Treebark Cameras	4.1	1 per minute	ProDuo Flash Card	Yes

3.1.2.2. Remotely Accessible Cameras

For real-time monitoring of ice conditions, two CC640 cameras [Campbell Scientific] were mounted on 4 inch by 4 inch wooden post, looking upstream and downstream, respectively. These cameras were interfaced with a CR1000 datalogger [Campbell Scientific], which collected the photographs from the cameras as they were taken and transmitted them to an office based data acquisition computer via a cellular modem. These cameras were part of a monitoring station that also collected air and water temperatures. The upstream camera was mounted in a large housing along with the datalogger, while the downstream camera was in a separate housing (Figure 3-4). The CC640 has a 0.3 megapixel resolution and is optimized for remote operations with its images being transmitted over a low bandwidth cellular connection (Campbell Scientific, 2007).

Due to its low resolution, this camera was primarily used for real time monitoring of field conditions and not for data analysis.

3.1.2.3. SLR Camera

For detailed photographs under both day and night time conditions, an EOS 5D SLR Camera [Canon USA Inc.] was used in sequence with a flood light. The ambient illumination provided by light pollution in the city also aided in the night time visibility of the ice cover at this location. The manufacturer's specifications for this camera are given in Table 3-6. A remote shutter switch was modified to allow electronic control of the camera by a CR1000 programmable data logger and to enable time lapse photography [Campbell Scientific]. The datalogger also controlled the flood light, synchronizing the operation of the two pieces of equipment. The camera was left in its automatic mode, the only setting chosen externally was the image acquisition rate controlled by the datalogger. This camera was mounted inside the trailer at station 56.8 km.

Table 3-6. Manufacturer's specifications for Canon EOS 5D SLR Camera (Canon Inc., 2007).

Maximum Resolution	12.8 megapixels
ISO Range	50-3200
Maximum Image Acquisition Rate	3 Hz
Shutter Speed	1/8000 second to 30 seconds

3.1.3. Submersible data loggers

Mini-Diver [Schlumberger Water Services] submersible dataloggers were used for the collection of both water temperature and pressure measurements. Table 3-7 presents the manufacturer's specifications for these dataloggers. These dataloggers are too small for deployments in rivers and so were mounted to 30 cm wide by 30 cm long concrete or steel platforms prior to their installation.

Table 3-7. Manufacturer specifications for Mini-Diver dataloggers (Schlumberger Water Services, 2011.

Temperature Range	-35°C to 50°C
Temperature Accuracy	±0.1
Temperature Resolution	0.01°C
Pressure Range	0 to 10 m
Pressure Accuracy	±0.5 cm
Pressure Resolution	0.02 cm

3.1.4. Acoustic Doppler Current Profiler

A 2 MHz Aquadopp ADCP [Nortek AS] was used for recording water velocity profiles in the water column above the sonar instruments. The ADCP converts the frequency shift of the reflected return signal into a velocity based upon the Doppler effect (Nortek AS, 2008). By concurrently operating three separate transducers, three-dimensional velocities can be measured. The ADCP calculates the velocity in range (i.e. distance from the transducer) intervals (called 'cells') from the transducer. The starting distance at which the ADCP begins to calculate velocities is referred to as the 'blanking distance'. The 'maximum range' is the distance from the transducer at which the furthest cell is recorded. Finally, the

'sampling rate' is the rate at which acoustic pulses are emitted and analyzed. The manufacturer's specifications for the 2 MHz Aquadopp are shown in Table 3-8.

Table 3-8. 2MHz Aquadopp Acoustic Doppler Current Profiler specifications for water velocity profile measurements (Nortek AS, 2008).

Maximum Profiling Range	4-10m
Cell Size	0.1-0.2m
Beam Width	1.7°
Minimum Blanking Distance	0.05m
Maximum # of Cells	128
Velocity Range	±10m/s
Accuracy	1% of measured velocity ± 0.5cm/s
Max. Sampling Rate	1 Hz

3.1.5. Sonar Instruments

A high (546 kHz) frequency sonar and a low (235 kHz) frequency sonar were used to measure suspended frazil and surface ice. These sonar instruments are bed mounted instruments that emit acoustic pulses into the water column and receive the reflected pulses. These acoustic pulses are reflected from targets in the water column or the water surface and are converted into voltage signals by the sonar instrument's transducer. The return signal is processed by the instrument's acquisition software to provide the distance or range to the target particle and the intensity of the signal. In addition to its acoustic measurements, each sonar instrument contains an onboard water temperature and pressure sensor which records measurements at the same rate as the sonar's transducer.

The sonar units have five important user selectable settings that influence data collection: ping period, digitization rate, pulse length, gain and range. The ping period determines the time between successive acoustic pulses. The digitization rate is the sampling rate used to acquire each ping, which determines the size of each bin in the profile. The pulse length specifies the duration of the acoustic pulse emitted by the transducer, and the gain setting (1, 2, 3 or 4) varies the amplification applied to the received signal. The range setting is the maximum distance from the transducer for which the sonar will record a measurement. The sonar also has a nonadjustable minimum lookout, which indicates the minimum distance from which a sonar can receive an acoustic reflection. The manufacturer's specifications for the high and low frequency sonar instrument are shown in Table 3-9.

Each sonar unit contains built-in hardware which filters, amplifies and digitizes the raw signals received from the transducer (Ghobrial *et al.*, 2012). The signals are filtered by a band pass filter and amplified using a Time Varying Gain (TVG) board. The TVG board applies a signal correction as a function of travel time in the water column, approximately correcting for losses due to signal spreading and absorption of sound by the water (Ghobrial *et al.*, 2012). The TVG board also applies a user selectable gain setting (1 to 4). The amplified signal passes through an envelope detector and then to a 16 bit analog to digital (A/D) converter. The A/D converter transforms the signal amplitude (volts) into raw digital counts, with values ranging from 0 to 65,535 (16 bit) at a rate of 64kHz (Ghobrial *et al.*, 2012).

Table 3-9. Manufacturer's specifications for high and low frequency SWIPS instruments (ASL Scientific Services Inc., 2011)

Parameter	Low Frequency SWIPS	High Frequency SWIPS
Frequency (kHz)	235	546
Maximum Range	36.0	25.4
Minimum Lookout (m)	0.5	0.5
Gain Setting Variable	1 to 4	1 to 4
Ping Rate (Hz)	1	1
Maximum Digitization Rate (kHz)	64	64
Pulse Length (μs)	10 to 10000	10 to 10000
Water Temperature Accuracy (˚C)	±0.1	±0.1
Water Temperature Resolution (˚C)	±0.01	±0.01
Water Pressure Accuracy (m)	±0.2	±0.2
Water Pressure Resolution (m)	±0.01	±0.01

3.2. Methods

3.2.1. Channel Bathymetry

The river was bathymetrically surveyed over a section 500 m upstream and 300 m downstream of station 56.8 km (the location of the sonar instruments). This survey was conducted on 15-Jun-10, using the depth sounder and RTK-GPS for depth and position measurements, respectively. The depths, easting, northing and elevation were collected using a data acquisition laptop which recorded the water surface coordinates and depths using a program written in Arcpad [ESRI]. The resulting depth contour map is shown in Figure 3-2. A grid spacing of approximately 20 m was used, with a denser spacing over the scour hole near the

right bank. The depths shown in this contour plot are those surveyed on 15-Jun-10, the actual depths were between 0.2 m and 0.80 m deeper during the winter than was indicated in Figure 3-2.

3.2.2. GBWTP Open Lead Shape

The width of the GBWTP open lead was estimated by three methods: a ground based photographic survey, an aerial photographic survey and a direct survey using a handheld Global Positioning System (GPS). The ground based photographic survey was conducted on 9-Dec-10 between stations 56.8 and 49 km. An aerial survey was not conducted during the 2010/11 season due to budget constraints (although an aerial survey completed on 24-Jan-08 was available for the entire study reach). The edge of ice along the open lead at station 56.8 km was recorded on 24-Feb-11 using a handheld GPS system.

3.2.3. Air Temperature

Air temperature measurements were collected by the monitoring station, located on the right bank at station 56.8 km. This sensor collected readings every 15 minutes from 30-Sept-10 to 31-Mar-11. Comparing the monitoring station's air temperature measurements against the Environment Canada air temperature data, it can be seen that the two stations displayed similar temperatures (Figure 3-6). The datasets differed by a mean of 0.2°C and standard deviation of 1.5°C over the entire winter. At cold air temperatures, the monitoring station occasional returned temperatures up to 3˚C lower than those determined by the Environment Canada

station. These differences are a result of the 11 km distance between the two stations and the different exposure conditions. Greater amounts of ambient heat in an urban environment would slightly dampen severe cold periods seen by the Environment Canada air temperature sensor. During analysis, the Environment Canada dataset was used for developing forecasting parameters. Using the City Center Airport station dataset will allow the results of this thesis to be applied to past and future winter seasons since this dataset is continuous from year to year.

3.2.4. Water Temperature and Stage Measurements

Water temperature and stage measurements were collected from station 57.3 km upstream to station 49.5 km using: submersible dataloggers, two sonars instruments, an ADCP and the near shore water temperature sensor (monitoring station based). The locations of these sensors are shown in Figure 3-7. Depths were calculated from pressure readings by subtracting the atmospheric pressure readings collected by Environment Canada and multiplying by the specific weight of water.

At station 57.1 km, a submersible datalogger was installed 15 meters from the right bank and recorded temperature and pressure data every 15 minutes from 30-Sept-10 to 31-Mar-11. Approximately 300 m upstream, at station 56.8 km, water temperatures were measured 15 and 45 m from the right bank. The monitoring station water temperature sensor was 15m from the right bank and the sonar instrument platform, was 45 m from the right bank. On the sonar instrument

platform the two sonar units and an ADCP measured water temperature and pressure measurements. The near shore sensor recorded water temperature measurements every 15 minutes and both sonar units recorded water temperatures at a rate of 1 Hz. The ADCP recorded water temperatures every 5 minutes prior to 5-Jan-11 and every 2 minutes after 13-Jan-11. The ADCP did not record any data between 5-Jan-11 to 13-Jan-11. The three acoustic instruments recorded water temperature and pressure measurements from 4-Nov-10 to 15-Mar-11.

It was known from a water temperature sensor calibration conducted in September-11 (documented in Appendix A) that the sonar instruments water temperature sensors tended to drift (i.e. to have a varying bias error). The same calibration test showed that the ADCP did not have a drifting bias error. As a result, the ADCP water temperature data was used as the reference water temperature for the instrument platform. During an 8 day period (5-Jan-11 to 13-Jan-11) when the ADCP was not recording data, water temperatures from the low frequency SWIPS were used as the reference temperature. Low frequency sonar water temperatures were adjusted by -0.09°C to match the ADCP on 5-Jan-11. The difference in the two datasets on 13-Jan-11 was 0.02°C indicating that the bias error resulting from the usage of the low frequency sonar was small but notable.

An outfall from the Clover Bar Energy Centre, a 243 megawatt natural gas-fired power plant, is located on the right bank approximately 50 m upstream of the sensors at station 56.8 km. This power plant is during peak demands peroids and

as a result it periodically discharges warm water into the river. The monitoring station's near shore temperature sensor, located 15m from the right bank, was located in plume of this outfall (Ghobrial *et al.*, 2010). The measured water temperatures at the sonar instrument platform were not affected by the outfall's warm water plume. This is verified in Figure 3-8, where water temperature time series data recorded at 15 m and 45 m from the bank from 8-Nov to 22-Nov-10 are plotted at the two locations. In the time series sampled at 15 m from the bank, sharp temperature spikes up to ~4˚C in amplitude appear periodically; however the time series sampled at the platform (45 m from shore) did not have these temperature spikes. At times when the temperature spikes are not present, the two time series are in close agreement.

At station 56.3 km, two submersible dataloggers were installed 15 m from the right and left banks. Each recorded water temperature and pressure measurements every 15 minutes. These dataloggers collected data from 30-Sept-10 to 31-Mar-11.

Two submersible data loggers were installed 300 m downstream and 800 m upstream of the GBWTP outfall (station 50.3 km). These loggers were used to monitor the discharges 300 m downstream from the GBWTP outfall and to determine if any additional thermal sources upstream were contributing to the GBWTP open water lead. Both loggers recorded water temperature and pressure measurements every 15 minutes from 30-Sept-10 to 30-Apr-11.

3.2.5. Water Surface Profile

To determine approximate depths in the reach between the GBWTP outfall (station 50.3 km) and station 56.3 km, water surface profiles were calculated using Alberta Environment's Flood Hazard Forecasting HEC-RAS model of the North Saskatchewan River. This model is not calibrated within the City of Edmonton and is intended for flood hazard forecasting downstream and upstream of the city limits (Northwest Hydraulic Consultants, 2007). Despite this limitation, this model presents the best available method of determining depths between stations 50.3 km to 56.3 km.

Using this model, discharges were chosen to calculate water surface profiles to match the minimum and maximum winter stage determined by the right bank submersible dataloggers located at station 56.3 km. Water surface elevations at the corresponding times, from the Water Survey of Canada gauge located at station 42.8 km (Environment Canada. 2011b) were then used to validate the computed water surface elevations.

A 0.50 m thick ice cover with an underside Manning's *n* roughness of 0.015 was added to the model to account for the winter ice conditions. The 0.50 m ice thickness was selected based upon pan thicknesses by the sonar instruments prior to the freeze-up front passing. The roughness of values of 0.015 were taken from Ashton (1986) (After Nezhikhovskiy, 1964), in which roughness range of 0.01 to 0.02 was suggested based the 0.50 m thick ice cover.

It was found that the calculated and observed water surface elevations at station 42.8 km were within 0.05 m. Since this HEC-RAS model was intended to predict high discharge (flooding) scenarios, the relative roughness calibration used in the model is lower than what was present in reality. As a result, only the calculated water surface elevations were valid and not the calculated discharge.

3.2.6. Time Lapse Camera Data

3.2.6.1. Camera Installations

A list of the installed camera types, locations and picture intervals is available in Table 3-10. Although most of these cameras had built in flashes, only those situated near river level (stations 56.2, 57.1 and 63.9 km) photographed night time ice conditions in any detail. All of the installed cameras recorded the progression of freeze-up, while those downstream of the GBWTP outfall (station 50.3 km) also documented open lead development and ice pans in the open lead. Camera installation locations were selected based upon their security, accessibility and a spacing of roughly 10 km between cameras, with greater detail in the vicinity of the sonar instrumentation. This spacing was determined by the number of available cameras and the distance of river that was desired to be covered. The furthest downstream cameras were located was at station 63.9 km, near the downstream end of the GBWTP open lead. In addition to monitoring freeze-up, these cameras recorded the variability in the location of the downstream end of the open lead.

A SLR camera, synchronized with spotlights, collected day and night images at station 56.8 km along with two remotely accessible cameras mounted on the monitoring station. The SLR camera was focused on the water surface above the sonar instruments. These photographs provide information about the surface ice conditions detected by the sonar instruments. The remotely accessible cameras were used for deployment planning during the winter season.

Table 3-10. List of Remote Cameras installed along the North Saskatchewan River from Station 9.2 to 63.9 km

Station (km)	Northing (m)	Easting (m)	Side of River	View Direction	Cameras Type	Date Installed	Date Removed	Photo Interval	Night Photos
9.2	5918432	321212	Left	Upstream	I65	5-Nov-10	25-Nov-10	1 hour	No
19.3	5925134	324698	Left	Upstream	I65	5-Nov-10	25-Nov-10	1 hour	No
28.2	5928864	328186	Right	Downstream	I65	5-Nov-10	15-Feb-11	1 hour	No
41.3	5933467	334726	Right	Downstream	I65	28-Oct-10	19-Nov-10	1 hour	No
49.8	5937777	339916	Left	Downstream	I65	8-Nov-10	9-Dec-11	1 hour	No
56.3	5939749	343412	Right	Across River	P41	19-Oct-10	9-Dec-11	1 hour	Occasional
56.8	5940261	343299	Right	Across River	SLR Camera	16-Nov-10	14-Apr-11	10 minute	Yes
56.8	5940275	343284	Right	Upstream & Downstream	2 x CC640	23-Sep-11	14-Apr-11	30 minute	No
57.1	5940639	343201	Right	Across River	PC85	19-Oct-10	14-Apr-11	1 hour	Occasional
63.9	5942706	348075	Right	Upstream & Downstream	2 x I65	8-Nov-10	9-Dec-11	1 hour	Occasional

3.2.6.2. Qualitative Analysis of Time Lapse Images

The automated time lapse camera images from the game cameras and the SLR camera were analyzed qualitatively. In each photograph, a percentage of the concentration of moving and station ice pans relative to the river width was estimated by visual inspection of the image. The resulting arrays of photograph times and ice concentrations were converted into figures referred to as 'cryographs' using a spreadsheet. A sample cryographs is shown in Figure 3-9.

With the exception of the freeze-up front, the ice conditions within each image were homogenous and there was no need to specify a particular region (near or far field) as the representative ice cover. In the case of the freeze-up front however, the intact ice cover could be seen propagating upstream over a 1 to 3 hour period at stations 9.2 km, 19.3 km and 28.2 km. The criteria for the identification of the 100 percent intact ice cover was set based upon the orientation of the camera; upstream or downstream.

Since the ice concentrations were referenced to the river station of the camera installation site, the representative freeze-up front locations would be the river cross section perpendicular to the camera. When facing the upstream direction (station 9.2 km and 19.3 km) this would correspond to the first appearance of the freeze-up front. If the camera was facing downstream (station 28.2 km), this would correspond to the image which first showed 100 percent intact ice. If the

freeze-up front passed overnight, the mid-point between the last observed open water image and the first intact ice image was taken as the observation time.

3.2.7. Velocity Data

Water velocity profiles were measured with an ADCP and used for determining water and ice travel times within the GBWTP open lead and for calculating pan lengths from the sonar data. The ADCP settings used during the 2010/11 season were: a maximum range of 4.5 m, cell size of 0.1 m, blanking distance of 0.2 m and a sampling rate of 1 Hz. The 1 Hz samples were recorded as profiles averaged over 5 minutes (prior to 13-Jan-11) and over 2 minute (after 13-Jan-11). The averaging time was decreased to make the ADCP's maximum data storage interval equal that of the sonars. The ADCP functioned continuously throughout the field season, with the exception of a loss of data between 5-Jan-11 and 13-Jan-11 when the onboard memory capacity was exceeded.

The velocity data were post processed to produce two values used in this study: surface velocity and mean velocity. Cells at depths above the water surface were removed from the dataset, as determined by the ADCP onboard pressure sensor. The shallowest remaining cell was recorded as the surface velocity. The cells between 0.20m above the ADCP transducer (the minimum measurement distance) up to the water surface then averaged to obtain a mean water velocity. The mean and surface water velocities were 0.70±0.1 meters per second (m/s) and 0.75±0.3, respectively, throughout the season.

3.2.8. Sonar Data

A sonar instrument platform was constructed to allow secure placement of the ADCP, high frequency sonar and low frequency sonar on the river bed. Several improvements have been made to the platform (Figure 3-10) since its initial construction in 2008. Previous field deployments of sonar instruments have experienced severe problems with adhesion of anchor ice to the platform or to the cables connecting the instruments to power and computers located on the river bank (e.g. Marko *et al.*, 2006). In one case, anchor ice buildup was so severe that the instrument platform became buoyant and was carried downstream by the flow (Marko *et al.*, 2006), risking a total loss of the instrument. In a more recent study, a water heater installed in the instrument platform melted any adhering ice particles eliminating this problem (Buermans *et al.*, 2011). For this study, the platform was covered with a low density polyethylene sheeting with non-stick surface in order to limit or prevent anchor ice adhesion. During the 2009/10 deployment, one minor episode of anchor ice adhesion was documented, but did not have a significant impact upon the instrument platform (Ghobrial et al, 2010). An upstream deflector was also installed to prevent floating weeds from becoming entangled in the platform.

The instrument platform was installed on 14-Oct-10 using a boat mounted crane. The platform was positioned 45m from the right bank, as shown in Figure 3-2, and at a depth of approximately 3.5 m. The data and power cables, as well as a mooring line (steel cable enclosed in a plastic conduit), were laid along the bed

from the instrument platform to the bank, where two data collection computers in the site trailer recorded output from the sensors in real time. These computers could be accessed remotely via a mobile internet key to ensure the instruments were operating correctly. Instrument data were downloaded in person from these computers at 1 to 2 week intervals. The instrument platform was removed from the river on 15-Mar-11.

The sonars' pulse length, gain and range settings were varied throughout the winter. The low frequency sonar gain was increased following freeze-up in order to the improve detection of the less dense frazil pans that were generated in the open lead. The high frequency sonar's gain and pulse length were also varied in an attempt to optimize the detection of suspended frazil. Table 3-11 summarizes variations in the sonars gain and pulse length settings. The ping period and digitization rates were kept at 1 Hz and 64 kHz (0.011m bin size), respectively throughout the entire season.

Table 3-11. Pulse length, gain and range settings used for the high and low frequency sonar instruments during the 2010/11 winter season.

		High Frequency Sonar			**Low Frequency Sonar**		
Start Date	**End Date**	**Pulse Length**	**Gain**	**Range (m)**	**Pulse Length**	**Gain**	**Range (m)**
4-Nov-10	9-Dec-10	34µs	3	4	68µs	1	4
9-Dec-10	21-Dec-10	34µs	3	4.5	68µs	3	4.5
21-Dec-10	17-Feb-11	68µs	1	4	68µs	3	4
17-Feb-11	15-Mar-11	34µs	3	4.5	68µs	3	4.5

3.2.8.1. Sonar Signal Processing

The raw sonar data (digital counts N) were pre-processed to correct for two factors. First, the envelope detector was originally thought to apply a linear transformation between signal amplitude (volts) and digital counts. However, testing by the manufacturer subsequently revealed that this transformation was non-linear at low voltages (Ghobrial *et al.*, 2012). Second, manufacturer also found the receiver circuit in the high frequency sonar to have a faster response time (i.e. higher frequency response) than that in the low frequency sonar.

A Matlab [Mathworks Inc.] program [SWIPSProcessor.m] developed by Ghobrial (2012) was used to correct for these two factors. In this program, a low pass filter was constructed based upon response time data supplied by the sonar instruments' manufacturer and applied to the high frequency sonar raw digital counts, N_r. The filter was designed so that the resulting filtered high frequency sonar dataset had the same frequency bandwidth as the lower frequency sonar's data (i.e. effectively making the frequency response of the two instruments equal). The algorithm then applied the second correction for the non-linear behavior of the envelope detector (Ghobrial *et al.,* 2012).

The pre-processed counts N were then converted to calibrated units using the transducer specifications and calibration data supplied by the manufacturer (Ghobrial *et al.*, 2012). The volume backscatter strength, S_v, is the calibrated unit

used because it can be related to frazil ice concentration and particle sizes (Urick 1983). S_v is given by;

$$S_v = 20log_{10}(N) - G[R] - OCV - \beta - TVR - 20log_{10}(V_{Tx}) \\ +20log_{10}(R) + 2\alpha R - 10log_{10}(\tfrac{1}{2}c\tau\psi) \quad [3\text{-}1]$$

where S_v is the volume backscatter strength in decibels (dB) per unit volume; N is the pre-processed digital counts; $G[R]$ is the receiver gain correction supplied by the instrument manufacturer; R is the range of the target from the transducer; OCV is the transducer receiving response in (dB), referred to as the Open Current Voltage; β is the analog to digital scaling factor (97.4 dB for 16 bit digitization) ; TVR is the transmit voltage response of the transducer; V_{Tx} is the actual RMS voltage applied to the transducer as a function of the supply voltage; α is the absorption coefficient expressed in dB/m; c is the speed of sound in water; τ is the user specified pulse length; and ψ is the transducer beam width. A more complete description of the sonar signal processing algorithm can be found in Ghobrial *et al.* (2012). Table 3-12 provides the acoustic parameters of the sonar instruments used in this calculation.

Table 3-12. Acoustic parameters of high and low frequency SWIPS instruments (Ghobrial *et al.*, 2012).

Parameter	High Frequency	Low Frequency
Frequency	546 kHz	235 kHz
Transducer beam width (ψ)	0.00861 Steridian	0.02893 Steridian
Transmitting Voltage Response (TVR)	176 dB	165 dB
Open Current Voltage (OCV)	-192 V	-187.5 V

The processing program [SWIPSProcessor.m] was only capable of processing discrete sections of data. Due to the memory restrictions of 32 bit computer systems, the maximum time span of sonar data that could be processed at one time was about 6 hours. The 2010/11 winter study produced about 6000 hours of low and high frequency sonar data. To streamline this process, a Matlab [Mathworks Inc.] parsing program [SWIPSParser.m] was written which divided these large datasets into discrete segments, processing each sequentially. A concatenation script then reassembled the processed datasets into figures of a chosen time span for analysis of surface and suspended ice data [SWIPSSurfaceIceFigs.m and SWIPSSuspIceFigs.m]. The processing, parsing and concatenation scripts are presented in Appendix B. The complete processed dataset is supplied on DVD in Appendix C. Processing the entire season of data took approximately 36 hours on a 2.13 GHz dual core computer.

3.2.8.2. Surface Ice Characteristics

The processing program [SWIPSProcessor.m] includes a pan detection algorithm which identifies the bottoms of frazil pans in the sonar dataset and records these as '*targets'*. These *targets* were then used to calculate pan thicknesses and lengths [SWIPSThicknessandLength.m] as well as surface ice concentration [SWIPSSurfaceConc.m]. These programs were adapted from an algorithm written by Ghobrial (2012). The pan detection algorithm analyzes the sonar datasets sequentially from the bed to the water surface, checking the volume backscatter strength (S_v) of each bin against a *threshold* value. If a bin at a given range exceeds the *threshold*, the next 6-12 bins above are also checked to see if the threshold is exceeded in all of these bins. The number of bins that are checked above the initial bin is referred to as the *persistence*. Checking for sufficient *persistence* is necessary to ensure that a detected target is a pan bottom and not a suspended ice particle. Likewise, the properly adjusted *threshold* would allow the accurate detection of frazil pans. If a *threshold* were too low suspended frazil would be erroneously detected as a pan; at too high of a *threshold,* some pans would not be detected at all. Once a frazil pan was identified by the algorithm, the initial bin in which the bottom of the pan was detected is recorded as the *target range.*

Frazil pans thicknesses were calculated by subtracting the *target range* from the pressure reading of the corresponding sonar unit. The pressure readings of the sonar instruments were adjusted to match the acoustic measurement of the water

surface under open water conditions prior to freeze-up to account for differences in the elevation of the pressure sensor and acoustic transducer of each sonar. The high frequency sonar pressure readings were adjusted by -0.227 m and the low frequency sonar pressure's adjusted by -0.214 m.

On occasion, negative thicknesses occurred when the *target range* was greater than the pressure reading of the sonar. These were caused by the pan detection algorithm not detecting the open water surface and returning the maximum sonar range. To remove these values, negative thicknesses were set to not-a-number (NaN) values, as were any thicknesses below 5 cm. The 5 cm threshold was chosen to reduce erroneous detections. A time series of surface ice concentrations was calculated by dividing the number of pings in which a thickness greater than NaN was detected by the total number of pings in a 5 minute (300 sample) time interval [SWIPSSurfaceIceConc.m].

Frazil pan lengths were calculated utilizing the Matlab Image Processing Toolbox [SWIPSThicknessandLength.m] in a procedure developed by Ghobrial (2012). Figure 3-11 provides an illustration of this procedure. The pan detection algorithm [SWIPSProcessor.m] produces a time series of ice thicknesses with a sampling rate of 1 Hz, equal to the ping rate. This time series was converted to a binary vector with false (0) indicating no pan detected and true (1) indicating a pan was detected. The assumption was made that a continuous series of true readings represented a continuous pan or raft. The binary vector was analyzed; the number of consecutive true readings for each pan and the time of the last true reading for

each pan were recorded. This produced a vector of the time in seconds that each pan was above by the sonar. Pan lengths in meters were calculated by multiplying this vector by the corresponding surface velocities measured by the ADCP.

The *persistence* and *threshold* values were calibrated by manually observing the suspended frazil flocs (frazil flocs are agglomerate frazil particles) in the high and low frequency sonar S_v datasets and determining the required persistence and threshold to avoid detecting them. The low frequency sonar S_v values were observed to be slightly lower than the corresponding high frequency sonar values, and therefore *threshold* settings of -37 dB and -40 dB were used when analyzing the high and low frequency sonars data, respectively. A *persistence* of 12 was used for both units.

The identification of a pan is based upon the acoustic S_v of a potential target exceeding the specified *threshold* and *persistence* settings. Many of the pans in the open lead were observed to be quite slushy, with a higher S_v nearer to the surface as illustrated in Figure 3-12. In this figure, the S_v values of the pans increase as the pan nears the surface. This made it difficult to define precisely when the acoustic return is strong enough to be considered a frazil pan. Consequently the identification of a pan was slightly ambiguous: a higher or lower threshold may render larger or smaller concentrations, thicknesses and lengths. The selected thresholds of -37 dB and -40 dB were selected as a

compromise between most complete detection of ice pans and a lower number of false *target* detections.

The pan thickness and length datasets were further processed to reduce erroneous values. The frazil pan thickness and length datasets were smoothed using a moving average filter of 300 samples (5 minutes) to prevent high frequency oscillations in the dataset. The *threshold* and *persistence* settings prevented most erroneous target detections, but occasionally a suspended ice particle was detected, creating a false positive as shown in Figure 3-13. These false positives could have a significant effect upon the thickness dataset when they were detected without any accompanying pans in the 300 sample range. To remove these extraneous values, any 300 sample time span which contained less than 3 target detections was set to a thickness of zero. This removal was unnecessary in the pan length and concentration datasets as a lone particle still produced near zero concentrations or lengths.

3.2.8.3. Suspended Ice Characteristics

As discussed in Section 1.1, the high and low frequency sonars are sensitive to different size ranges of particles; the high frequency sonar is sensitive to suspended frazil while the low frequency sonar is sensitive to larger features like slush ice and flocs. Increases in a sonar's acoustic return are correlated with increases in either frazil particle sizes or concentrations (Gartner, 2004). To quantify the differences in the sonar returns, two values were calculated: depth

averaged S_v and the ratio of the volume backscatter coefficient for the high to low frequency sonars, s_{v1}/s_{v2}. The volume backscatter coefficient is the backscattering cross sectional area per unit volume (s_v) of the population of target particles (Ghobrial *et al.*, 2012). The parameter s_v (defined below) is the linear form of S_v and can be arithmetically averaged in time and space, unlike the logarithmic S_v (Ghobrial *et al.*, 2012).

Values of s_{v1}/s_{v2} greater than ambient levels (ambient levels are conditions without any suspended or surface ice present) would indicate the presence of suspended frazil. Similarly, increases in the low frequency sonar depth averaged S_v would indicate the presence of slush ice. Depth averaged S_v and s_{v1}/s_{v2} values have been used in laboratory studies to calculated suspended frazil concentrations; however this requires knowledge of the particle size distributions through direct measurements (Ghobrial *et al.*, 2012).

To calculate depth averaged S_v, the sonar data were first converted from the logarithmic S_v(dB) to the arithmetic s_v(m^{-1}). The relationship between S_v and s_v is given by,

$$S_v = 10log_{10}(s_v R_o) \qquad [3\text{-}2]$$

where R_o is the reference distance (1.0 m used by Ghobrial *et al.*, 2012). The s_v of each bin, beginning 60 bins above the transducer, to the detected *target* (either the bottom of a pan or the water surface) was then averaged and converted back to the logarithmic form, depth averaged S_v. The 60 bins separation above the transducer

is required because a background noise approximately -50 dB in strength is present in the first ~50 bins of each ping. The ratio of high frequency sonar's s_v to low frequency sonar's s_v (s_{v1}/s_{v2}) was then calculated.

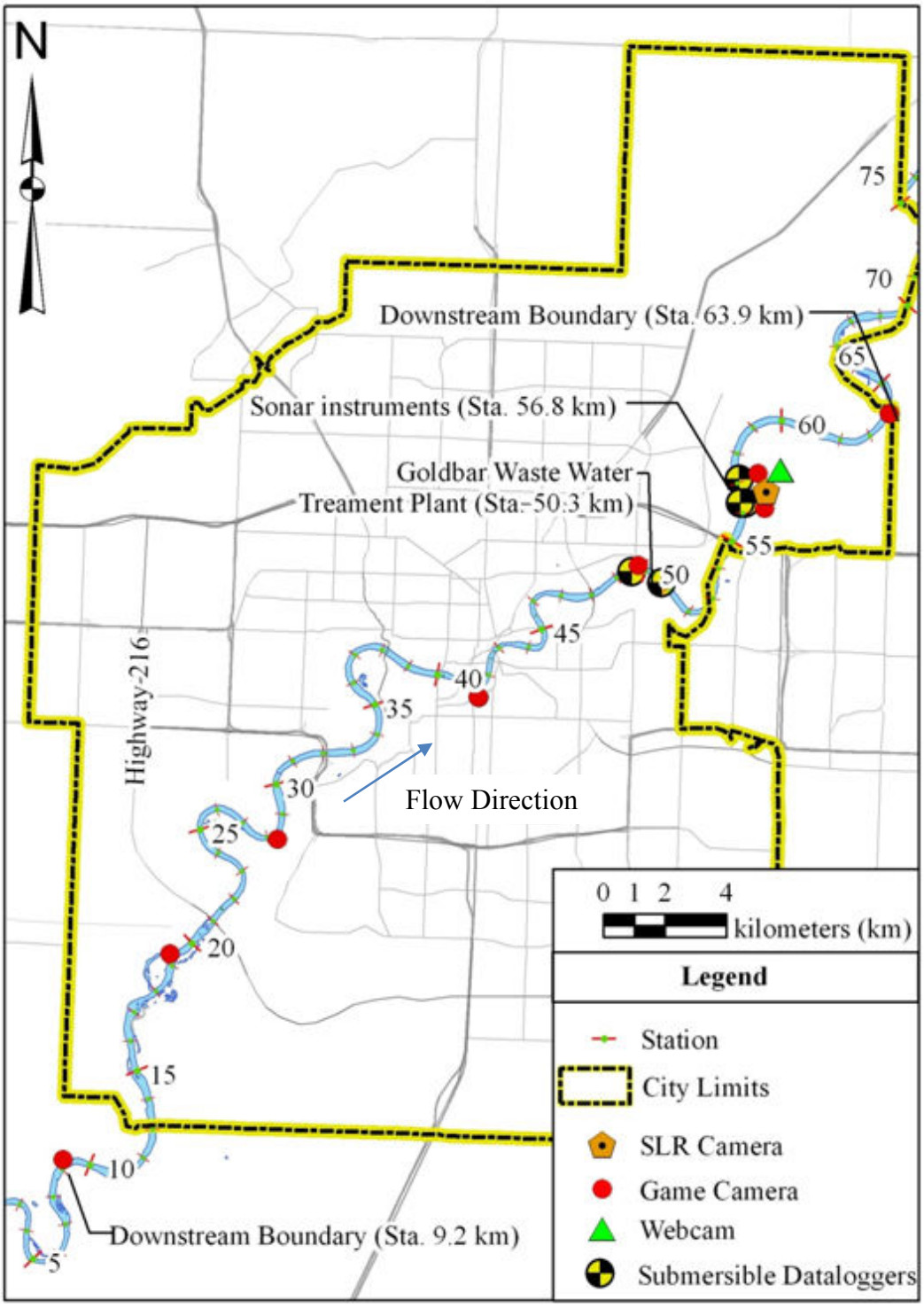

Figure 3-1. North Saskatchewan River study reach, with locations of installed instrumentation.

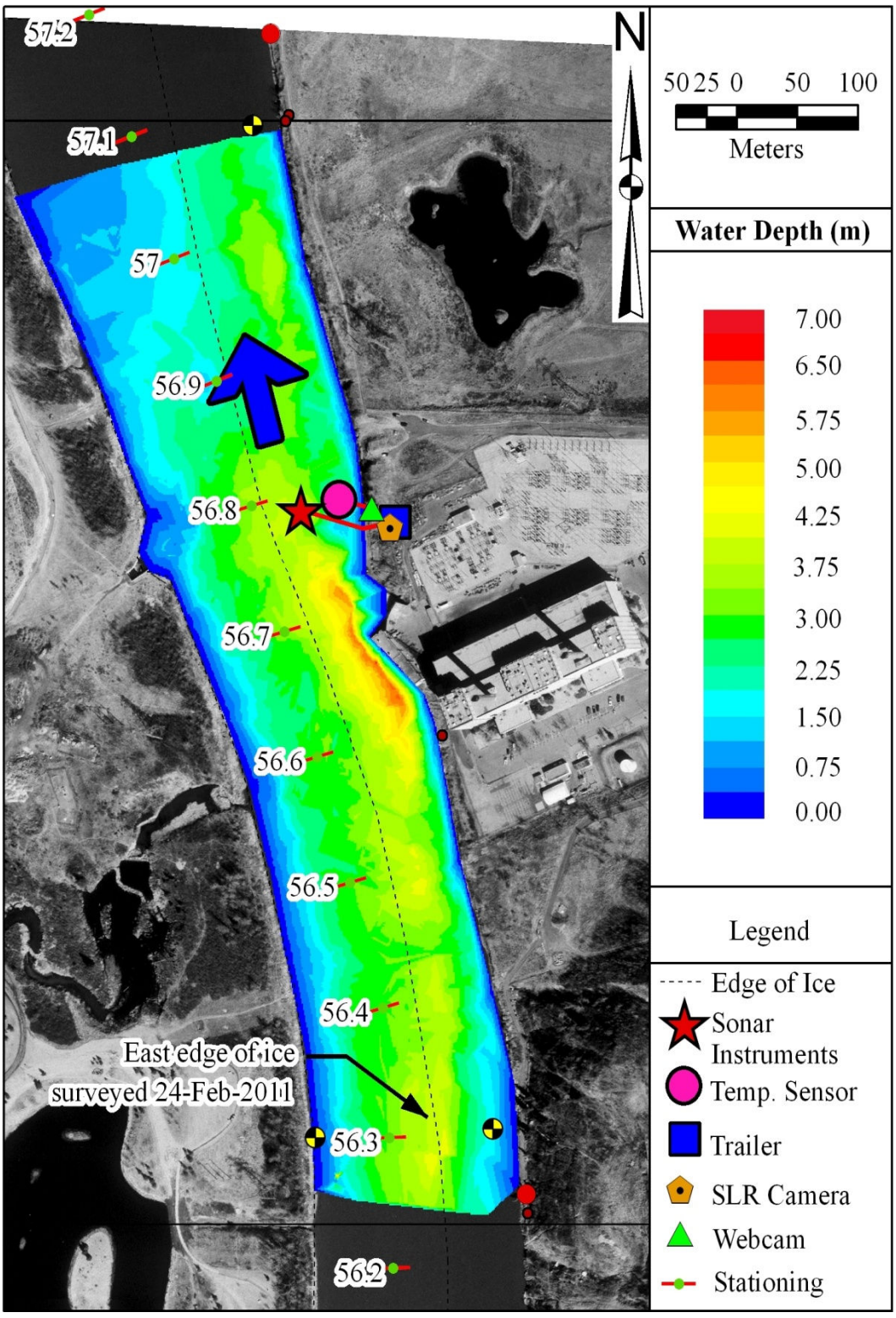

Figure 3-2. Location plan for in-stream sonar instrumentation site

Figure 3-3. Inside and outside picture of site trailer at station 56.8km, housing data collection computers and SLR camera.

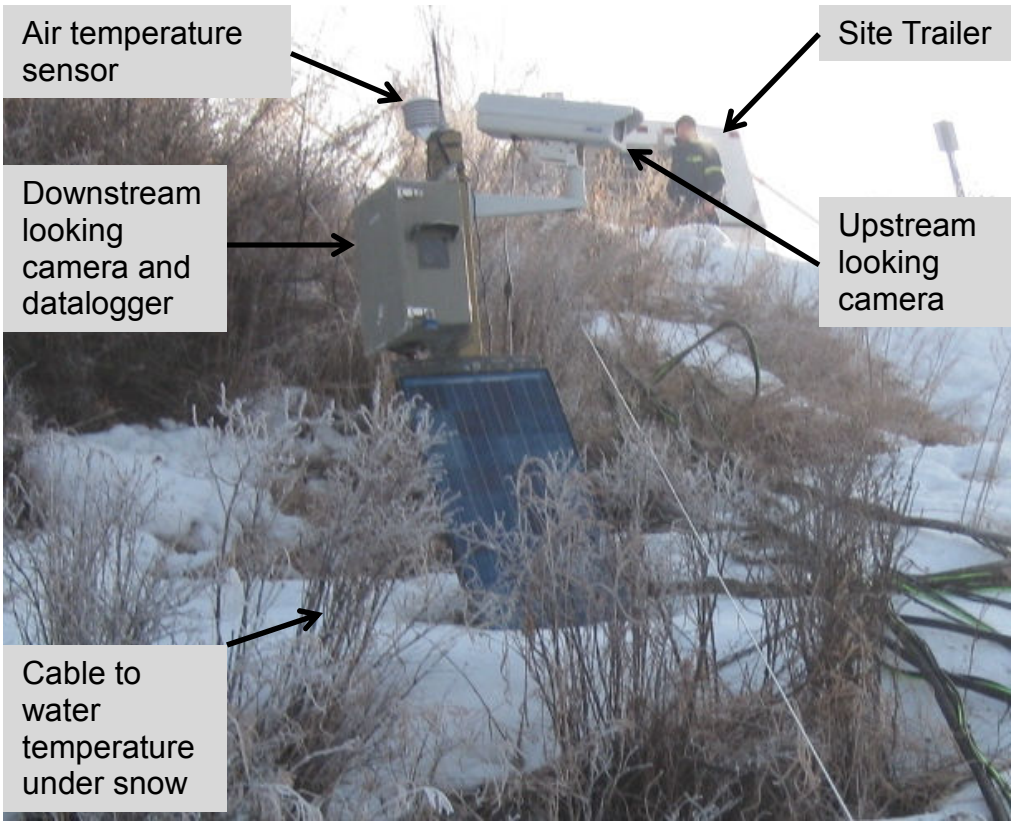

Figure 3-4. Picture of monitoring station located at station 56.8 km.

Figure 3-5. Picture of a Moultrie I65 Gamespy camera installed at station 9.2 km.

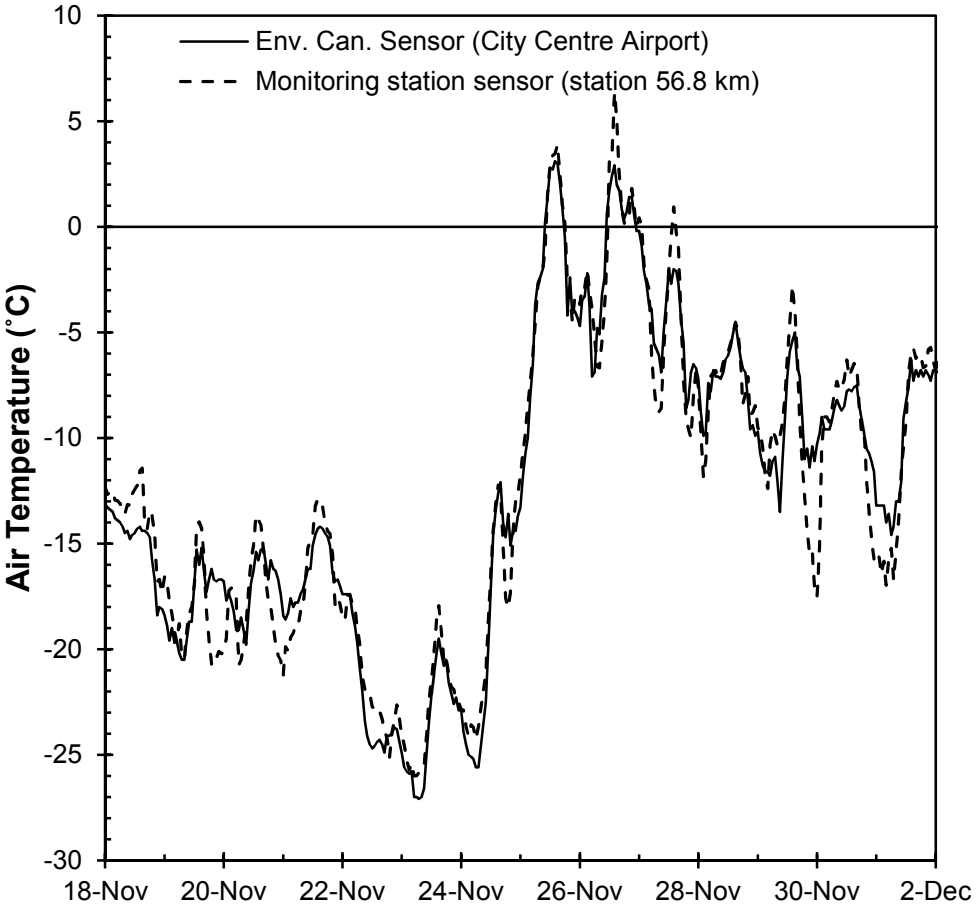

Figure 3-6. Comparison of air temperatures recorded by Environment Canada City Centre Airport station and monitoring station based air temperature sensor located at station 56.8 km.

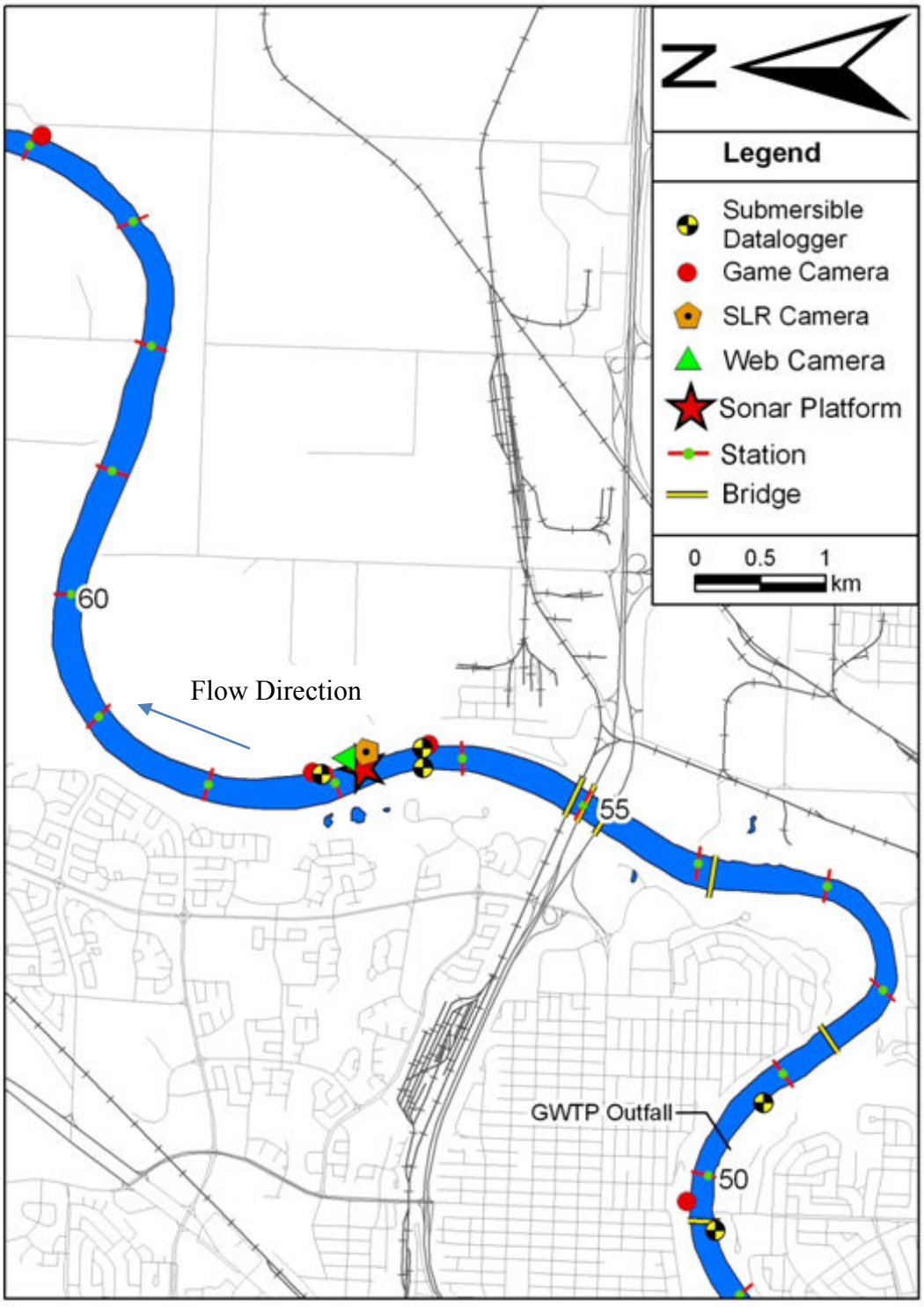

Figure 3-7. Locations of water temperature and pressure sensors in study reach.

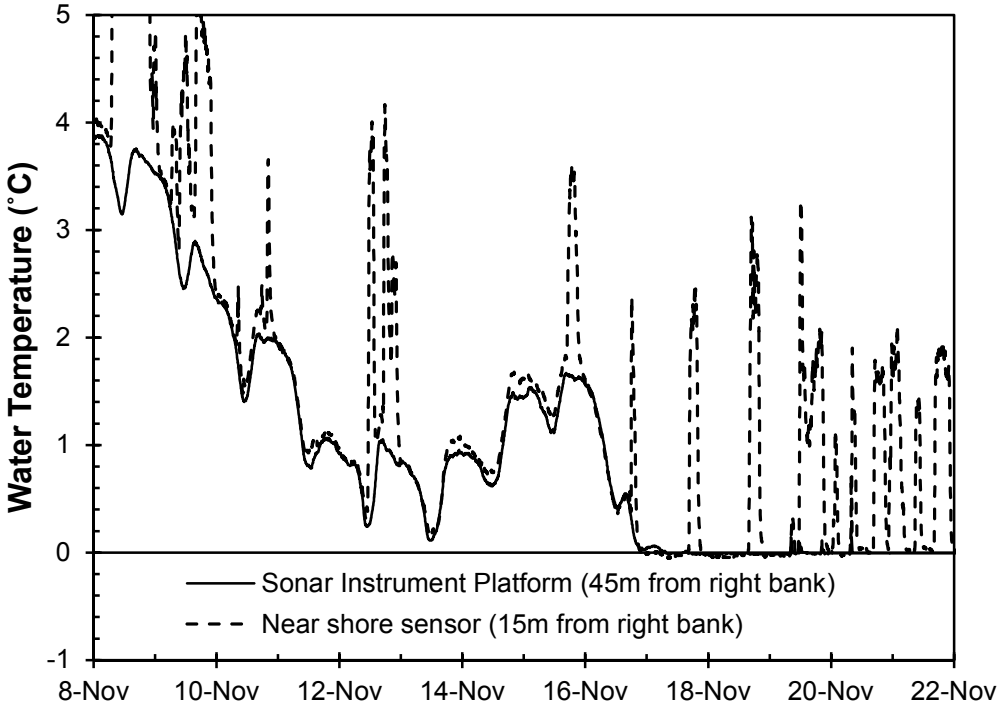

Figure 3-8. Comparison plot of water temperatures recorded at station 56.8 km by the sonar instrumentation platform (located 45 m from right bank) and the near shore water temperature sensor (located 15 m from right bank).

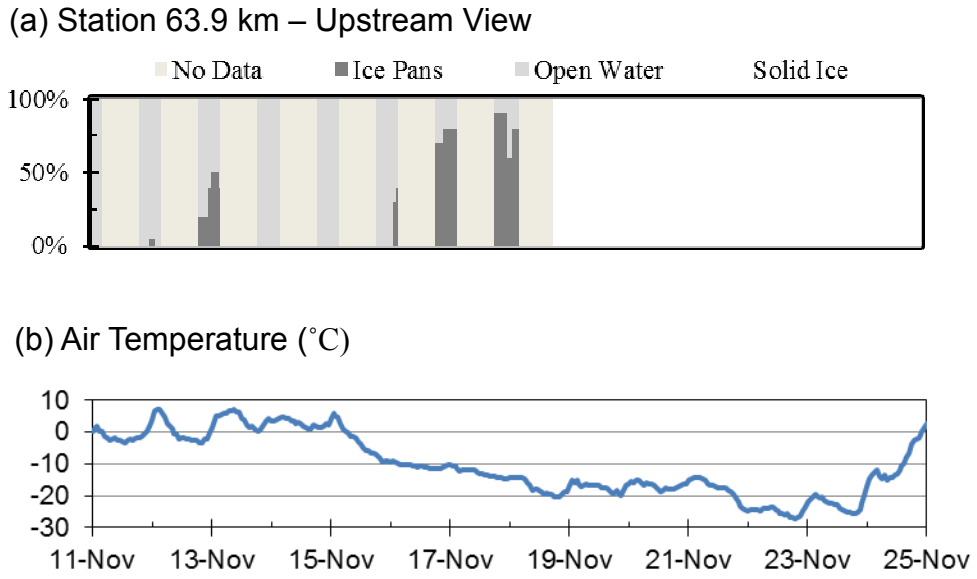

Figure 3-9. Sample cryrograph showing (a) Station 63.9 km relative percentages of ice pans, open water and solid ice cover and (b) Air temperatures. Dates shown are 12:00am (noon).

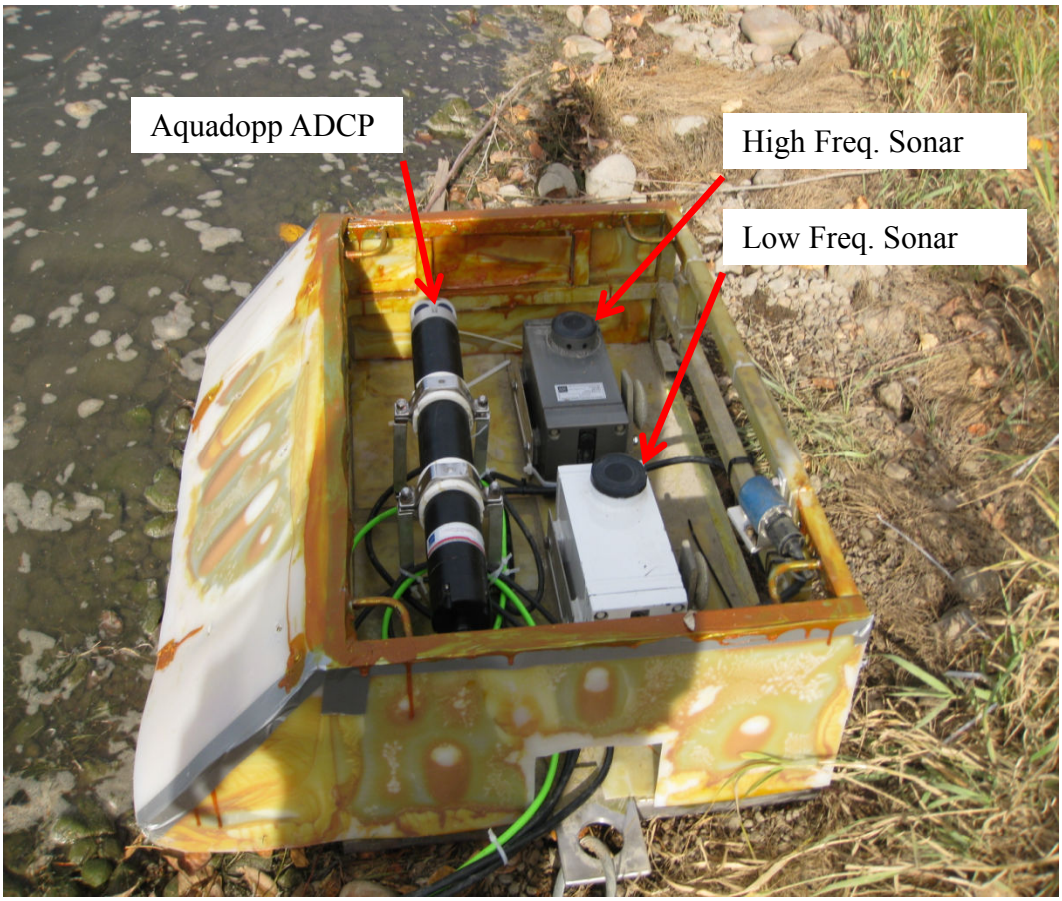

Figure 3-10. Photograph of sonar instrument platform prior to being installed on the river bed.

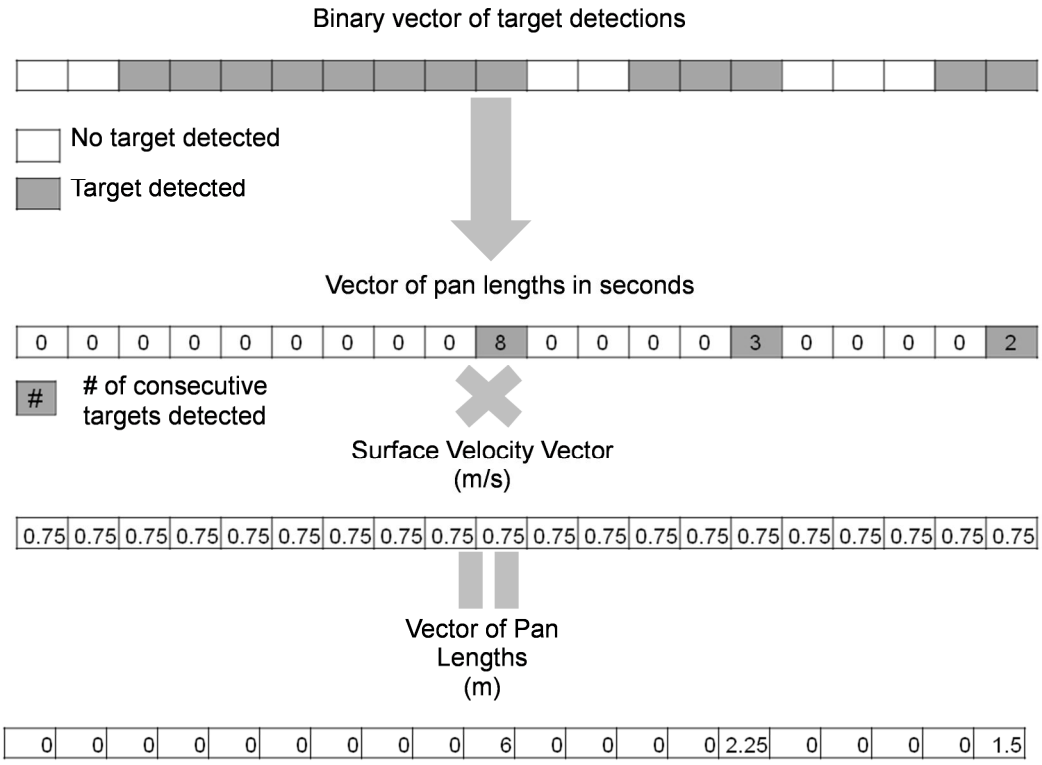

Figure 3-11. Illustration of process used for calculate pan lengths from a binary vector of target detections.

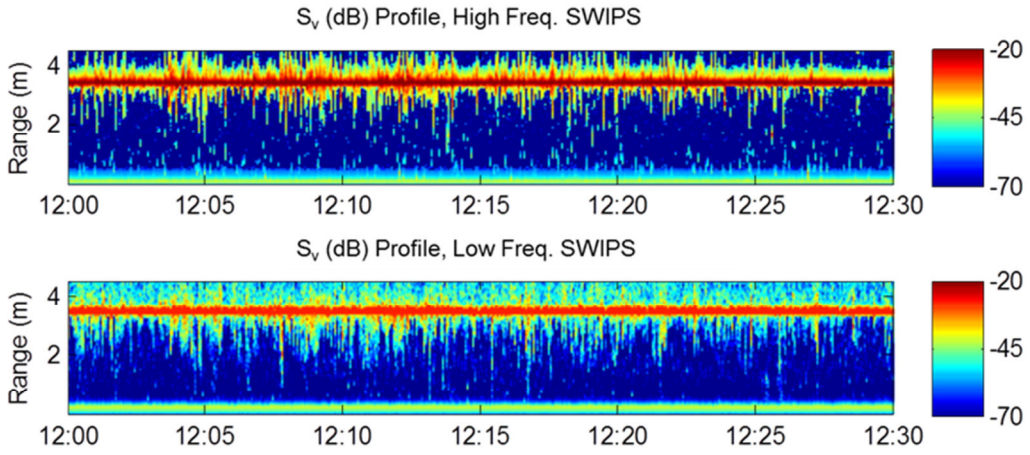

Figure 3-12. High and low frequency sonar S_v plot illustrating the vertical variation in the acoustic return of a pan.

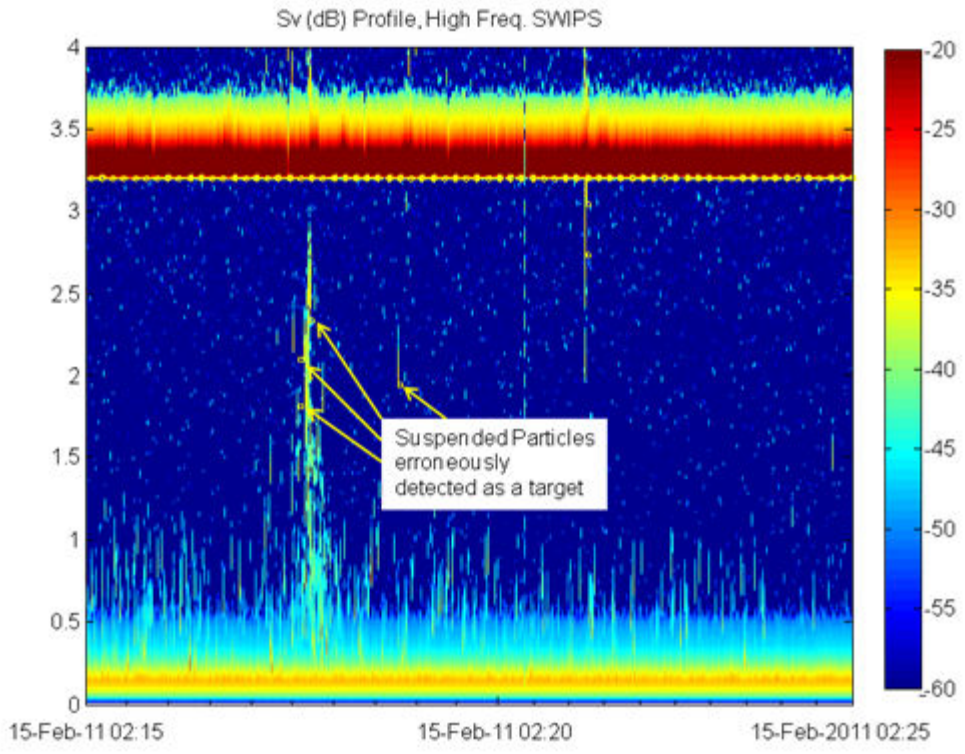

Figure 3-13. Example figure showing suspended particles being falsely detected as targets.

4. Freeze-up and Open Lead Development

The freeze-up cryographs shown in Figure 4-1 through Figure 4-4 were the primary data source for the analysis of freeze-up. Using these figures, the characteristics of the 2010 freeze-up season were identified including ice cover development, bridging locations and the freeze-up front celerity. The GPS and ground based photographic observations of the GBWTP open lead dimensions were used to determine the widths of the open lead between station 50.3 km and station 56.8 km. In person observations and time lapse camera photographs were used to identify other opening in the winter ice cover.

4.1. Freeze-up Progression[5]

The first frazil pans were observed in morning of 12-Nov-10 at station 57.1 km (Figure 4-4(a)). These pans were thin (~10 cm thick based upon the sonar measurements) and visually appeared to be slushy as the air temperatures were relatively warm (near 0˚C). These frazil pans were recorded by the time lapse cameras on 12-Nov-10 and 13-Nov-10 from station 28.2 km to 63.9 km (Figure 4-1 to Figure 4-4). No other pan events were observed for the next two days. This was due to a period of warm (near 0˚C) air temperature lasting until 12:00 on 15-Nov-10 (Figure 4-1(d)).

Air temperatures dropped steadily from 0˚C at 12:00 on 15-Nov-10 to -20˚C at 12:00 on 19-Nov-10 (Figure 4-1(d)). Ice pans appeared at the time lapse cameras sites downstream of station 49.8 km at approximately 15:00 on 16-Nov-10. By

[5] Portions of this section have been published (Maxwell *et al.*, 2011).

8:00 on 17-Nov-10, ice pans were recorded at every time lapse camera in the study reach. Downstream of station 49.8 km, ice pan concentrations rose from ~30% in the morning of 17-Nov-10 to approximately 80% on 19-Nov-10. The freeze-up first appeared at the downstream cameras (station 63.9 km) at 09:00 on 19-Nov-10, having bridged somewhere further downstream (Figure 4-4(b, c)). The ice cover subsequently propagated upstream, and the entire river within the Edmonton city limits was ice covered by 23-Nov-10.

Table 4-1 displays locations and times that the freeze-up front was observed and the calculated celerity of the freeze-up front, whenever accurate times could be obtained. Figure 4-5 displays a plot of the observed freeze-up front locations and the corresponding air temperatures. The celerity of the 2010 freeze-up front (average of 10.7 km/day) was faster than the 1981 freeze-up front celerity of 7 km/day measured by Gerard and Andres (1982), possibly due to colder air temperatures in the 2010 season. Gerard and Andres (1982) recorded air temperatures between 0°C and -10°C during the 1981 freeze-up of the Edmonton reach, whereas the 2010 freeze-up season air temperatures between -10°C and -25°C (Figure 4-1(d)).

Table 4-1. Locations, times and celerity of freeze-up front observations

Station (km)	Time Freeze-up Front Observed	Celerity of Freeze-up Front (km/day)	Notes
63.9	11/19/2010 9:00		
57.1	11/20/2010 1:00		Front passed at night
56.8	11/19/2010 23:30	11.8	
56.3	11/19/2010 4:00		Front passed at night
49.8	11/20/2010 14:00	11.6	
41.3	11/21/2010 1:00		Front passed at night
39.5	11/21/2010 14:34	10.0	
28.2	11/22/2010 11:00	14.0	Bridged 2 hours before front arrived
19.3	11/23/2010 13:00	7.9	
9.2	11/20/2010 12:00		Bridged between Station 9.2 and 19.3km

Freeze-up characteristics were different in the reaches upstream and downstream of the Highway 216 bridge. The islands and mid-channel bars in the upstream reach exhibited substantial border ice and thermal ice growth as illustrated in Figure 4-6(a,b,c,d). Somewhere between station 9.2 and 19.3 km, a bridging event (Figure 4-1(a)) occurred three days prior to the arrival of the downstream ice front. The exact bridging location could not be determined because it did not occur within the view of a camera station; however the camera at station 9.2 km photographed the resulting ice front propagating upstream (Figure 4-1(b,c)). The bridging site was likely located at one of the mid-channel features of the upstream reach (between station 9.2 and 19.3 km). These types of features could provide potential bridging locations for a developing ice cover (Choles, 1997).

In the downstream reach, ice features during freeze-up were dominated by frazil pans, rafts and the freeze-up front. Border ice was minimal except near islands and shallow flow regions. Figure 4-7(a,b,c,d) and Figure 4-8(a,b,c,d) shows the progression of freeze-up from frazil ice pans to an intact ice cover at two locations in the reach downstream of the Highway 216 bridge. In Figure 4-7(d), the stationary ice on the right bank is not border ice, but instead ice pans that have been arrested by friction with the bank.

The passing of the freeze-up front introduced additional flow resistance by the ice cover, which caused an increase in river stage. This increase was observed at every pressure sensor in the study reach, as shown in Figure 4-9. The increase in stage from the previous day's peak level to post-freeze-up day's peak levels diminished as the ice front traveled upstream. Between stations 57.3 km and station 56.3 km, the river staged up uniformly by approximately 80 cm. Further upstream at the GBWTP outfall, the river level increased by 50 cm as the freeze-up front passed. Finally, at the WSC gauge located at station 42.8 km, the river staged up by about 40cm. The reason for these differential increases is likely to be due to differences in river widths between these locations (120 m, 140 m and 150 m, respectively, as measured in Google Earth [Google]).

These observations of freeze-up only covered a single season of data, and therefore cannot be treated as a comprehensive characterization of freeze-up of the North Saskatchewan River. Different freeze-up scenarios are possible under varied meteorological conditions or water levels. Despite the lack of extra

seasons of data, it is likely that the tendency of bridging in the upstream reach is a repeatable occurrence as this can be attributed to the geomorphological differences between the reaches upstream and downstream of the Highway 216 bridge.

4.2. Open Leads

As part of this study, the open leads occurring on the North Saskatchewan River within Edmonton during the 2010/11 winter were documented. The GBWTP open lead, Edmonton's largest; is known for episodic mid-winter frazil events, which are a major focus of this thesis. To understand to the ice events occurring within this open lead, the formation and physical dimensions of this lead were documented in detail. Additional openings in the ice cover were also recorded, but not to the same extent as the GBWTP open lead.

4.2.1. Gold Bar Wastewater Treatment Plant Open Lead

Following the freeze-up front passing the Gold Bar Wastewater Treatment plant (GBWTP) outfall (station 50.3 km) on 20-Nov-10 at 14:00, the GBWTP open formed rapidly. Discharging between 1.5 and 3.5m^3/s of ~13˚C effluent, the thermal plume produced by the outfall melted the ice cover downstream of the outfall. The ice cover above the in-stream sonar instruments, 6.5 km downstream of the GBWTP outfall, was melted out at 22:00 on 26-Nov-10. The cameras at the downstream end of the study reach recorded the appearance of the open lead at 8:00 on the 6-Dec-10.

For the remainder of the winter, the downstream tail of this open lead moved upstream and downstream of the cameras located at station 63.9 km. The distance the open lead tail travelled upstream and downstream is unknown because no additional cameras were installed near station 63.9 km; however, Table 4-2 gives the times during which the open lead tail was known to be upstream or downstream of station 63.9 km. In total, the open lead was downstream of station 63.9 km for 85 days of the ice covered season and upstream for 32 days of the season.

Table 4-2. Location of Wastewater Treatment Plant Open Lead Tail Relative to Station 63.9 km.

Time Span		Open Lead Tail Location Relative to Station 63.9 km
Beginning	Ending	
19-Nov-10 00:00	14-Dec-10 08:00	Downstream
14-Dec-10 08:00	15-Dec-10 08:00	Upstream
15-Dec-10 08:00	4-Jan-11 12:00	Downstream
4-Jan-11 12:00	12-Jan-11 08:00	Upstream
12-Jan-11 08:00	24-Jan-11 08:00	Downstream
24-Jan-11 08:00	24-Jan-11 13:00	Upstream
24-Jan-11 13:00	24-Jan-11 15:00	Downstream
24-Jan-11 15:00	31-Jan-11 08:00	Upstream
31-Jan-11 08:00	4-Feb-11 08:00	Downstream
4-Feb-11 08:00	20-Feb-11 07:00	Upstream
20-Feb-11 07:00	15-Mar-11 16:00	Downstream

In addition to monitoring the downstream tail of the open lead, the width of the open lead was investigated. The section of interest spanned from the GBWTP outfall (station 50.3 km) downstream to the sonar deployment site at station 56.8 km.

The width of the GBWTP open lead was determined by scaling the lead width against either bridge pier spacing or the channel width. Satellite photos in Google Earth were used to determine the actual distance between bridge piers and river widths. These actual widths were required to provide a reference pixel size for the scaling. While the majority of the ground based survey images were unsuitable for scaling, three sets of bridge piers were suitable: the Ainsworth Dyer bridge (station 51.4 km), the Rundle Park bridge (station 53.9 km) and the Highway 16 railway bridge (station 55.1 km). An example photograph for the Ainsworth Dyer bridge is shown in Figure 4-10. In this photograph, yellow scaling lines indicate points where pixels were measured for scaling.

The aerial survey photographs were then similarly analyzed at the locations of the bridge piers seen in the ground survey and at stations in between. These measured widths are summarized in Table 4-3 along with those widths measured in the ground based survey. By comparing the measured widths of the two surveys, it was found that the scaled distances differed by a maximum of 6 m. This level of accuracy indicated that the open leads recorded during the two seasons were probably similar in shape and size.

Table 4-3. Open Lead Widths calculated using scaled photos or GPS survey.

	Jan 24, 2008 Flight Observations	Dec 9, 2010 Ground Observations	Feb 24, 2011 Edge of Ice survey	Selected Dimension
Station (km)	Width (m)	Width (m)	Width (m)	Width (m)
50.3	-	-	-	18
51.4	16	20	-	18
51.5	72	-	-	72
52.0	32	-	-	32
52.5	65	-	-	65
53.9	85	79	-	82
55.1	124	130	-	127
55.3	68	-	-	68
55.7	137	-	-	137
56.1	-	-	-	60
56.3	-	-	60	60
56.8	-	-	60	60

The 2008 aerial survey and the 2010 ground survey was combined to create an estimate of GBWTP open leads from station 50.3 km to 56.3 km. The GPS survey of the open lead at station 56.8 km was extrapolated upstream to station 56.3 km as no aerial photographs suitable for scaling were available in this reach.

Similarly, the width measured at the Ainsworth Dyer bridge (station 51.4 km) was extrapolated upstream to station 50.3 km, because no photographs suitable for scaling were available. In both these cases, the photographs did indicate there was little change in the open lead width over the distances these measurements were extrapolated across. The final shape of the GBWTP open lead is shown in Figure 4-11.

Combining the open lead widths with the available bathymetric data, several important features were noted. These features will be used to analyze the formation of suspended and surface ice in the open lead in Chapters 5 and 6. Upstream of the Highway 16 bridges (near station 54.8 km), the open lead was divided into two regions, a deep and shallow region. The deep region (depth ~1.2 m) was ~40 m wide and located near the centre of the channel and the shallow region (depth ~0.6 m) was ~70 m wide and located against the right bank (Figure 4-12). Downstream of the Highway 16 bridges, the channel undergoes a sudden constriction due to a point bar along the right bank; this constriction is visible in the open lead map and in Figure 4-13. The bathymetry of this constriction is unknown as no cross sections are available in this location. Downstream of the constriction, the deepest portion of the flow shifts again to the right bank. Immediately upstream of the sonar instrumentation platform deployment site, an intake/outfall structure creates a deep scour pool (Figure 3-2). The instrument platform is located at the downstream end of this scour pool.

Water temperature sensors between station 49.5 km and station 57.1 km collected water temperature measurement in the GBWTP open lead during throughout the 2010/11 winter season as presented in Figure 4-14. Upstream of the GBWTP outfall, no spikes in water temperature were observed following freeze-up (Figure 4-14(a)), indicating there were no notable thermal effluents contributing to the GBWTP open lead upstream of station 50.3 km. At station 50.8 km (Figure 4-14(b), the thermal impact of the GBWTP outfall caused the water temperatures to remain at ~5˚C throughout the winter. Further downstream, at station 56.3 km, the temperature sensor adjacent to the left bank (Figure 4-14(c)) appears to have been frozen in ice throughout the entire winter as the sensor recorded a constant temperature of 0˚C. The sensor adjacent to the right bank at station 56.3 km, (Figure 4-14(d)) follows very similar trends to the those recorded at station 56.8 km (Figure 4-14(e)). This would indicate that the Clover Bar Energy Centre outfall plume does not affect the sonar instrument sensors. Finally, the mixing of the effluent from Clover Bar Energy Centre outfall (Figure 4-14(f)) with the GBWTP open lead can be seen in the water temperature recorded at station 57.1 km (Figure 4-14(g)).

4.2.2. Additional Openings in the Ice Cover

Outfalls that had a visible melting effect upon the ice cover during the 2010/11 winter were identified during field monitoring in this study. In other years and under different meteorological conditions, additional openings may be present in the ice cover.

Three notable features were observed during the 2010/11 winter. A mid-river outfall at the University of Alberta created a smaller open lead, beginning at station 39.5 km and ending at around station 40.3 km. It was also documented that at stations 28.2 km and 38.2 km, surface flooding was intermittently present throughout the winter. At the station 28.2 km, this flooding was probably due to mid-winter snowmelt runoff from an outfall on the right bank. In the case of station 39.5 km, the surface flooding was either due to snowmelt runoff or water released by construction work which was being conducted on the Quesnel bridge approximately 300 m upstream.

(a) Station 9.2 km

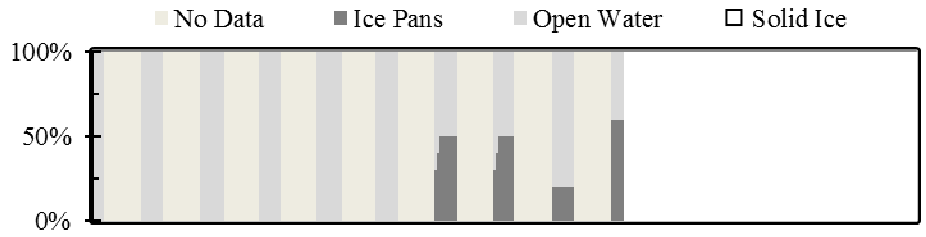

(b) Station 19.3 km

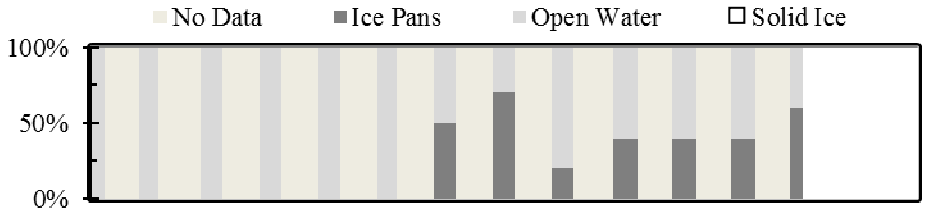

(c) Station 28.2 km

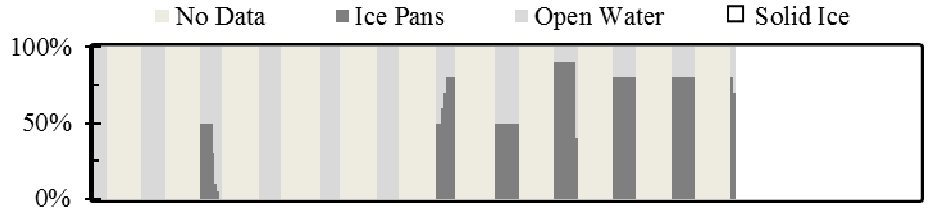

(d) Air Temperature (˚C)

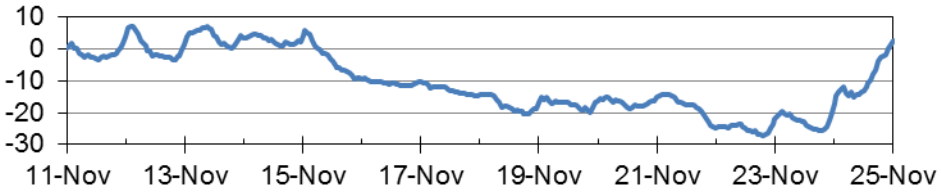

Figure 4-1. Cryographs produced from remote automated time lapse camera images at (a) Station 9.2 km, (b) Station 19.3 km, (c) Station 28.2 km and (d) Air temperature. Dates shown are 12:00am (noon).

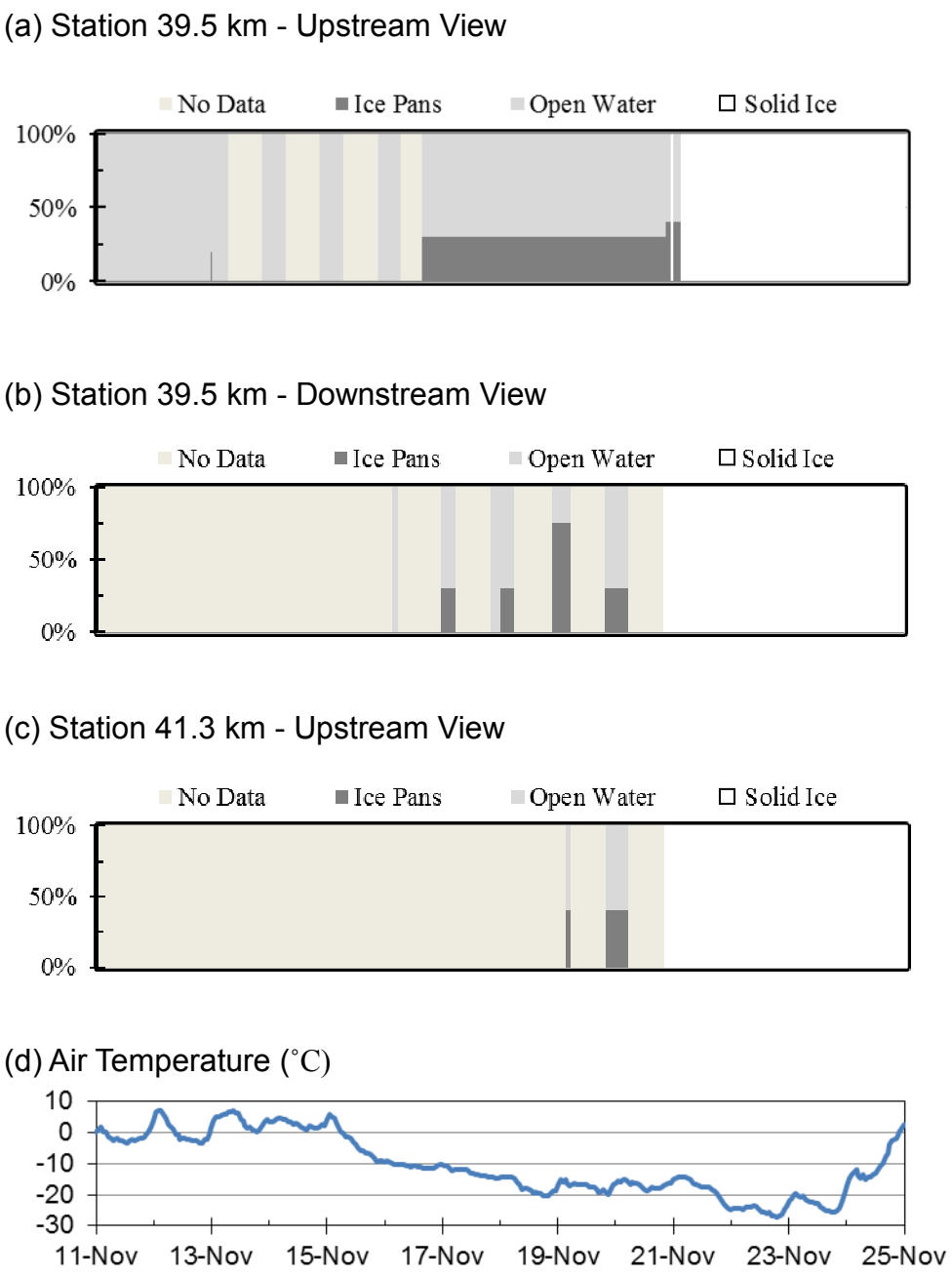

Figure 4-2. Cryographs produced from remote automated time lapse camera images at (a) Station 39.5 km-Upstream View, (b) Station 39.5 km-Downstream View, (c) Station 41.3 km-Upstream View and (d) Air temperature. Dates shown are 12:00am (noon).

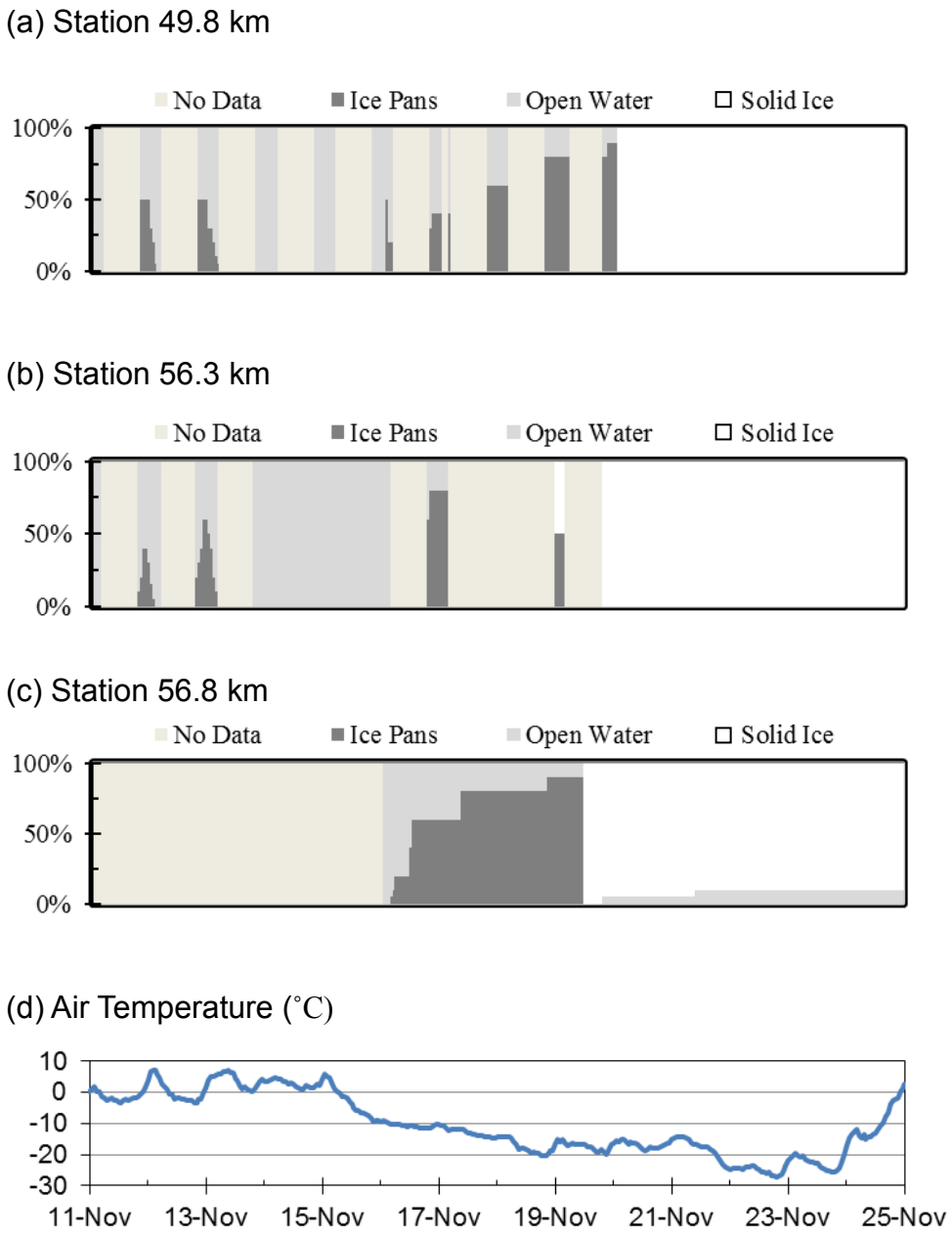

Figure 4-3. Cryographs produced from remote automated time lapse camera images at (a) Station 49.8 km, (b) Station 56.3 km, (c) Station 56.8 km and (d) Air temperature. Dates shown are 12:00am (noon).

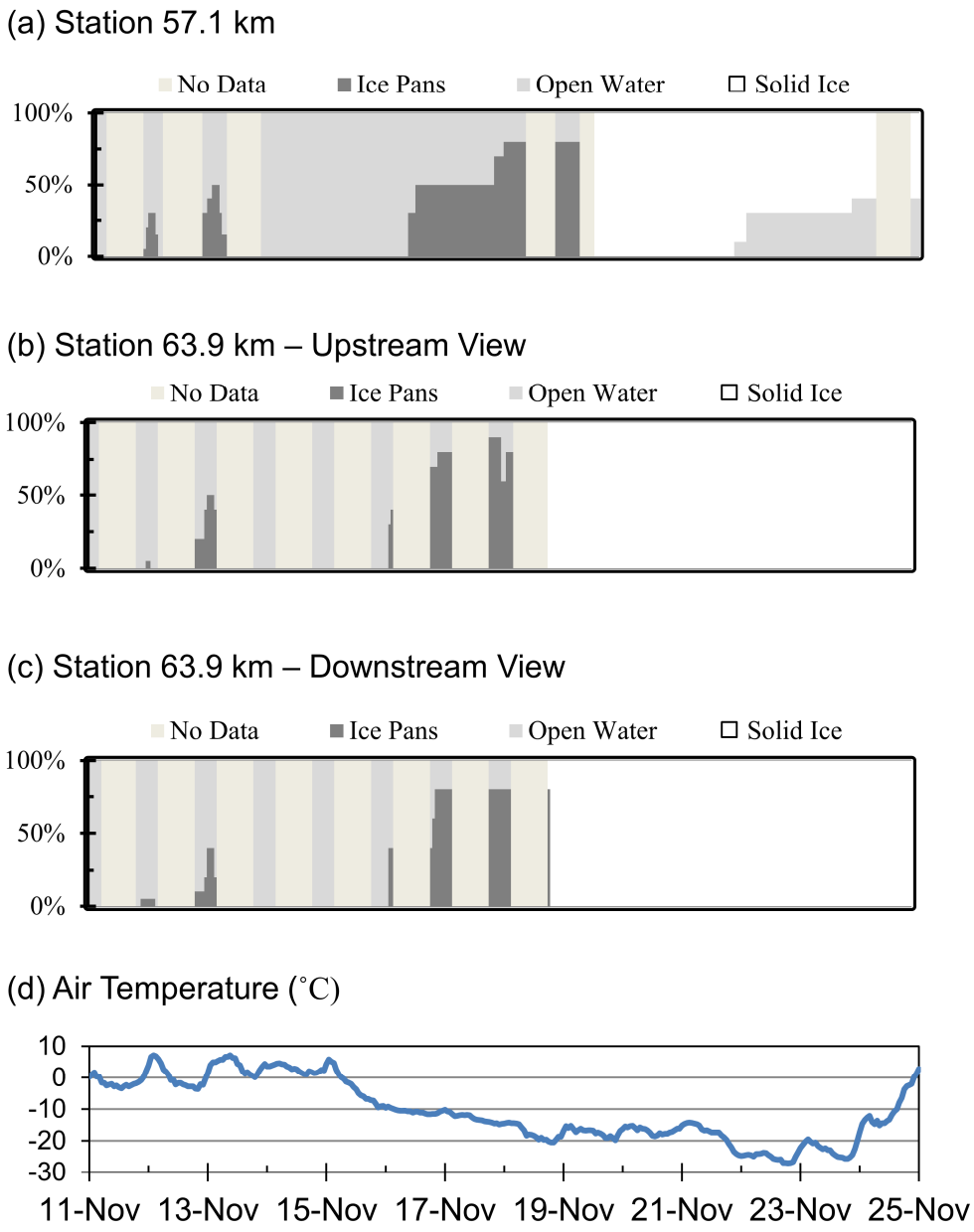

Figure 4-4. Cryographs produced from remote automated time lapse camera images at (a) Station 57.1 km, (b) Station 63.8 km, upstream view,(c) Station 28.2 km, downstream view and (d) Air temperature. Dates shown are 12:00am (noon).

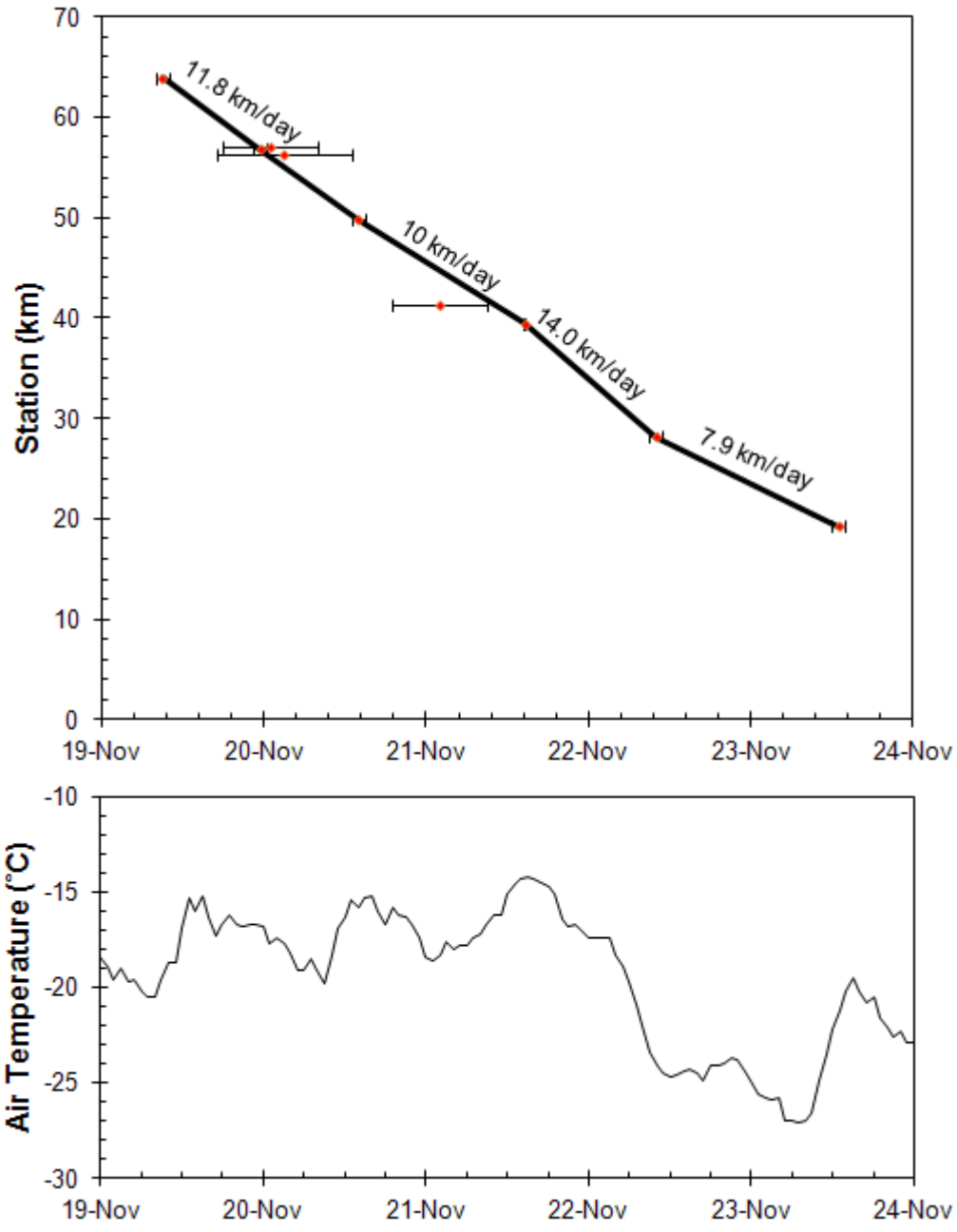

Figure 4-5. Observed 2010 freeze-up front locations with horizontal error bars representing uncertainty of observations and corresponding air temperatures.

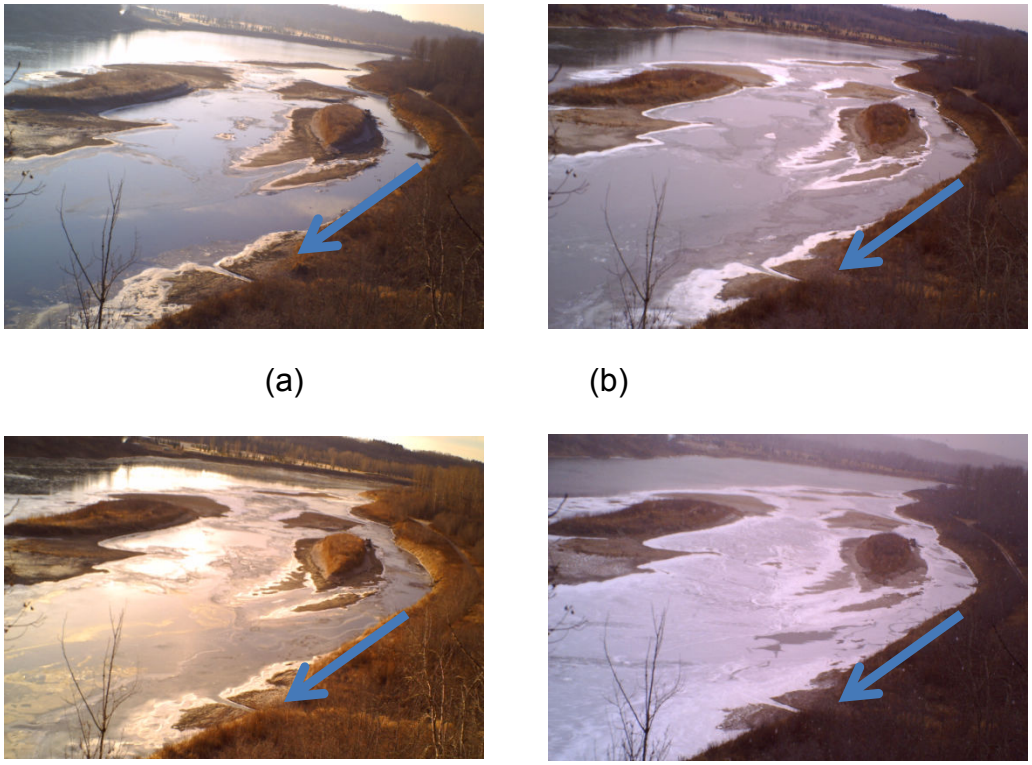

Figure 4-6. Images illustrating thermal freeze-up of upstream reach of river from a game camera located at Sta. 19.3. (a: 10:00 10-Nov-10; b: 09:00 on 12-Nov-10; c: 09:00 on 13-Nov-10; d: 15:00 on 16-Nov-10)

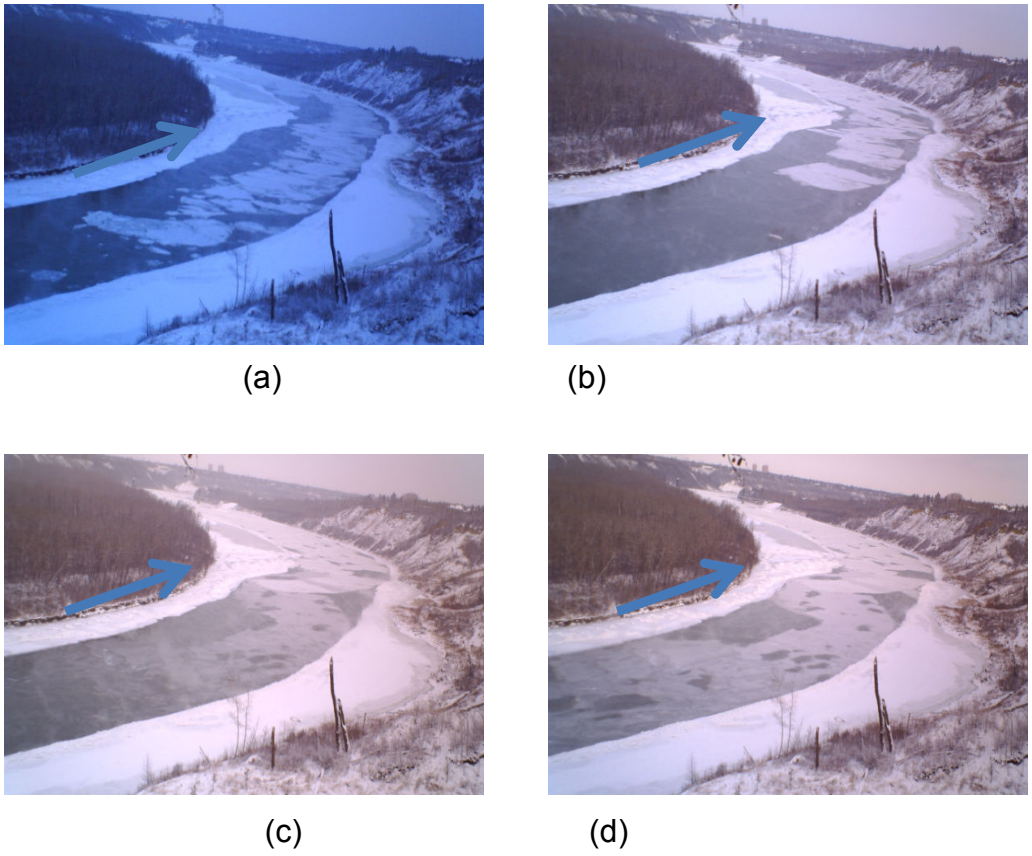

Figure 4-7. Images recording freeze-up front passing camera located at station 28.2 km. (a: 08:00 22-Nov-10; b: 09:00 on 22-Nov-10; c: 10:00 on 22-Nov-10; d: 11:00 on 22-Nov-10)

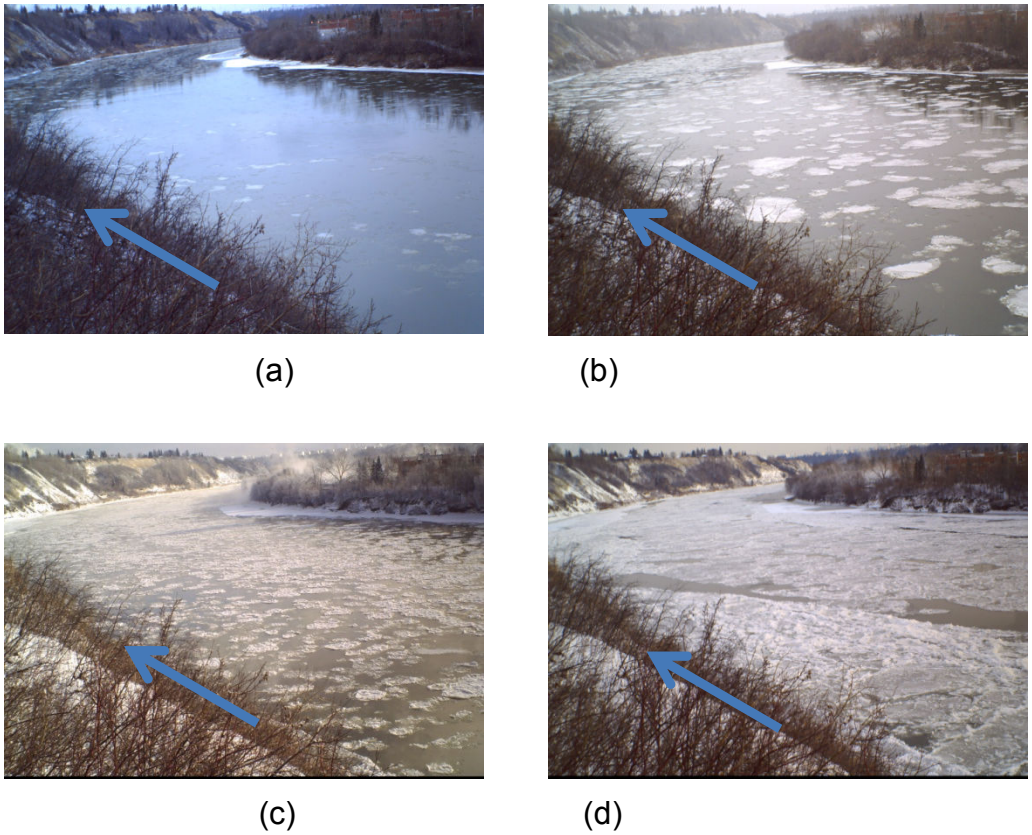

Figure 4-8. Images showing freeze-up front passing Gold Bar Wastewater Treatment Plant at station 49.8 km. (a: 16:00 16-Nov-10; b: 11:00 on 17-Nov-10; c: 13:00 on 19-Nov-10; d: 15:00 on 20-Nov-10)

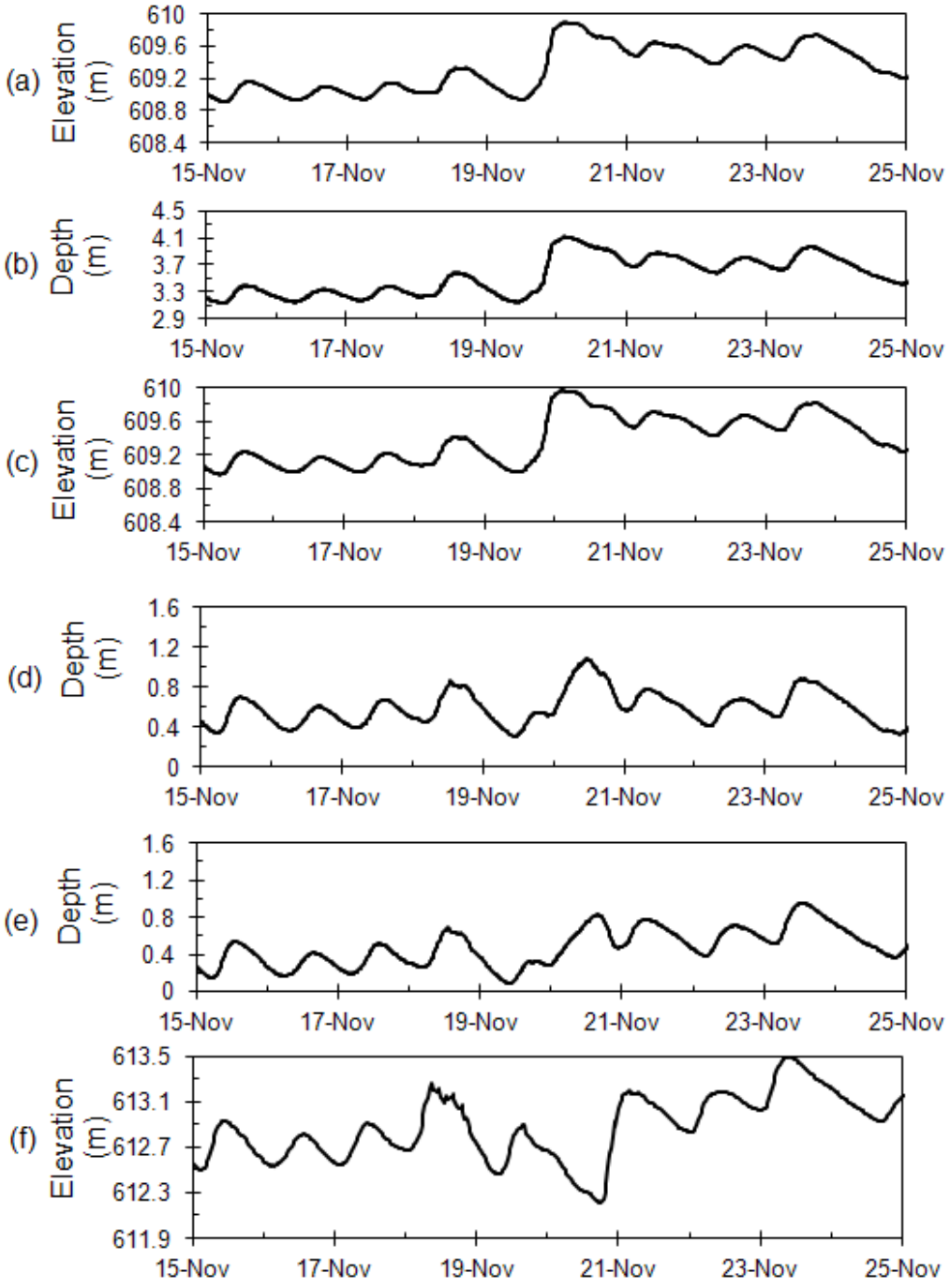

Figure 4-9. Water level hydrographs recorded during the 2010 freeze-up stations (a) 57.1 km, (b) 56.8 km, (c) 56.3 km, (d) 50.6 km, (e) 49.5 km and (f) 42.8 km.

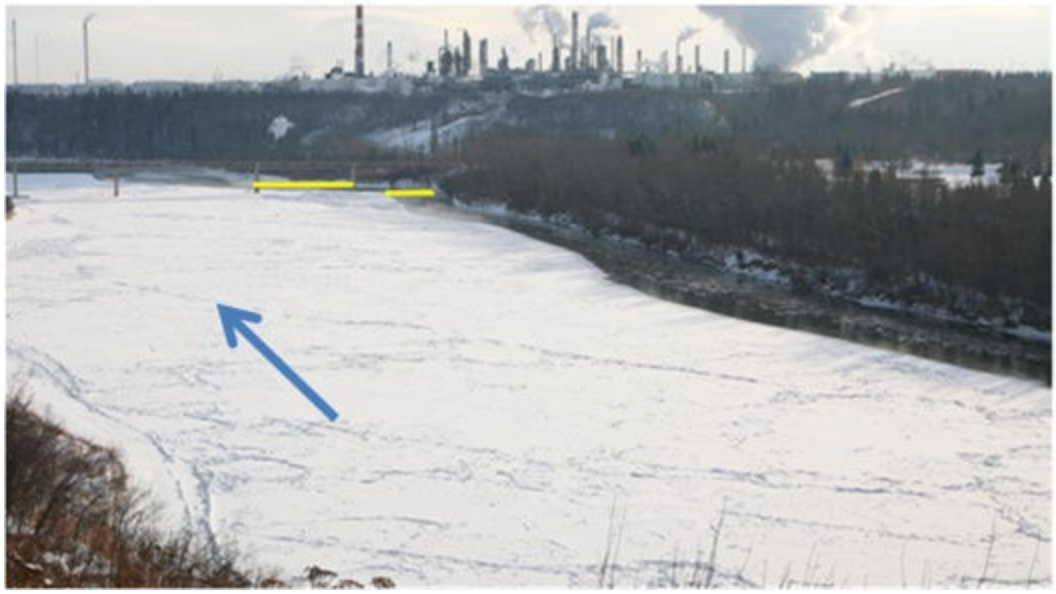

Figure 4-10. Ground based photograph of open lead at the Ainsworth Dyer bridge. (Taken 9-Dec-10)

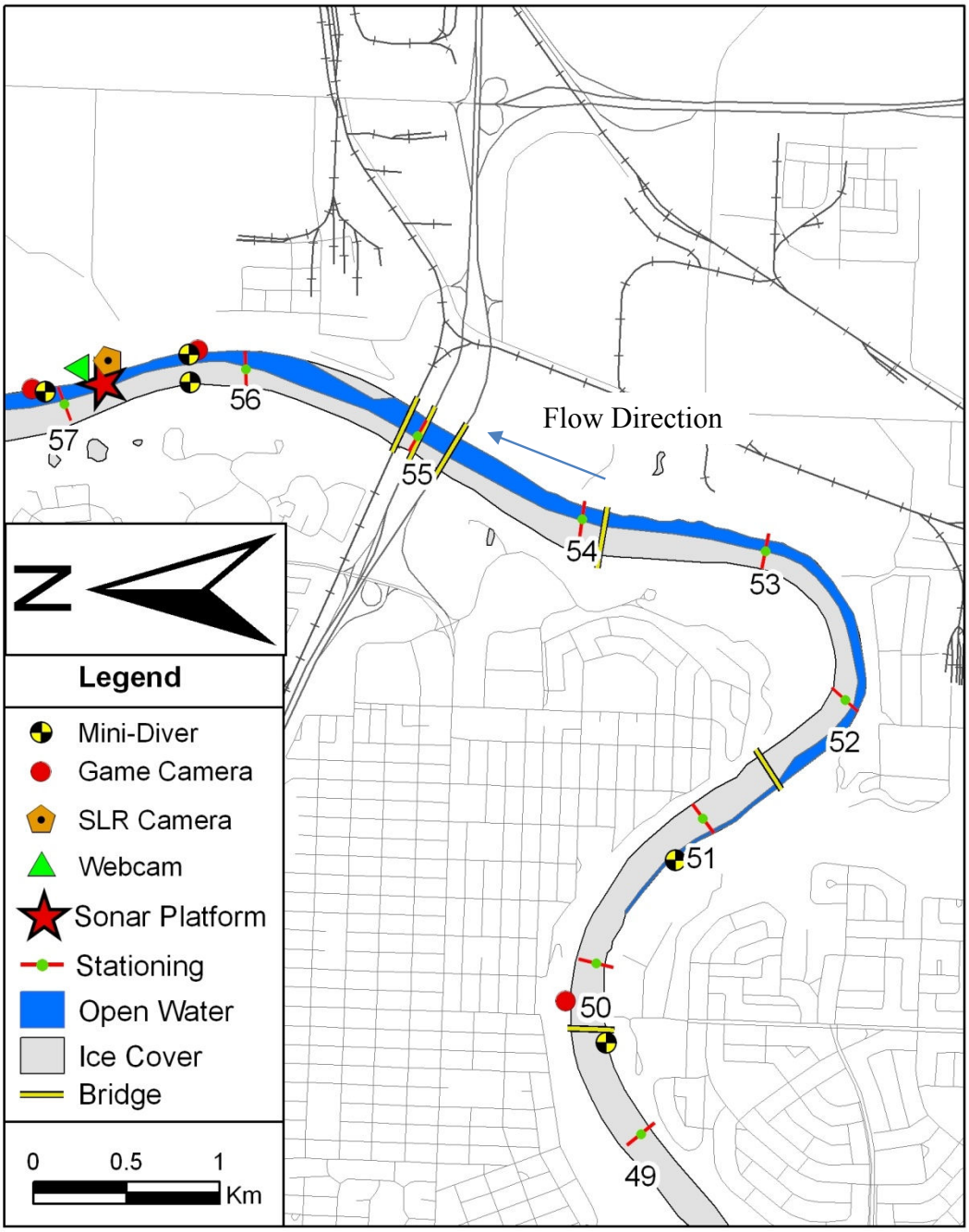

Figure 4-11. Illustration of GBWTP open lead shape from station 50.3 to 57.0 km

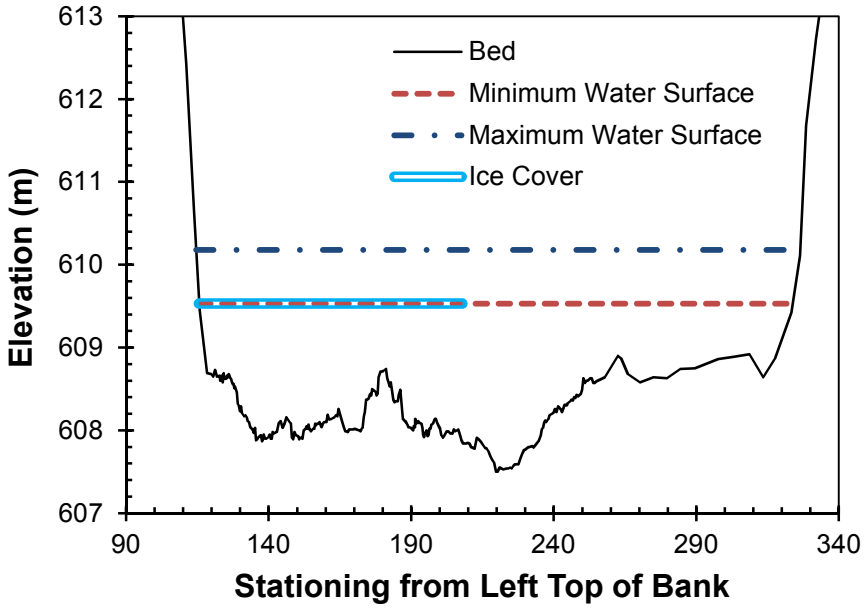

Figure 4-12. Cross section at station 54.8 km extracted from Alberta Environment's flood risk mapping study HEC-RAS model (Northwest Hydraulics Consultants, 2007).

Figure 4-13. Aerial photograph taken 24-Jan-08 illustrating constriction downstream of Highway 16 Railway bridge.

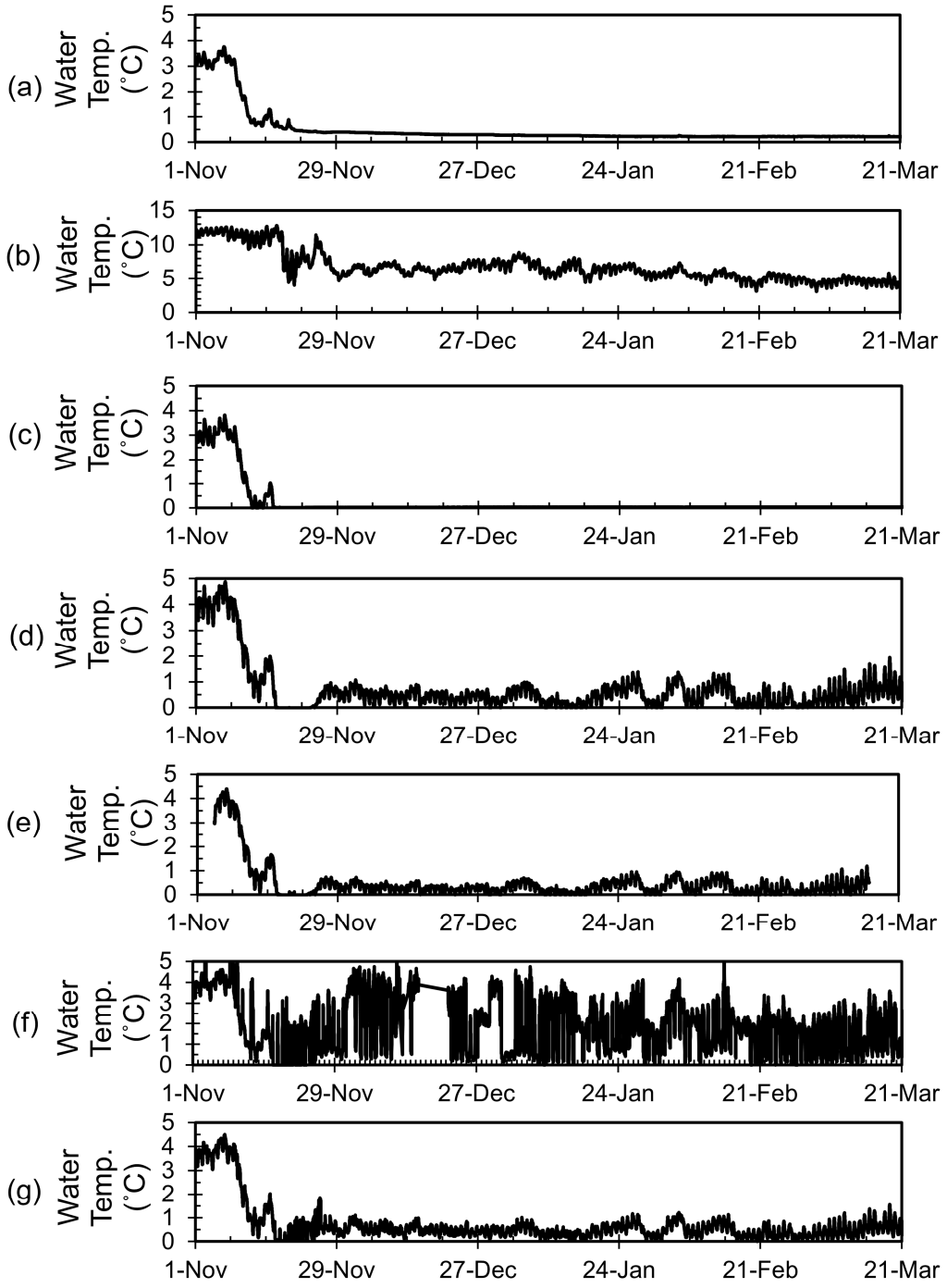

Figure 4-14. Water temperatures recorded at stations (a) 49.5km (20 m from right bank), (b) 50.6 km (10 m from right bank), (c) 56.3 km (15 m from right bank), (d) 56.3 km (15 m from left bank), (e) 56.8 km (45 m from right bank, (f) 56.8 km (15 m from right bank) and (g) 57.1 km (15 m from right bank).

5. Measuring and Characterizing Frazil Pans

Using the acoustic data recorded by the two sonar units, frazil pan thicknesses, lengths and concentrations were calculated quantitatively (Section 3.2.8.2). An algorithm was developed and used for detecting frazil pans in the sonar dataset. This algorithm detected the underside of ice pans and calculated pan concentration, thickness and length.

In this chapter, the ice pan dimensions from the high and low frequency sonars and the approximate concentrations estimated from images collected by the automated time lapse SLR camera were compared against each other. Using the validated pan dimension dataset, open lead pan events were identified and classified into one of two categories. The formation mechanisms for each of these pan types were then explored.

5.1. Validation of Sonar Measured Pan Concentrations, Thicknesses and Lengths

The calculated pan dimensions were validated using two methods: comparison between the high and low frequency sonar datasets and comparison of the sonar determined ice concentrations with concentrations determined from a visual analysis of the SLR camera images (Section 3.2.6.2).

5.1.1. Comparison of high and low frequency sonar surface ice dimensions

The results from the high and low frequency sonars were evaluated over time periods when the gain and pulse length settings of the sonars were held constant (Table 3-11). These time periods were also separated for freeze-up pans and open lead pans, prior to 19-Nov-10 and after 26-Nov-10. The calculated means and standard deviations shown in these tables were calculated based only on non-zero measurements (i.e. they excluded times when no ice was present above the sonars) to prevent biasing of the mean towards zero and erroneously high standard deviations. The means and standard deviations of the high and low frequency sonar computed concentrations, thicknesses and lengths are presented in Table 5-1 through Table 5-3, respectively. In Table 5-2, the calculations of mean and standard deviations of pan thicknesses neglected values above 1.5 m because they were known to be erroneous from observations of the surface ice analysis figures (pan thicknesses ranged up to ~70 cm).

Table 5-1. Comparison of mean and standard deviation of ice pan concentrations calculated from the high and low frequency sonar datasets.

		High Freq. Sonar		Low Freq. Sonar	
From	To	Mean (%)	St. Dev. (%)	Mean (%)	St. Dev. (%)
4-Nov-10	19-Nov-10	45.8	33.9	47.5	30.8
26-Nov-10	9-Dec-10	7.5	10.3	3.9	5.8
9-Dec-10	21-Dec-10	8.6	13.4	5.0	7.4
21-Dec-10	17-Feb-11	13.4	13.4	7.4	7.4
17-Feb-11	15-Mar-11	15.7	15.8	14.5	15.3

Table 5-2. Comparison of mean and standard deviations of ice pan thicknesses calculated from the high and low frequency sonar datasets.

		High Freq. Sonar		Low Freq. Sonar	
From	To	Mean (m)	St. Dev. (m)	Mean (m)	St. Dev. (m)
4-Nov-10	19-Nov-10	0.35	0.22	0.28	0.17
26-Nov-10	9-Dec-10	0.15	0.15	0.12	0.09
9-Dec-10	21-Dec-10	0.15	0.11	0.13	0.08
21-Dec-10	17-Feb-11	0.23	0.24	0.13	0.08
17-Feb-11	15-Mar-11	0.15	0.09	0.13	0.06

Table 5-3. Comparison of the mean and standard deviations of ice pan lengths calculated from the high and low frequency sonar datasets.

		High Freq. Sonar		Low Freq. Sonar	
From	To	Mean (m)	St. Dev. (m)	Mean (m)	St. Dev. (m)
4-Nov-10	19-Nov-10	9.5	14.9	8.6	13.0
26-Nov-10	9-Dec-10	1.4	1.2	1.2	0.8
9-Dec-10	21-Dec-10	1.3	1.0	1.1	0.7
21-Dec-10	17-Feb-11	1.7	3.2	1.4	1.1
17-Feb-11	15-Mar-11	2.1	1.9	1.6	1.3

In the first time period (4-Nov-10 to 19-Nov-10), the mean and standard deviations of the high and low frequency sonars concentrations were within 2% and 3%, respectively. This agreement can be attributed to the strong S_v returns of the freeze-up pans, which allowed the pan identification algorithm to avoid the ambiguities associated with the identification of the bottom of the pan that were discussed in Section 3.2.8.2.

In the final four time periods (i.e. in the open lead), the high frequency sonar's ice concentrations were slightly larger than the low frequency sonar's concentrations by a average of 3% (For the interval between 21-Dec-10 and 17-Feb-11, the mean high frequency sonar's concentration was 13.4% versus a low frequency sonar's mean concentration of 7.4%). This increase may be a result of the change in the high frequency sonar's pulse length from 34μs to 68μs and the reduction in the high frequency sonar's gain from 3 to 1 during that interval. The standard deviations of the high frequency sonar's ice concentrations were notably larger than those of the low frequency sonar (~13% compared to ~8%), except during the 17-Feb-11 to 15-Mar-11 interval (when they were 15.8% and 15.4%, respectively.

The high frequency sonar's concentrations were consistently higher than the low frequency sonar but were within a margin of ±10%, ~90% of the time. During two suspended frazil events (29-Dec-10 and 17-Feb-11), the high frequency sonar's surface concentrations registered values near 100%, while the low frequency sonar's values were approximately 50%. Figure 5-14 illustrates the 29-Dec-10 event. The suspended frazil can be seen in Figure 5-14(a) in the middle of the water column from approximately 08:30 to 09:30. Figure 5-14(d) presents the corresponding photographs of the surface ice conditions during these events, in which the surface ice concentration appears to be ~20% and definitely not 100%. This indicated that the low frequency sonar's results were more accurate in these cases. The false 100 percent surface ice concentration events coincide with

suspended frazil events. A detailed 15 minute plot of the 29-Dec-11 event (Figure 5-15) shows that while the frazil pans were visually discernable on both high and low frequency sonars' S_v profile plots the suspended frazil returns were above the specified *threshold*. Note that the *threshold* (-37dB on the high frequency sonar and -40 dB on the low frequency sonar) could not be raised without making certain pan events, such as the one shown plotted in Figure 5-12, undetectable.

During freeze-up (4-Nov-10 to 19-Nov-10) the high frequency sonar's ice floe thicknesses and lengths values were greater by 7 cm and 0.90 m, respectively. In the open lead (26-Nov-10 to 15-Mar-11) the mean and standard deviations of the pan thicknesses and lengths compared well between the high and low frequency sonars (3 cm and 50 cm, respectively), except for the 21-Dec-10 to 17-Feb-11 interval (10 cm and 30 cm greater, respectively). Mean pan lengths did not appear to vary during this interval but the standard deviation of the high frequency sonar pan lengths increased to 3.2 m (from an average of ~1.5 m).

Histograms displaying the calculated ice thicknesses during freeze-up and in the open lead are displayed in Figure 5-13(a, b and c, d, respectively). During freeze-up, the high and low frequency sonars histograms are very similar in terms of magnitude and distribution although the high frequency sonar plot Figure 5-13(a) exhibits a slightly higher peak than the low frequency sonar. By comparison, the ice thicknesses of pans occurring in the open lead varies significantly between the

high (Figure 5-13(c)) and low (Figure 5-13(d)) frequency sonars with significantly thicker and more numerous detections by the high frequency sonar.

Overall, the high frequency sonar's concentrations were larger than the low frequency sonar's concentrations by a bias error of approximately 2 to 5%. Similarly, the high frequency sonar's pan thicknesses and lengths were between 10% and 20% larger than the low frequency sonar's measurement. These bias errors were a result of the high frequency sonar being saturated easier when suspended particles or slush ice is present. The primary scenario where the high frequency sonar's returns erroneously higher results compared to the low frequency sonar was during suspended frazil events. These bias errors could be corrected by raising the *threshold*; however, this would result in some pan events with S_v intensities of approximately -35 dB being left undetected. The low frequency sonar appeared to offer the more accurate surface ice concentration results, and will thus serve as the primary reference for surface ice concentrations for remainder of this chapter.

5.1.2. Comparison of sonar ice concentrations against photographic ice concentrations

The surface ice concentrations determined from an analysis of the SLR camera images (documented in Section 3.2.6.2) were compared against those concentrations measured by the low frequency sonar. Figure 5-16 presents an example of a photograph from freeze-up and the corresponding high and low

frequency sonar ice concentrations. The white frazil ice pans seen in Figure 5-16(c) are well contrasted against the water, resulting in easy visual identification. Figure 5-2a presents the photographic and sonar based concentrations for the entire freeze-up period. It is evident from this figure that the two were in reasonably close agreement. Over the freeze-up period the photographic ice concentrations were an average of 5.5% greater than the low frequency sonar based concentrations with a standard deviation of 11.9%.

In the open lead, the surface ice concentrations calculated from the low frequency sonar's concentration series were on average 4.7% higher than the photographic ice concentrations, with a standard deviation of 11.9%. However, during pan events having a concentration above approximately 30%, such as the one that occurred on 15-Jan-11 (Figure 5-17) the sonar based concentrations were 10 to 50% higher than those estimated from photographs. In Figure 5-17, the estimated concentration from the sonar data peaked at ~40% (at 9:49) whereas the concentration estimated from the photograph was 15%.

These differences in concentration arise from the difficulty in visually detecting the often translucent pans occurring in the open lead (Figure 5-17(d)). In addition, in the evening and during the night, blurring of the images further reduced the accuracy with which ice concentrations could be estimated from the images. Concentrations were estimated during these time but these ice concentrations proved to be little better than a binary (true or false) measure of ice

presence. As a result, the visually determined ice concentrations during freeze-up tended to be more accurate than those in the open lead.

To summarize, the estimates of the surface ice concentrations obtained from the SLR camera images differed from those measured by the low frequency sonar by an average of -5.5% during freeze-up and +4.7% in the open lead. However, for open lead pan events with surface ice concentrations above ~30%, the low frequency sonar measured ice concentrations between 10 and 50% greater than those estimated by the photographic method. This difference was a result of the freeze-up ice pans being visually distinct from the open water while the open lead pans were highly translucent and difficult to identify visually.

5.2. Synopsis of Surface Ice Data

To facilitate detailed analyses, daily surface ice analysis figures were plotted. These figures included time series of high and low frequency sonar profiles (S_v as a function of range and time), surface ice concentration, pan thickness, pan length, water temperature, air temperature and precipitation presence. Also shown in these figures are the surface ice concentrations determined from SLR camera images on the adjacent right bank. Figure 5-1 presents one example of these figures with the remaining 90 figures available on DVD in Appendix C.

A series of plots showing longer time series of the calculated ice pan concentrations, thicknesses and lengths during the 2010/11 winter are presented in Figure 5-2 to Figure 5-6. Surface ice concentrations determined from the SLR camera (which was focused on the water surface above the sonar instruments) are

also plotted in these figures. The analysis of the photographic data was conducted prior to the calculation of the sonar based surface ice concentrations, making the photographic concentrations estimated from the photographs independent of the sonar dataset.

5.2.1. Freeze-up

Frazil pans first appeared in the river on 12-Nov-10 and from 16-Nov-10 to 19-Nov-10 surface ice concentrations increased from zero to 100% as seen in Figure 5-2. Detailed surface ice analysis plots from the time of freeze-up are shown in Figure 5-7 through Figure 5-10. Pan and raft dimensions varied throughout freeze-up, with a trend of increasing concentrations, thicknesses and lengths. In the early stages of freeze-up (beginning 18:00 on 16-Nov-10), surface ice concentrations were below 50 percent, pan thicknesses were 0.15 to 0.30 m and the pan lengths were 5 to 10 m (Figure 5-7 and Figure 5-8). As freeze-up progressed, surface ice concentrations climbed steadily, reaching ice concentrations between 85% and 100% on 19-Nov-10. Pan thicknesses reached 0.5 m and lengths ranged between 5 and 35 m (Figure 5-10). The freeze-up front passed the sonar instruments (station 56.8 km) at 23:00 on 19-Nov-10 and the corresponding strong signals reflected from the solid ice cover are visible in both sonars' profile times series shown in Figure 5-10. Throughout freeze-up, the signals (S_v) from the high and low frequency sonars were near saturation (approximately -20dB).

From 19-Nov-10 to 26-Nov-10, the ice cover above the sonar instruments gradually thinned, as seen in the ice thickness plots in Figure 5-2. The high frequency sonar registered higher thicknesses than the low frequency sonar, due to fact it saturated sooner (i.e. at a lower depth) as it propagated through the ice cover. By 21:30 on 26-Nov-10, the ice cover above the sonars was completely melted. The ice cover can be seen fragmenting in the high frequency sonar S_v plot from 26-Nov-10 (Figure 5-11(a)).

5.2.2. Open Lead

For the remainder of the winter, episodic surface pan events occurred in the open lead and were detected by the sonar instruments (Figure 5-3 through Figure 5-6). A detailed example of an open lead pan event is shown in Figure 5-12. Open lead pan events averaged ~6.5 hours in length and occurred during air temperatures ranging between -30˚C to 2˚C and water temperatures ranging between -0.05˚C to 1˚C.

Open pan events were between ~1 hour and 24 hours in length and tended occur each day over 3 day to 2 week long intervals throughout the winter. Surface ice concentrations during these events typically reached a maximum during the morning hours (06:00 to 12:00); although the maximum ice concentrations during each event were highly variable, ranging between 10% and 70%. During the month of Dec-10, the pan events were fairly sporadic, not following any notable trend (Figure 5-3). However, for the remainder of the winter (Jan-11 to Mar-11),

the pan events strongly correlated with drops in air temperature as can be seen in Figure 5-4 and Figure 5-5.

5.3. Open Lead Pan Identification and Characterization

Most of the pan events observed in the open lead had a distinct start and end time, such as the events shown in Figure 5-12 and Figure 5-14. However, when two events were closely spaced, like those shown in Figure 5-18 identifying the point where one event stopped and the next began was slightly subjective. In these cases, discrete events were divided based upon differences in the S_v profiles and surface pan concentrations. For example, for the case shown in Figure 5-18 two pan events were identified. The dividing time was determined to be 6:00 on 17-Jan-11, just as the ice concentrations begins to rise for the second event. The division of those two events was based upon the stronger returns shown in the low frequency sonar S_v profile and the rise in surface ice concentration, both of which began at 06:00.

By visually inspecting the surface ice analysis figures (Appendix C), it was found that the open lead ice pan events could be categorized into two classes: slushy pans and crusty pans. Figure 5-19 and Figure 5-20 present examples of slushy and crusty ice pans, respectively. These pan types were primarily differentiated based upon the S_v from the high and low frequency sonars; crusty pans had S_v values near -20 dB while slushy pans had S_v values near -35dB. Slushy pans also tended to have a layer of low density slush (S_v less than -40 dB) on their

undersides that could be as thick as 2 m. These slushy and crusty pan types were extremely difficult to differentiate visually from photographic observations, as both appeared quite translucent from the surface (as discussed in the previous subsection).

In total, 104 pan events were detected in the open lead sonar dataset of these, 54 were classified as crusty pan events and 50 as slushy pan events. The start and end times of each event were recorded in a table and cross referenced with the available hydrological and meteorological conditions (Appendix D). Abridged versions of this table display the recorded crusty pan (Table 5-4 and Table 5-5) and slushy pan events (Table 5-6 and Table 5-7).

Histograms displaying the distribution of ice thicknesses and the mean as detected by the high and low frequency sonars during the crusty and slushy pan events outlined in the above tables are shown in Figure 5-21while the corresponding pan lengths are shown in Figure 5-22. Both crusty (Figure 5-21(a, b)) and slushy (Figure 5-21(c, d)) pans exhibit a larger number of detections by the high frequency sonar compared to the low frequency sonar. The mean thicknesses of slushy pans were between 0.04 and 0.06 m thicker than those of crusty pans. The mean lengths of crusty pans were between 0.4 and 1.0 m longer than those of slushy pans. Despite these differences in mean values, ~99% of crusty and slushy pans exhibit a similar range of thicknesses (0 to 0.7 m) and lengths (0 to 10m). Thus, identification of either pan type still requires examination of the S_v profile plots.

Table 5-4. List of Identified Crusty Pan Events from Dec-10 to Jan-11.

Start Time	End Time	Water Temp (˚C)	Air Temp (˚C)	Snowing? (Yes/No)	Concurrent Suspended Frazil? (Yes/No)
6-Dec-10 3:00	6-Dec-10 13:00	0.11	-14.7	No	No
7-Dec-10 7:00	7-Dec-10 14:00	0.07	-16	No	No
9-Dec-10 8:00	9-Dec-10 12:00	0.08	-13.9	No	No
10-Dec-10 7:00	10-Dec-10 11:00	0.05	-17	No	No
11-Dec-10 7:30	11-Dec-10 12:00	0.09	-16	Yes	No
12-Dec-10 10:00	12-Dec-10 13:00	0.03	-14.4	Yes	No
18-Dec-10 9:00	18-Dec-10 12:00	0.09	-11.8	Yes	No
20-Dec-10 8:00	20-Dec-10 10:00	0.11	-13.8	Yes	No
21-Dec-10 4:00	21-Dec-10 14:00	0.04	-19.7	No	No
22-Dec-10 2:00	22-Dec-10 13:00	0.09	-20.9	No	No
24-Dec-10 0:00	24-Dec-10 10:30	0.15	-19.4	No	No
29-Dec-10 6:00	29-Dec-10 14:00	-0.02	-20.9	No	Yes
31-Dec-10 6:00	31-Dec-10 12:00	0.00	-20	No	Yes
9-Jan-11 7:00	9-Jan-11 14:00	0.00	-15.8	Yes	Yes
10-Jan-11 6:00	10-Jan-11 13:00	0.01	-16.4	Yes	Yes
11-Jan-11 3:00	11-Jan-11 14:30	-0.01	-21.2	No	Yes
12-Jan-11 4:00	12-Jan-11 14:00	0.01	-27.3	Yes	Yes
13-Jan-11 5:00	13-Jan-11 14:00	0.01	-23	No	Yes
14-Jan-11 3:00	14-Jan-11 14:00	-0.01	-25.1	No	Yes
15-Jan-11 5:00	15-Jan-11 14:00	-0.02	-25.8	Yes	Yes
16-Jan-11 6:00	16-Jan-11 16:00	-0.02	-21	Yes	Yes
17-Jan-11 6:00	17-Jan-11 12:00	-0.02	-22.7	Yes	Yes
29-Jan-11 6:00	29-Jan-11 14:00	-0.01	-15.6	Yes	No
30-Jan-11 3:00	30-Jan-11 15:00	0.01	-21.3	No	No
31-Jan-11 6:00	31-Jan-11 12:00	-0.02	-28.6	No	Yes

Table 5-5. List of Identified Crusty Pan Events from 1-Feb-11 to 15-Mar-11.

Start Time	End Time	Water Temp (˚C)	Air Temp (˚C)	Snowing? (Yes/No)	Concurrent Suspended Frazil? (Yes/No)
1-Feb-11 3:00	1-Feb-11 13:00	-0.04	-21.3	No	Yes
6-Feb-11 7:00	6-Feb-11 10:00	0.08	-18.2	No	No
7-Feb-11 6:00	7-Feb-11 12:00	0.05	-16.0	No	No
7-Feb-11 7:00	7-Feb-11 10:00	0.05	-16.2	No	No
7-Feb-11 17:30	8-Feb-11 12:00	0.20	-16.0	No	No
8-Feb-11 7:00	6-Feb-11 11:00	0.05	-23.1	No	No
9-Feb-11 5:30	9-Feb-11 10:00	0.07	-19.2	No	No
16-Feb-11 5:30	16-Feb-11 15:00	-0.03	-21.0	No	Yes
17-Feb-11 3:00	17-Feb-11 5:30	-0.04	-21.5	No	No
17-Feb-11 5:30	17-Feb-11 13:00	-0.03	-22.0	No	Yes
18-Feb-11 4:00	18-Feb-11 13:00	-0.01	-21.5	No	Yes
19-Feb-11 4:00	19-Feb-11 13:00	-0.02	-25.4	No	Yes
19-Feb-11 18:00	20-Feb-11 13:00	0.07	-19.5	No	Yes
20-Feb-11 22:00	21-Feb-11 9:00	0.14	-15.9	No	No
23-Feb-11 3:00	23-Feb-11 13:00	0.03	-20.5	No	Yes
23-Feb-11 18:00	24-Feb-11 14:30	0.11	-18.7	No	Yes
25-Feb-11 1:30	25-Feb-11 12:30	0.00	-25.3	No	Yes
28-Feb-11 0:00	28-Feb-11 16:30	-0.03	-20.2	No	Yes
1-Mar-11 1:00	1-Mar-11 11:00	0.07	-28.4	No	Yes
2-Mar-11 0:00	3-Mar-11 14:00	0.11	-24.0	No	Yes
3-Mar-11 3:00	3-Mar-11 13:00	0.02	-21.7	Yes	No
4-Mar-11 3:00	4-Mar-11 12:00	0.02	-18.3	No	No
5-Mar-11 2:00	5-Mar-11 11:30	0.11	-16.1	Yes	No
6-Mar-11 2:00	6-Mar-11 12:00	0.06	-16.7	Yes	No
7-Mar-11 3:00	7-Mar-11 11:00	0.05	-20.3	No	No
8-Mar-11 2:00	8-Mar-11 10:30	0.09	-23.2	No	No
11-Mar-11 5:00	11-Mar-11 12:00	-0.01	-22.5	No	No
12-Mar-11 2:00	12-Mar-11 10:00	0.09	-18.9	No	No
13-Mar-11 7:00	13-Mar-11 8:30	0.11	-17.4	No	No

Table 5-6. List of slushy pans identified from Dec-10 to Jan-11

Start Time	End Time	Water Temp (˚C)	Air Temp (˚C)	Snowing? (Yes/No)
2-Dec-10 17:30	2-Dec-10 18:30	0.65	-5.1	Yes
2-Dec-10 20:00	2-Dec-10 22:00	0.54	-5.6	Yes
3-Dec-10 8:00	3-Dec-10 9:30	0.33	-6.2	Yes
8-Dec-10 17:30	8-Dec-10 18:30	0.49	-10.3	Yes
8-Dec-10 20:30	9-Dec-10 7:00	0.38	-10.3	Yes
9-Dec-10 6:30	9-Dec-10 8:00	0.25	-12.2	Yes
9-Dec-10 17:00	9-Dec-10 19:00	0.36	-14.2	Yes
9-Dec-10 23:30	10-Dec-10 6:00	0.31	-14.7	Yes
10-Dec-10 23:00	11-Dec-10 6:00	0.29	-16.2	Yes
12-Dec-10 9:00	12-Dec-10 15:00	0.04	-14.5	Yes
12-Dec-10 23:00	13-Dec-10 1:00	0.37	-10.8	Yes
14-Dec-10 17:30	14-Dec-10 20:30	0.44	-5.4	Yes
15-Dec-10 5:00	16-Dec-10 4:00	0.21	-6.9	Yes
19-Dec-10 7:30	19-Dec-10 8:00	0.20	-13.3	Yes
19-Dec-10 10:00	19-Dec-10 14:00	0.10	-12.5	Yes
26-Dec-10 22:00	26-Dec-10 23:00	0.36	-9.0	Yes
1-Jan-11 13:00	1-Jan-11 19:30	0.32	-6.5	Yes
1-Jan-11 21:00	2-Jan-11 1:00	0.52	-1.4	Yes
2-Jan-11 4:00	2-Jan-11 5:30	0.45	-1.7	Yes
2-Jan-11 9:00	2-Jan-11 12:00	0.18	-4.9	Yes
7-Jan-11 13:30	7-Jan-11 17:00	0.48	-2.4	Yes
7-Jan-11 19:00	7-Jan-11 20:00	0.44	-4.4	Yes
7-Jan-11 21:30	8-Jan-11 0:30	0.32	-4.9	Yes
8-Jan-11 3:00	9-Jan-11 9:00	0.23	-7.3	Yes
9-Jan-11 17:00	9-Jan-11 23:30	0.22	-15.8	Yes
12-Jan-11 14:00	13-Jan-11 3:00	0.15	-24.3	Yes
13-Jan-11 14:00	13-Jan-11 20:00	0.16	-22.7	Yes
14-Jan-11 13:00	15-Jan-11 3:00	0.02	-25.1	Yes

Table 5-7. List of slushy pans events identified from 15-Jan-11 to 15-Mar-11.

Start Time	End Time	Water Temp (˚C)	Air Temp (˚C)	Snowing? (Yes/No)
16-Jan-11 5:00	16-Jan-11 8:00	0.13	-20.8	Yes
16-Jan-11 15:00	16-Jan-11 21:00	0.13	-22.1	Yes
16-Jan-11 23:00	17-Jan-11 6:00	0.14	-22.5	Yes
17-Jan-11 12:30	17-Jan-11 14:00	0.12	-20.5	Yes
19-Jan-11 7:30	19-Jan-11 9:00	0.25	-4.7	Yes
19-Jan-11 12:30	19-Jan-11 13:00	0.27	-10.8	Yes
20-Jan-11 7:00	20-Jan-11 8:30	0.11	-11.1	Yes
21-Jan-11 19:00	22-Jan-11 1:00	0.32	-7.1	Yes
29-Jan-11 0:30	29-Jan-11 2:00	0.26	-13.1	Yes
29-Jan-11 14:00	29-Jan-11 21:00	0.26	-17	Yes
5-Feb-11 3:00	5-Feb-11 6:00	0.92	1.4	Yes
5-Feb-11 7:00	5-Feb-11 16:00	0.61	0.4	Yes
13-Feb-11 5:00	13-Feb-11 6:00	0.70	1.9	Yes
15-Feb-11 8:00	15-Feb-11 9:00	0.22	-7.8	Yes
16-Feb-11 19:00	17-Feb-11 5:00	0.10	-20.9	Yes
18-Feb-11 2:30	18-Feb-11 4:00	0.14	-21.2	Yes
26-Feb-11 4:00	26-Feb-11 10:00	0.20	-8.1	Yes
27-Feb-11 3:00	28-Feb-11 0:00	0.14	-8.1	Yes
3-Mar-11 20:30	3-Mar-11 22:00	0.17	-19.0	Yes
5-Mar-11 19:30	5-Mar-11 21:00	0.36	-15.0	Yes
5-Mar-11 22:00	5-Mar-11 23:00	0.30	-16.0	Yes
10-Mar-11 17:00	10-Mar-11 18:00	0.57	-13.6	Yes

5.4. Pan Formation Processes

5.4.1. Slushy Pan Formation

Slushy pan events were always associated with snowfall, the start time of each slushy pan event (documented in Appendix D) coincided with snowfall. Figure 5-23 shows an example of a slushy pan event occurring in the presence of snowfall and stopping once that snowfall ceased at approximately 7:00. When the snowfall resumed at 16:00, the slushy pans reappear. These slushy pan events occurred in above zero water temperatures between 0°C and 1.0°C and in air temperatures between 2°C and -25°C. These warm temperatures and the prevalence of snowfall during these events indicate that suspended snowfall is the source of these slushy pans.

Based upon the concept that slushy pans are formed from entrained snowfall, the parameters which are likely to determine whether slushy pans will form include: snowfall presence, snowfall rate, air temperature and water temperature. Examining the surface ice analysis figures (available in Appendix C), it was found that occasionally snowfall occurred without slushy pans. It is likely that slushy pans did not occur during these snowfall events because the quantity of snow crystals was not sufficient to overcome the ambient air and water temperatures and survive in the flow long enough to be detected by the sonars. It is also possible that the snowfall observed at the City Centre Airport did not occur

over the river upstream of station 56.8 km, resulting in a false detection of snowfall.

5.4.2. Crusty Pan Formation

Crusty pan events are strongly linked to suspended frazil event, as every suspended frazil event was concurrent with the appearance of crusty pans. Of the 54 detected crusty events, 24 coincided with suspended frazil. Figure 5-24(a, c) presents an example from 29-Dec-10, where crusty pans appeared before, during and after a suspended frazil event. In addition, the S_v returns from crusty pans were similar to that of the freeze-up pans (-20dB), which are known to be produced from suspended frazil events (Ashton, 1986).

The 30 crusty pan events that occurred without local suspended frazil coincided with drops in water temperatures to values between 0°C and 0.2°C. An example of this dip is shown in Figure 5-20(f). The timing of maximum surface ice concentration during this event (09:00 to 12:00) also coincides with the minimum water temperature, which may indicate a correlation between the two parameters. The air temperatures during crusty pan events ranged between -11 and -25°C. The cold air temperatures and depression in water temperature seen during crusty pan events suggest that although suspended frazil was not being generated locally during these events, it may have been generated upstream.

It is known from the cross sectional bathymetry profiles extracted from Alberta Environment's HEC-RAS model (documented in Section 2.2.1) that there is a shallow shelf located against the right bank of the channel within approximately 500 m upstream of the Highway 16 Bridges (station 54.8 km). The exact length or width of this shelf is unknown due to the coarse spacing of the bathymetry cross sections, but based upon the cross section at station 54.8 (Figure 4-12) this shelf is between 0.6m and 1.3m deep and could be up to 500m long. The left portion of the open lead is deeper, between 2.0 m and 2.7 m deep.

The variation in depths seen in Figure 4-12 could have allowed for frazil pans to form under the following scenario. Flow over through this reach may have split into a right and left flow with separate temperature regimes. The flow along the right bank may become super-cooled due to the shallow depth and produce suspended frazil and crusty pans. The temperature of the left bank flow may remain above 0°C due to its lower surface area to volume ratio. The two flows would then recombine downstream, bringing the water temperature above 0°C but preserving the newly formed frazil pans. This mechanism could explain the presence of frazil pans in water temperature above 0°C at the sonar platform and it would also explain the appearance of crusty pans before and after suspended frazil events. It is also possible that other shelves exist further upstream where frazil is generated via the same mechanism.

5.5. Discussion of Results

The formation of crusty pans without the appearance of suspend frazil was hypothesized to be a result of differential transverse cooling somewhere in the upstream reach. The shelf at station 54.8 km was one possible location for this occurrence. To validate this mechanism of crusty pan production additional field measurements are required. Photographic documentation of the frazil pans and water temperature measurements in the right and left portion of the flow would provide the evidence required to verify this hypothesis. Two dimensional (longitudinal and transverse) modeling may also capture the transverse cooling but would require more detailed bathymetry in the reach upstream of the Highway 16 bridges.

From the list of slushy pan events recorded in Table 5-6 and Table 5-7, it was discovered that slushy pans never occurred in super-cooled water temperatures. It was found that during freeze-up, no slushy pans were detected despite the presence of snowfall during most of the day on 17-Nov-10 and 18-Nov-10 (Figure 5-8 and Figure 5-9). One explanation for this lack of slushy pans in super-cooled water is that suspended frazil agglomerates with the snow slush and all of these ice particles contribute to the formation of crusty pans. Evidence of this can be seen in Figure 5-18 where a slushy pan event occurred from 0:00 to ~5:30. As the water temperature at the sonar instrument platform neared zero degrees, crusty pans appeared and slushy pans disappeared; despite the fact snowfall continued

until 13:00. After the water temperature warmed again, slushy pans briefly reappeared (Figure 5-18 at 13:00).

It is not possible to quantify the volume of ice present in the open lead slushy pans, the S_v plots shown in the surface ice analysis figures (Appendix C). However, these figures indicate that these slush layers are present to a depth of approximately 2 m; with the upper ~40 cm being sufficiently dense to be considered pans (based upon a high and low frequency sonar threshold of -37 dB and -40 dB, respectively). This indicates that entrained snowfall may contribute a significant volume of ice to this open lead.

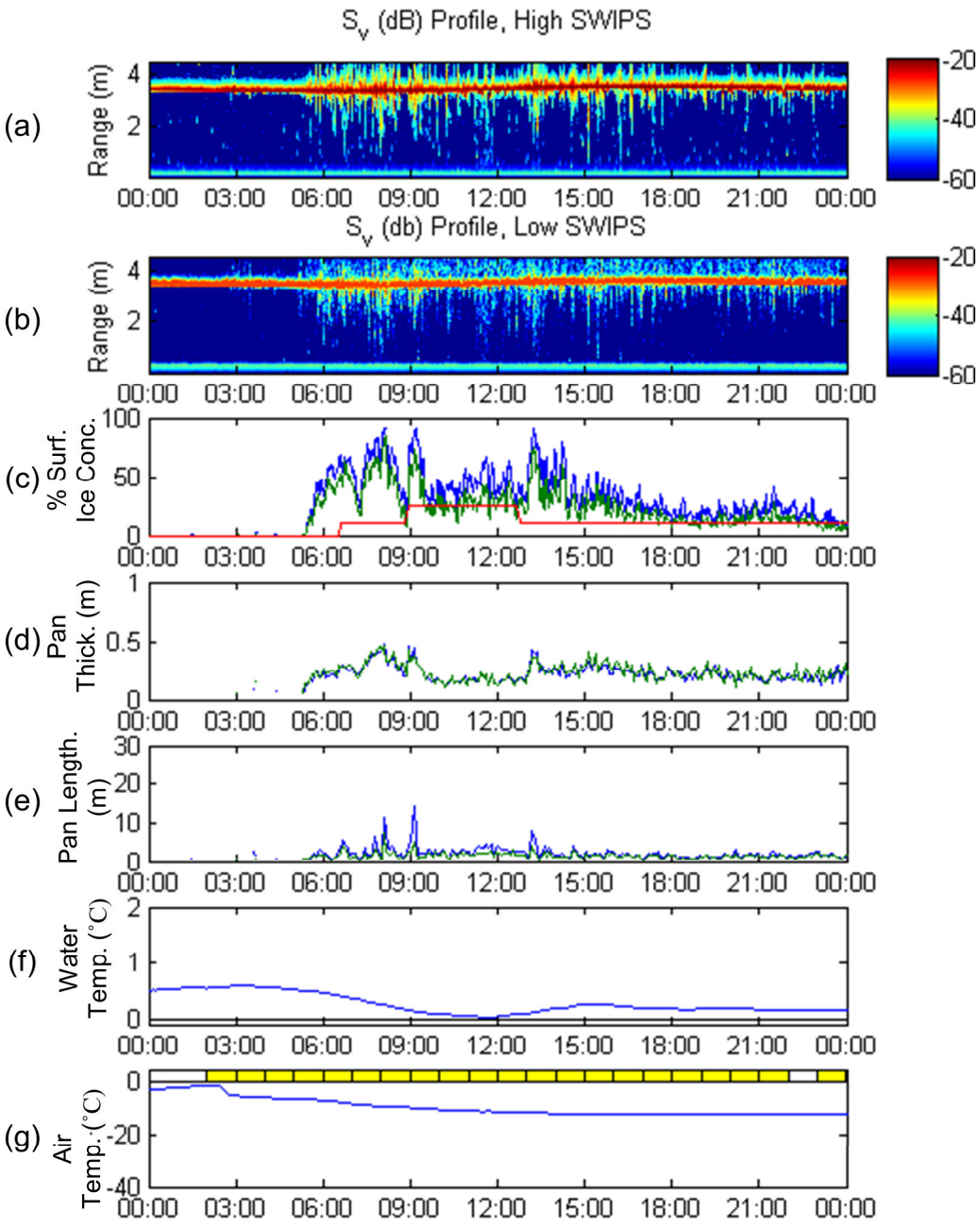

Figure 5-1. Surface ice analysis figure from 15-Dec-2010 displaying: (a) high frequency sonar S_v profile, (b) low frequency sonar S_v profile, (c) surface ice concentrations from the SLR camera (red), high (blue), low (green) frequency sonars, (d) High (blue) and low (green) frequency pan thicknesses, (e) High (blue) and low (green) frequency pan lengths, (f) water temperatures 45 m (blue) and 15 m (green) from the right bank and (g) Air temperature (blue) and snowfall presence (yellow).

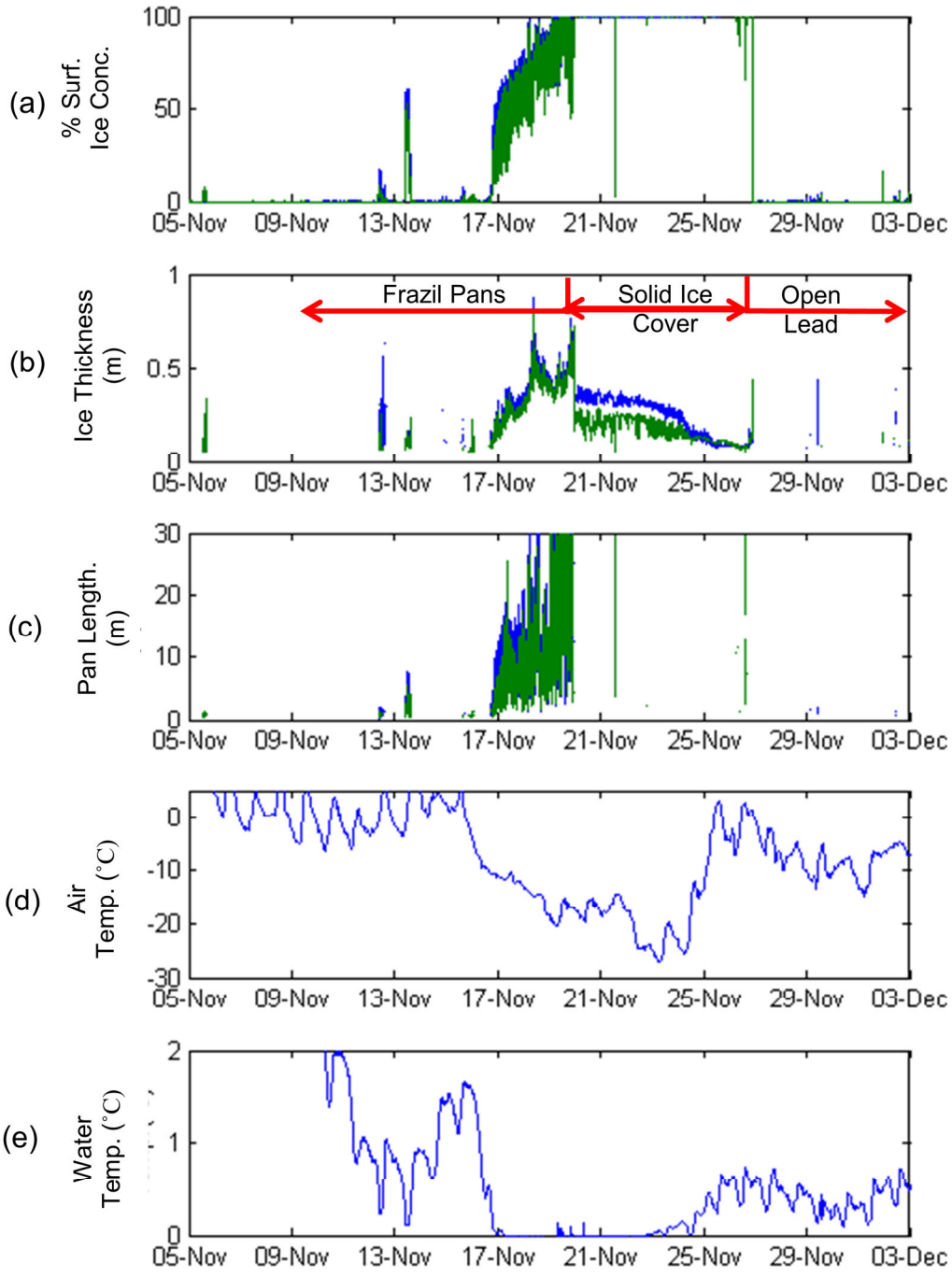

Figure 5-2. Summary of surface ice (a) concentration, (b) thickness, (c) length, (d) air temperature and (e) water temperature, from 5-Nov-10 to 3-Dec-10.

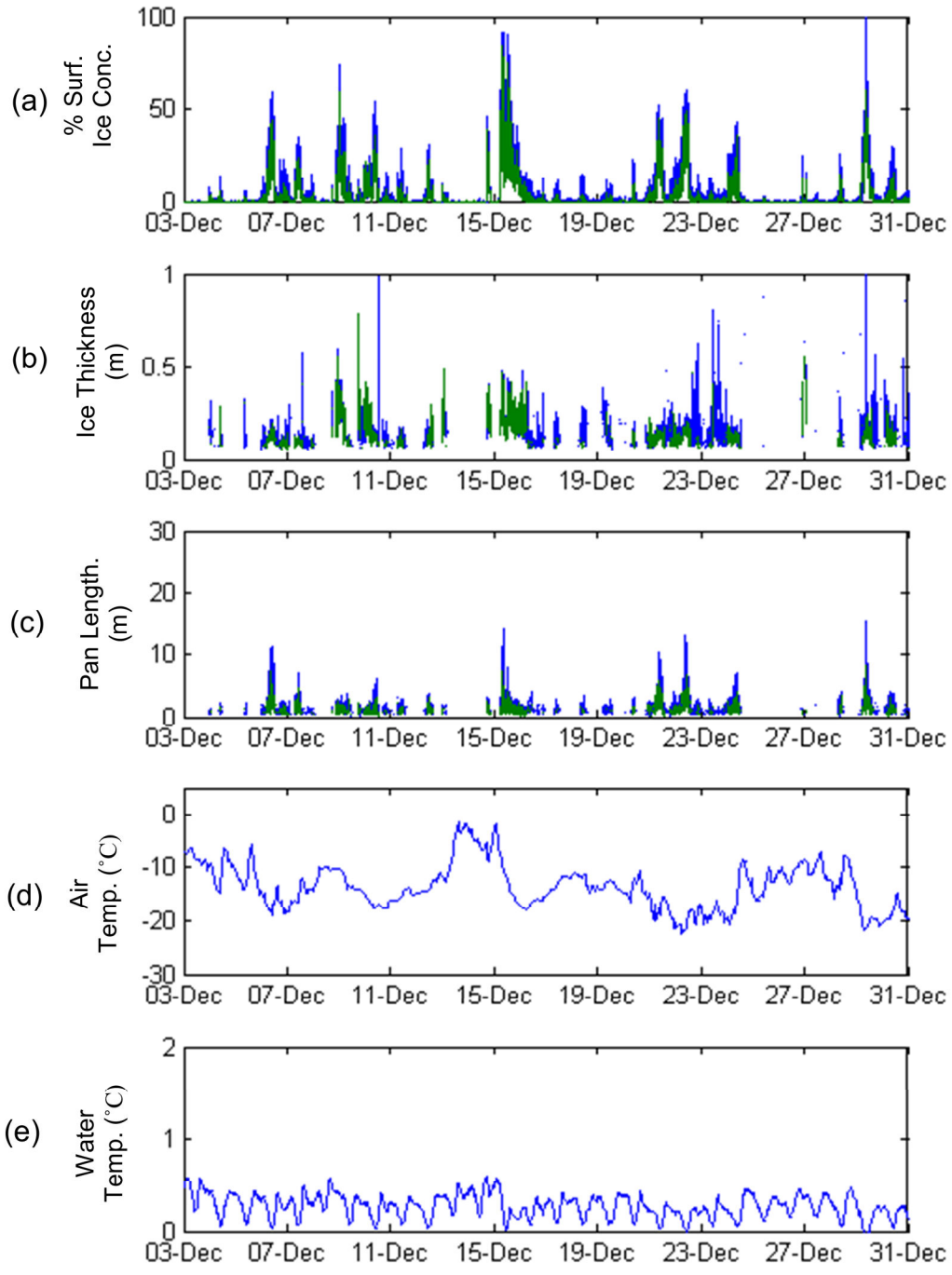

Figure 5-3. Summary of surface ice pan (a) concentration, (b) thickness, (c) length, (d) air temperature and (e) water temperature, from 3-Dec-10 to 31-Dec-10.

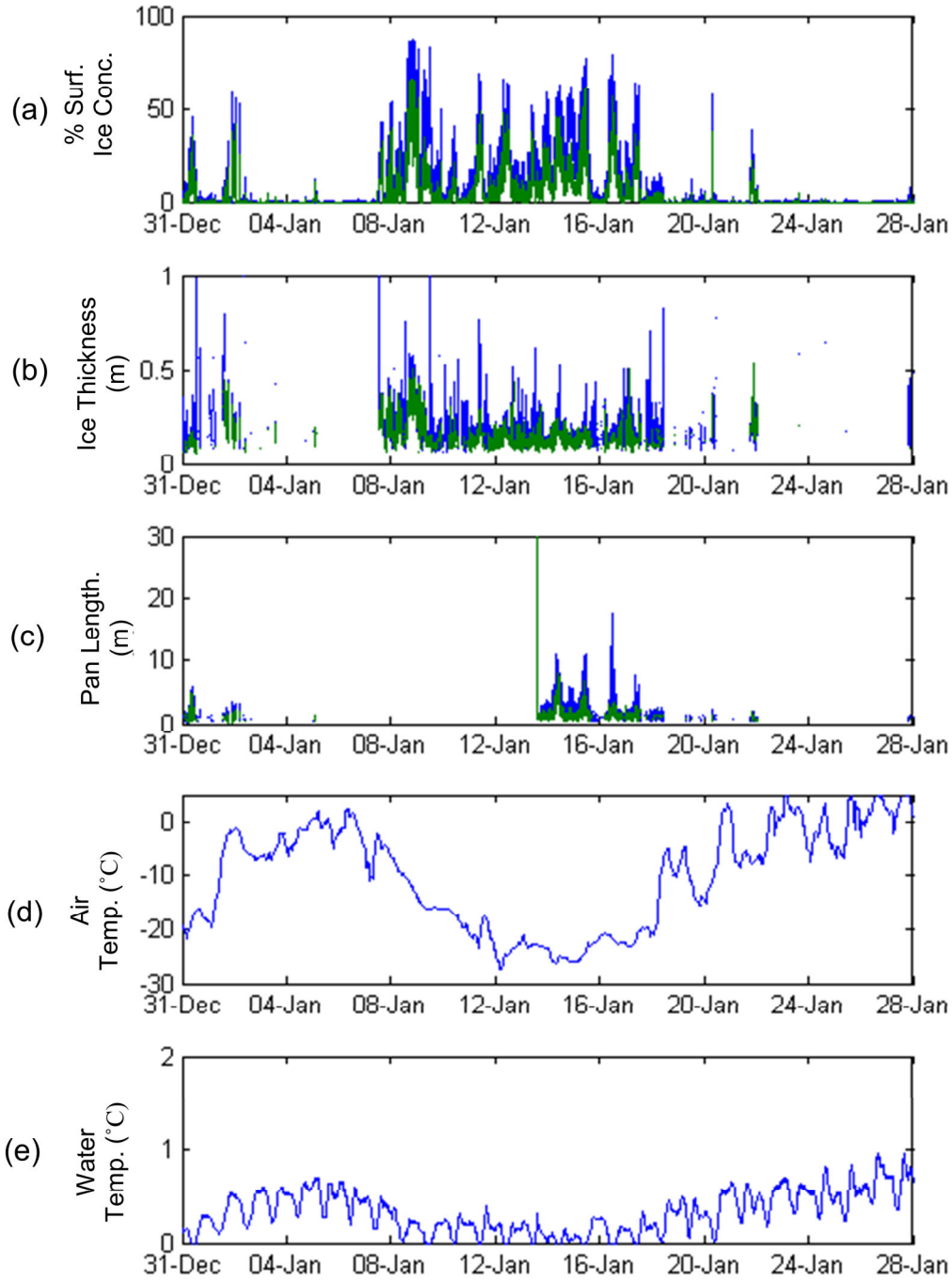

Figure 5-4. Summary of surface ice pan (a) concentration, (b) thickness, (c) length, (d) air temperature and (e) water temperature, from 31-Dec-10 to 28-Jan-11.

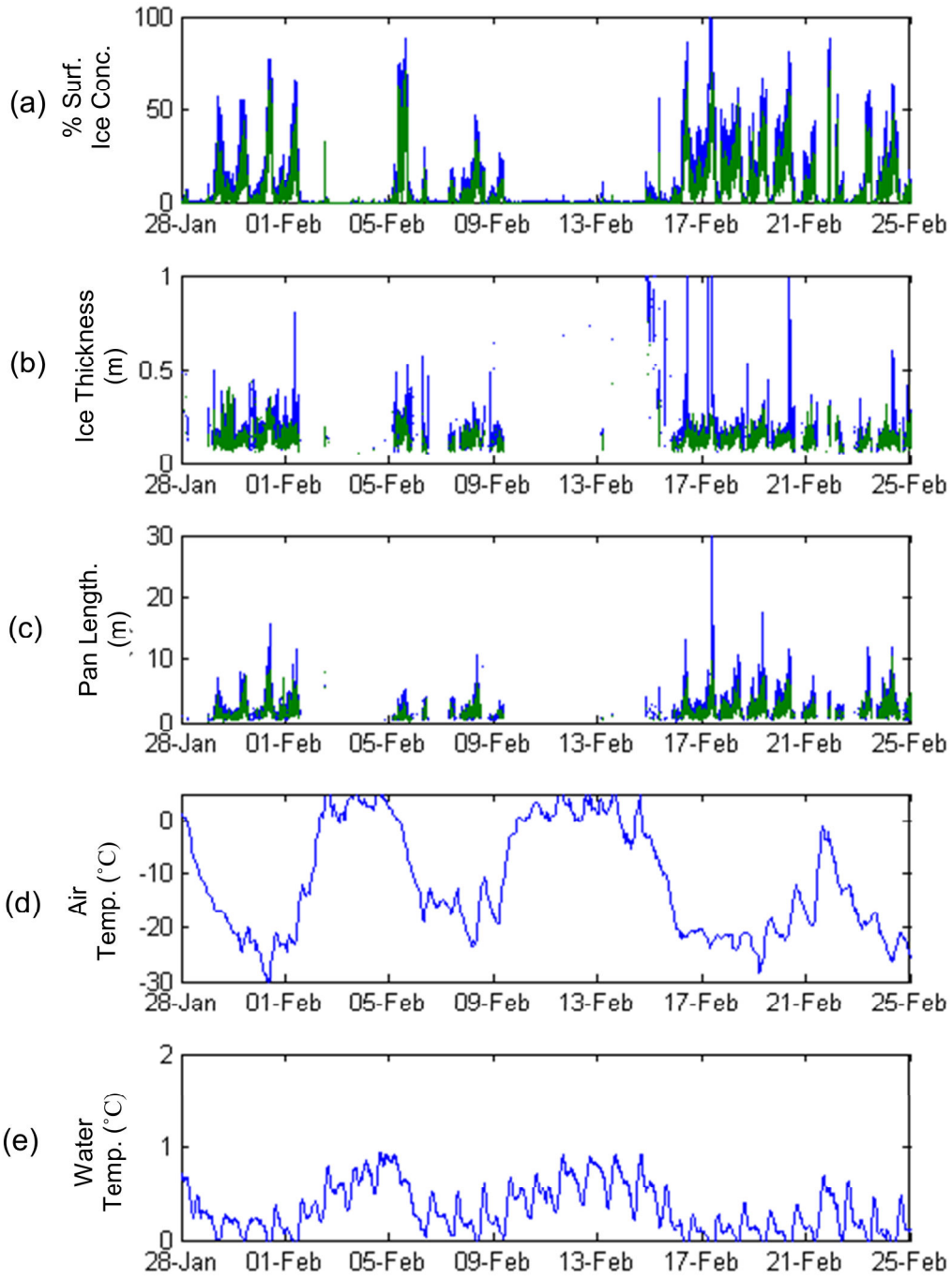

Figure 5-5. Summary of surface ice pan (a) concentration, (b) thickness, (c) length, (d) air temperature and (e) water temperature, from 28-Jan-11 to 25-Feb-11.

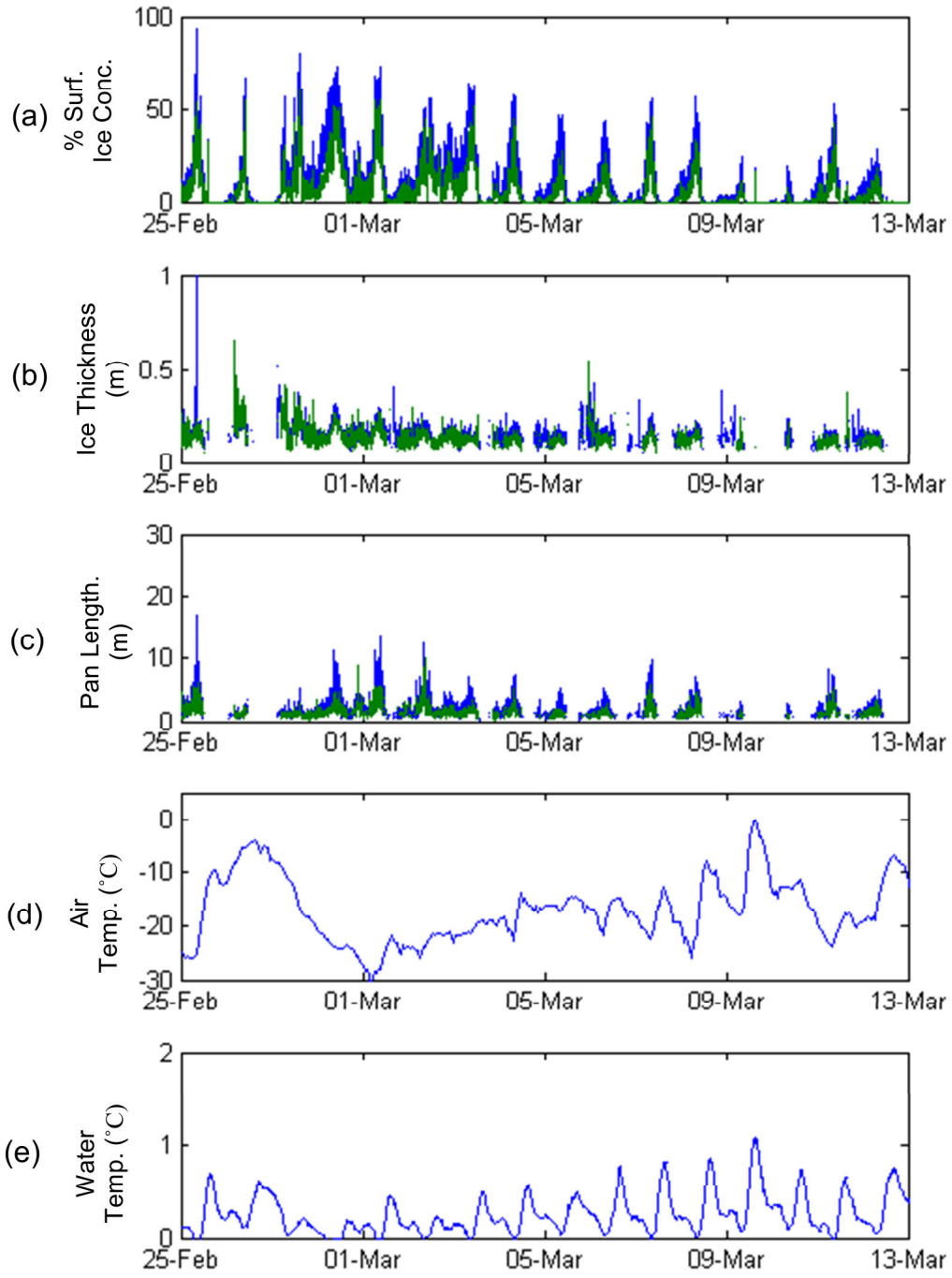

Figure 5-6. Summary of surface ice pan (a) concentration, (b) thickness, (c) length, (d) air temperature and (e) water temperature, from 25-Feb-11 to 13-Mar-11.

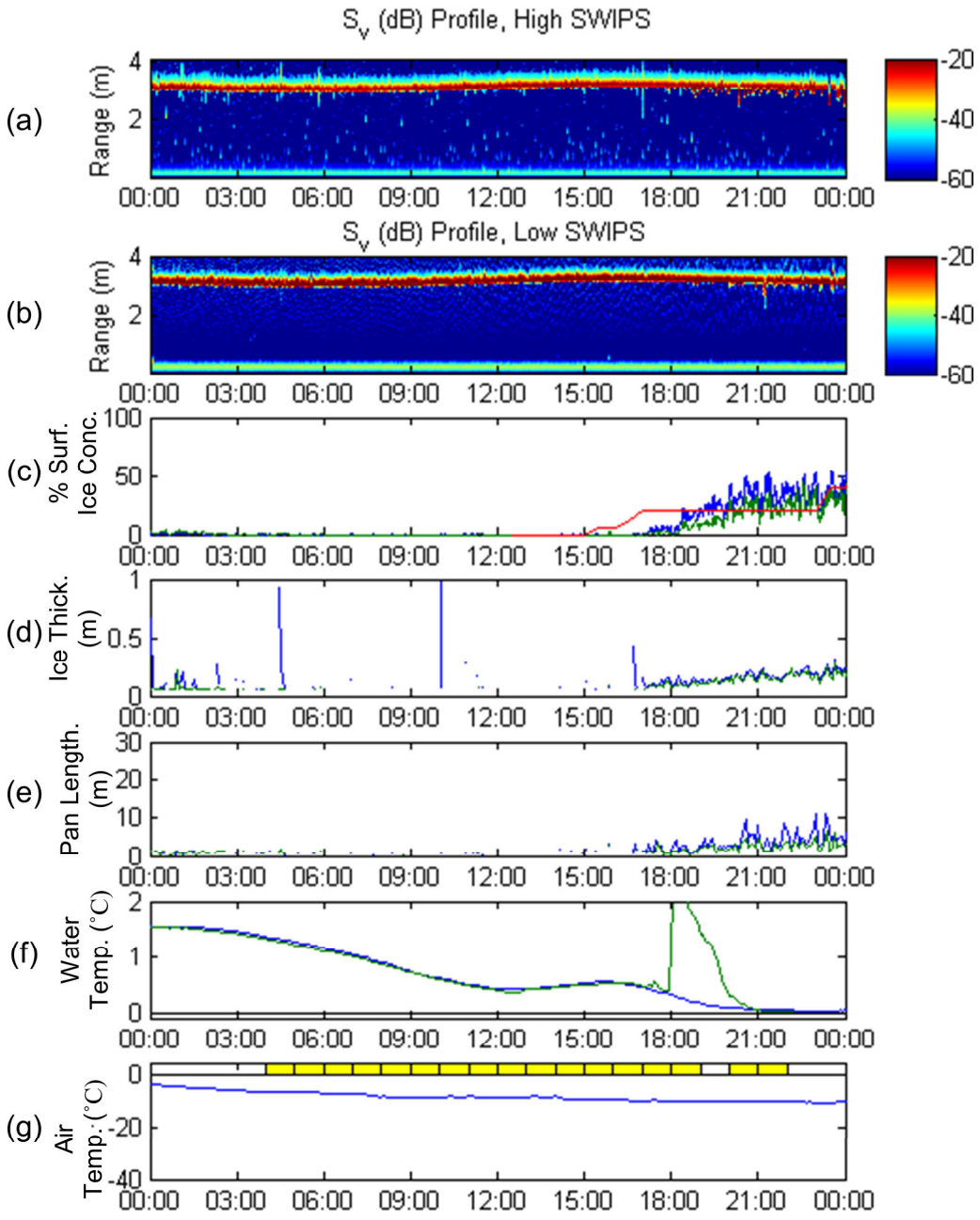

Figure 5-7. Surface ice analysis figure from 16-Nov-2010 displaying: (a) High frequency sonar S_v profile, (b) Low frequency sonar S_v profile, (c) Surface ice concentrations from the SLR camera (red), high (blue), low (green) frequency sonars, (d) High (blue) and low (green) frequency pan thicknesses, (e) High (blue) and low (green) frequency pan lengths, (f) water temperatures 45 m (blue) and 15 m (green) from the right bank and (g) Air temperature (blue) and snowfall presence (yellow).

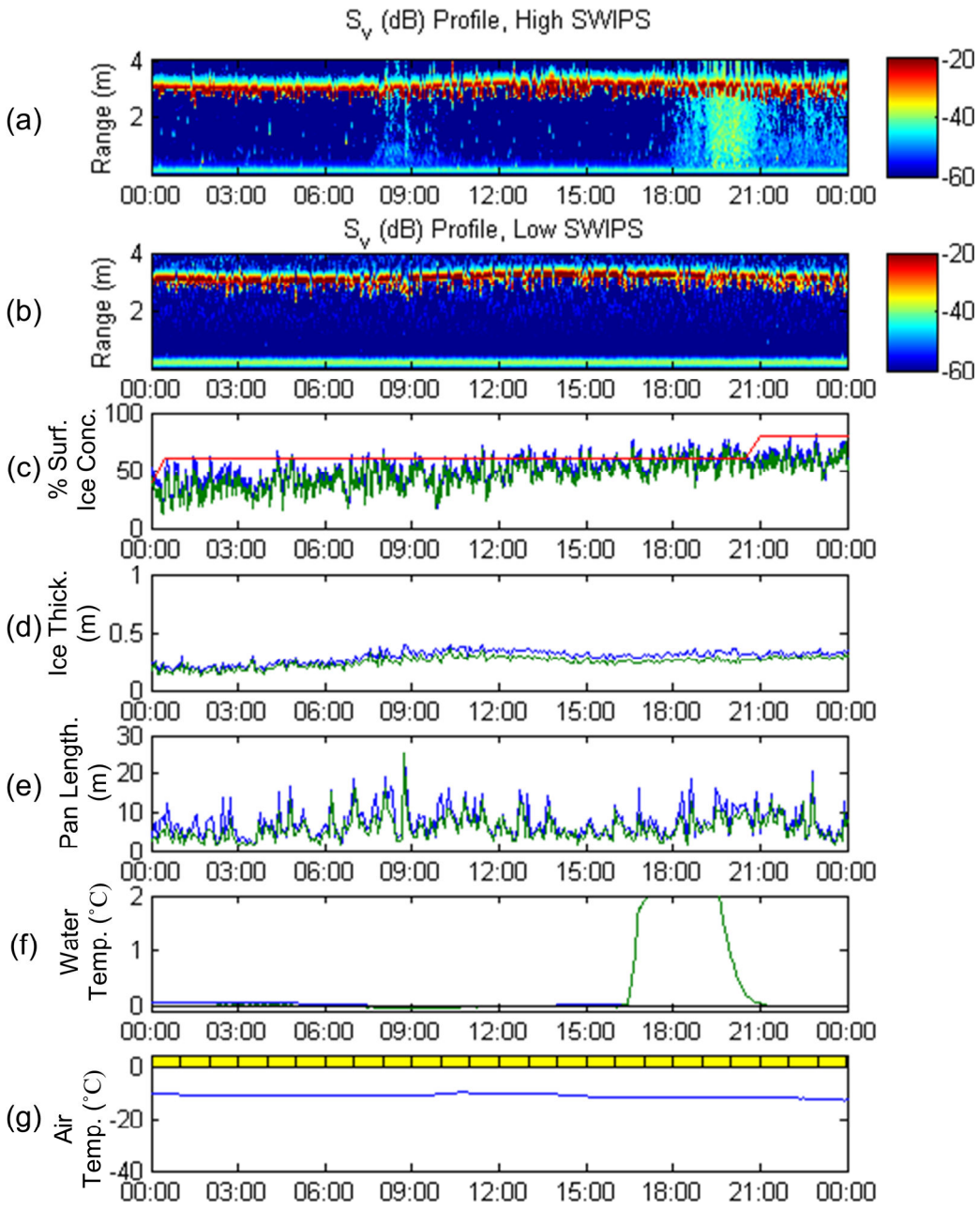

Figure 5-8. Surface ice analysis figure from 17-Nov-2010 displaying: (a) high frequency sonar S_v profile, (b) low frequency sonar S_v profile, (c) surface ice concentrations from the SLR camera (red), high (blue), low (green) frequency sonars, (d) High (blue) and low (green) frequency pan thicknesses, (e) High (blue) and low (green) frequency pan lengths, (f) water temperatures 45 m (blue) and 15 m (green) from the right bank and (g) Air temperature (blue) and snowfall presence (yellow).

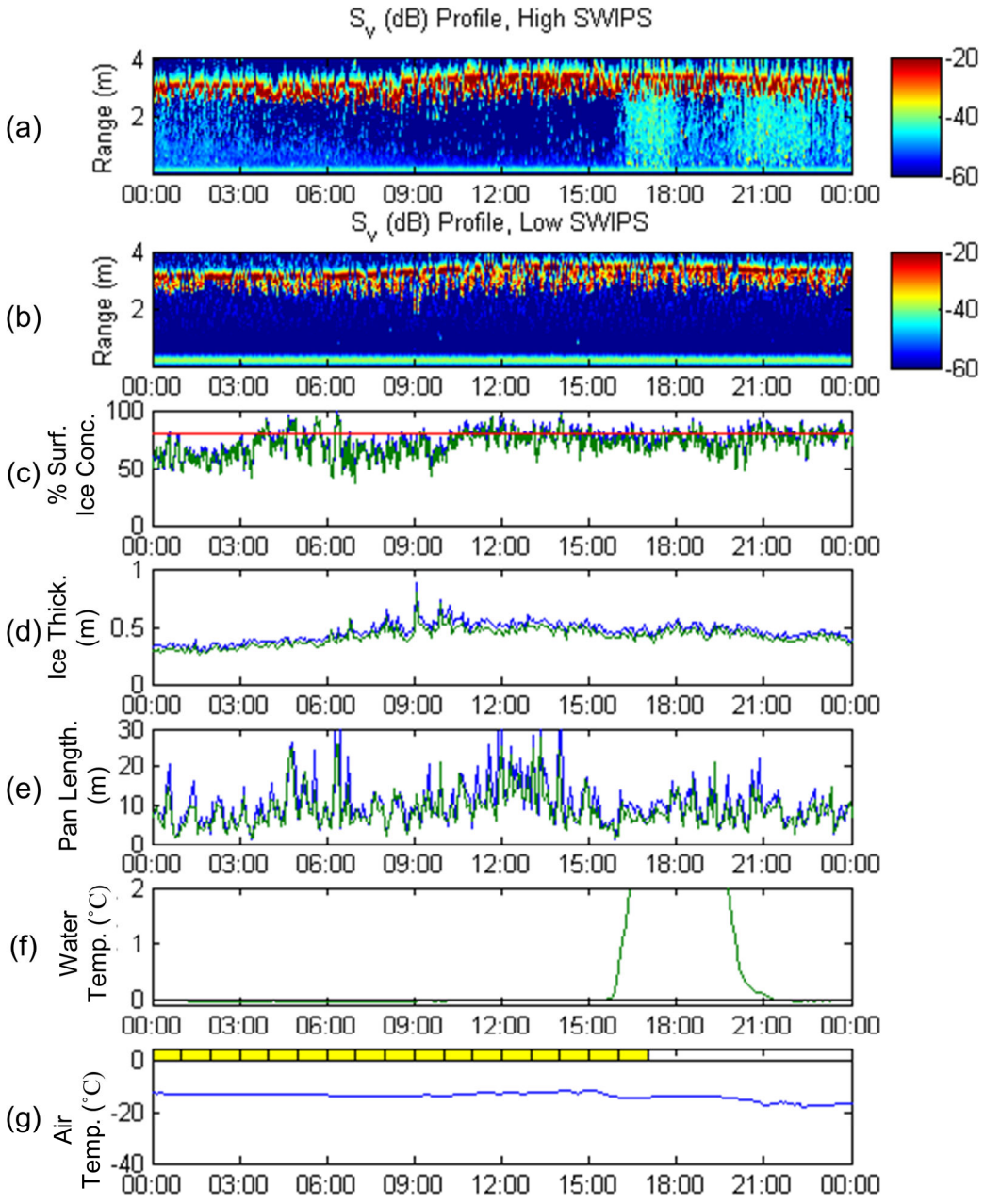

Figure 5-9. Surface ice analysis figure from 18-Nov-2010 displaying: (a) high frequency sonar S_v profile, (b) low frequency sonar S_v profile, (c) surface ice concentrations from the SLR camera (red), high (blue), low (green) frequency sonars, (d) High (blue) and low (green) frequency pan thicknesses, (e) High (blue) and low (green) frequency pan lengths, (f) water temperatures 45 m (blue) and 15 m (green) from the right bank and (g) Air temperature (blue) and snowfall presence (yellow).

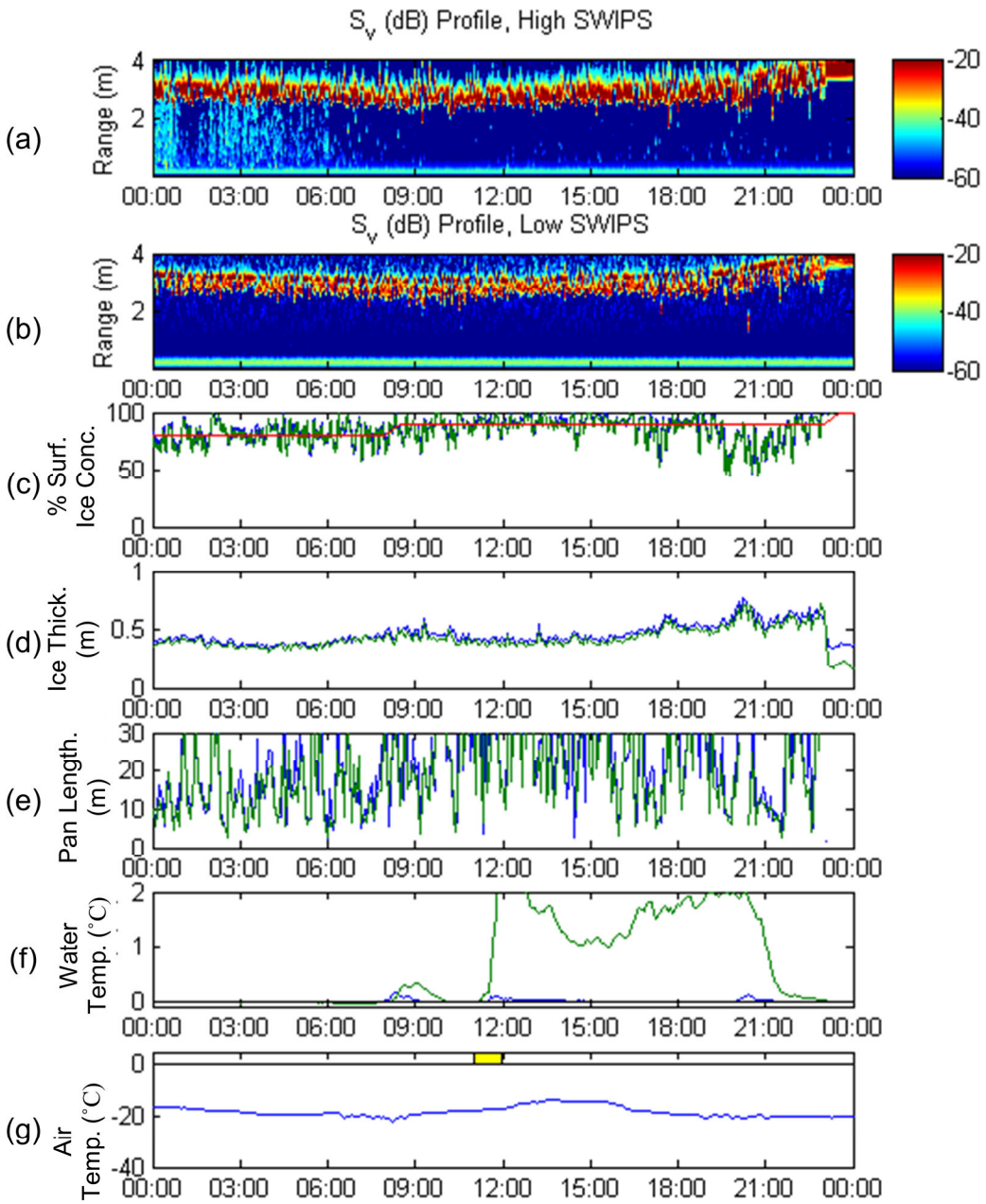

Figure 5-10. Surface ice analysis figure from 19-Nov-2010 displaying: (a) high frequency sonar S_v profile, (b) low frequency sonar S_v profile, (c) surface ice concentrations from the SLR camera (red), high (blue), low (green) frequency sonars, (d) High (blue) and low (green) frequency pan thicknesses, (e) High (blue) and low (green) frequency pan lengths, (f) water temperatures 45 m (blue) and 15 m (green) from the right bank and (g) Air temperature (blue) and snowfall presence (yellow).

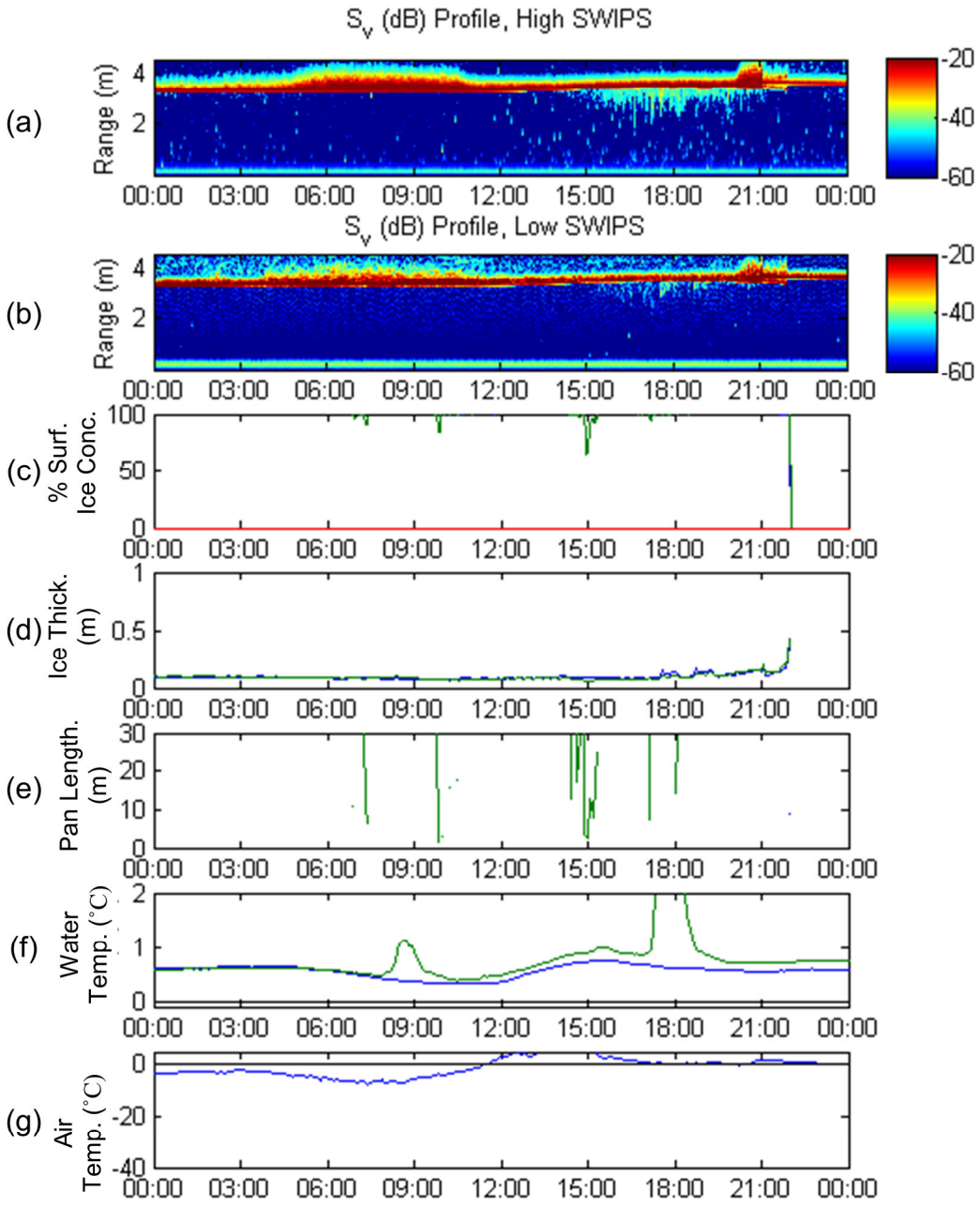

Figure 5-11. Surface ice analysis figure from 26-Nov-2010 displaying: (a) high frequency sonar S_v profile, (b) low frequency sonar S_v profile, (c) surface ice concentrations from the SLR camera (red), high (blue), low (green) frequency sonars, (d) High (blue) and low (green) frequency pan thicknesses, (e) High (blue) and low (green) frequency pan lengths, (f) water temperatures 45 m (blue) and 15 m (green) from the right bank and (g) Air temperature (blue) and snowfall presence (yellow).

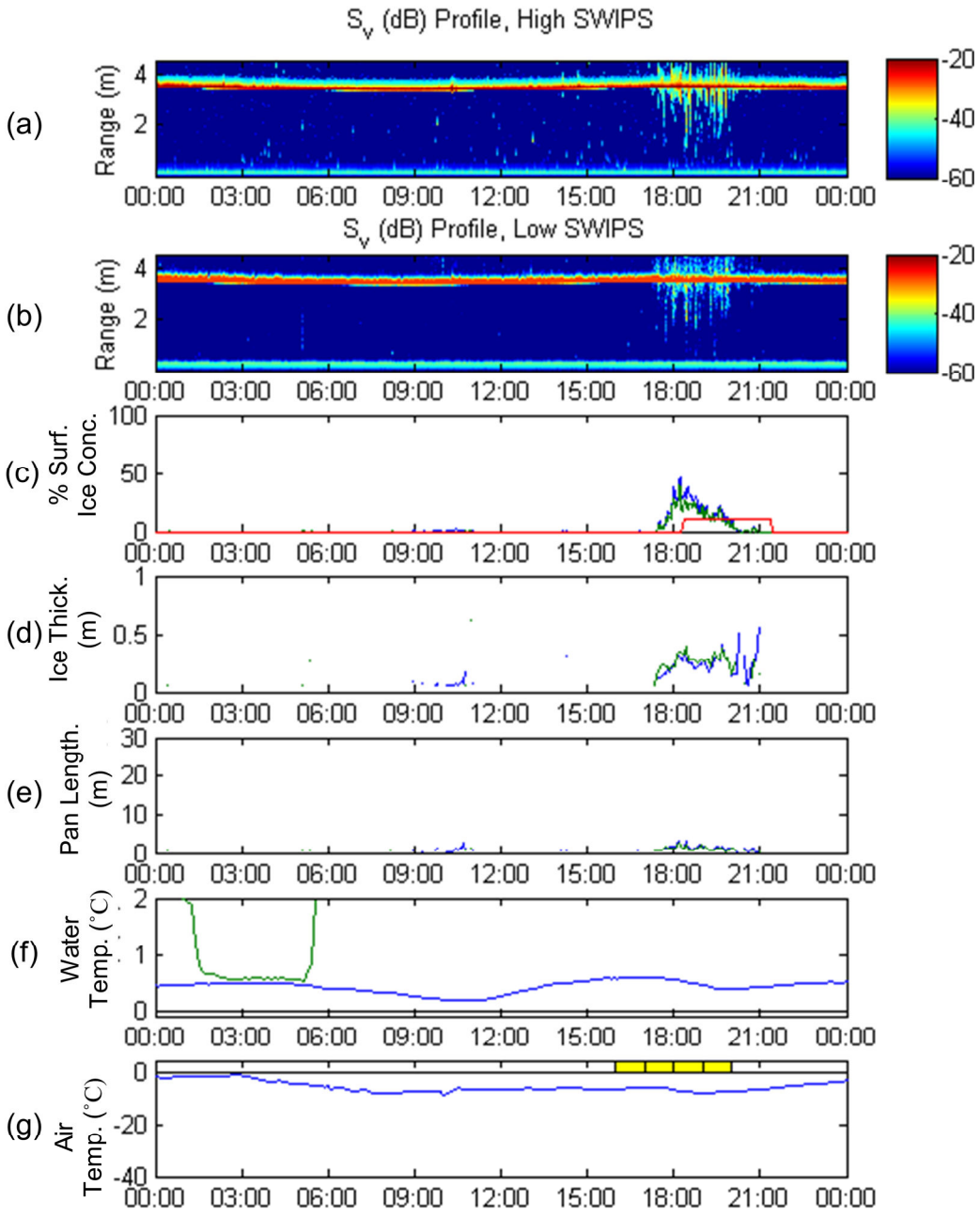

Figure 5-12. Surface ice analysis figure from 14-Dec-2010 displaying: (a) high frequency sonar S_v profile, (b) low frequency sonar S_v profile, (c) surface ice concentrations from the SLR camera (red), high (blue), low (green) frequency sonars, (d) High (blue) and low (green) frequency pan thicknesses, (e) High (blue) and low (green) frequency pan lengths, (f) water temperatures 45 m (blue) and 15 m (green) from the right bank and (g) Air temperature (blue) and snowfall presence (yellow).

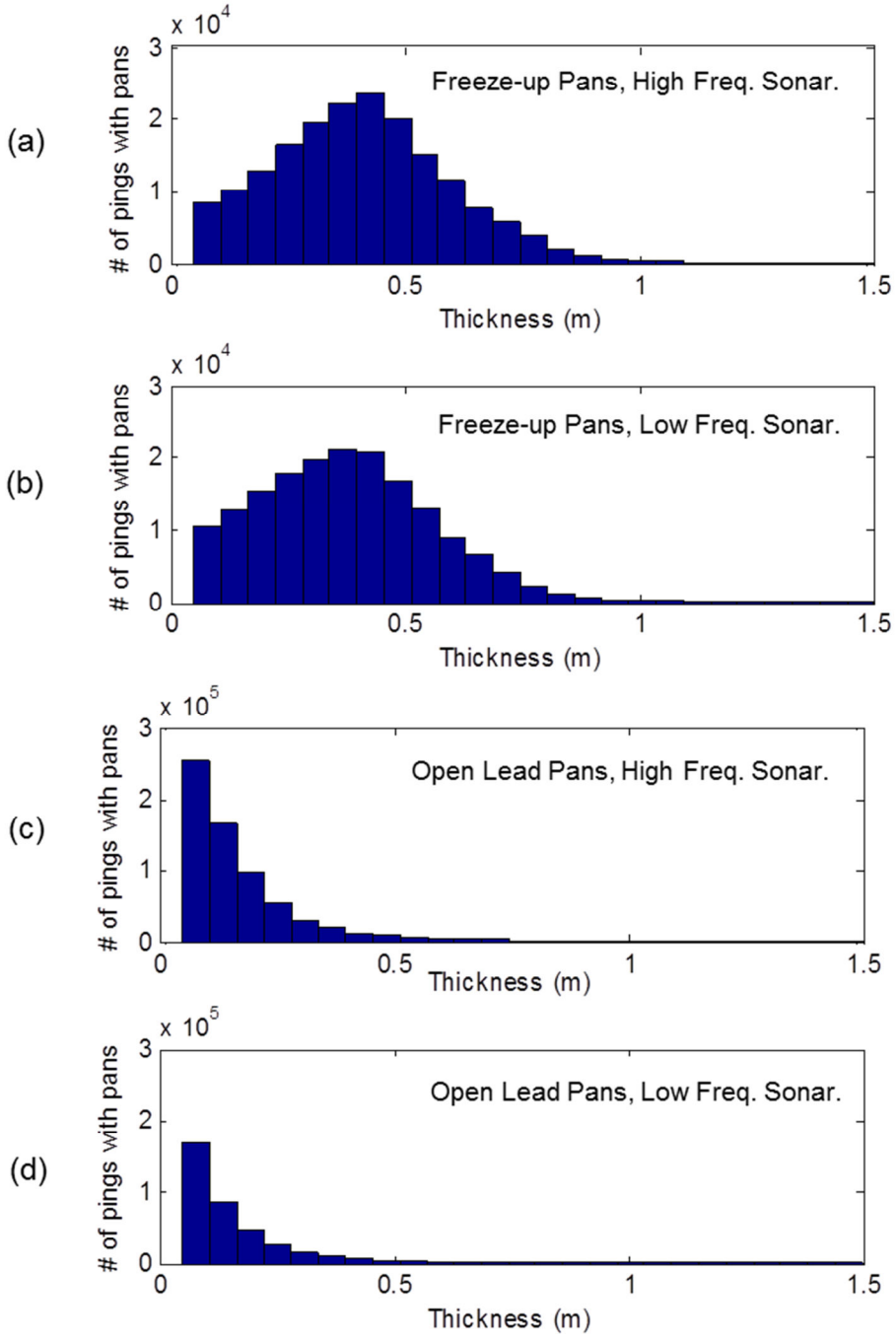

Figure 5-13. Histograms of the calculated ice thicknesses during freeze-up by the (a) high frequency sonar and (b) low frequency sonar and the ice thicknesses occurring in the open lead detected by the (c) high frequency sonar and (d) low frequency sonar

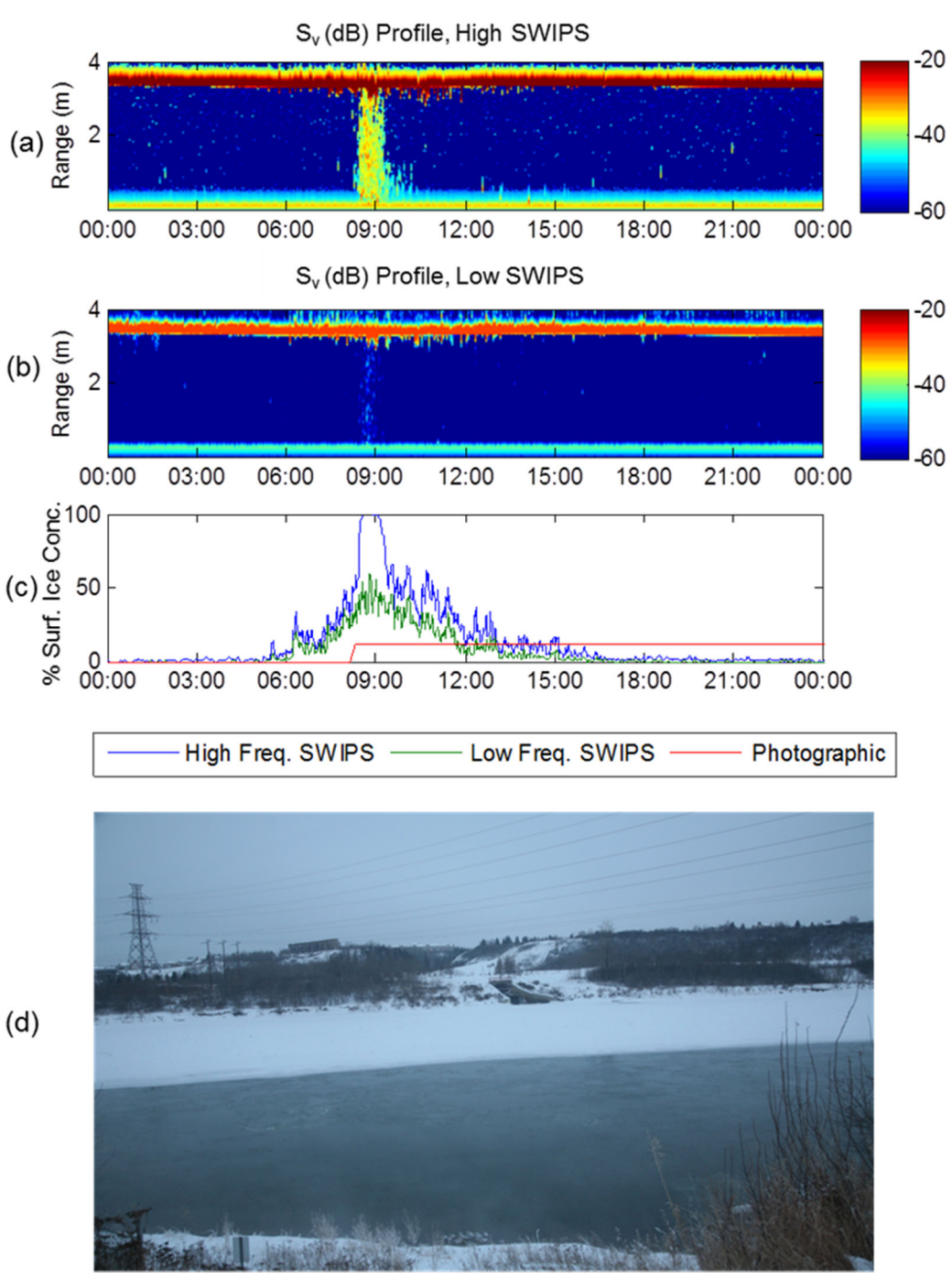

Figure 5-14. (a) High and (b) low frequency sonar S_v plots, (c) calculated ice concentrations. (d) Photograph from 29-Dec-10 at 09:00 at station 56.8 km illustrating the absence of 100% surface ice concentration indicated by the high frequency SWIPS unit.

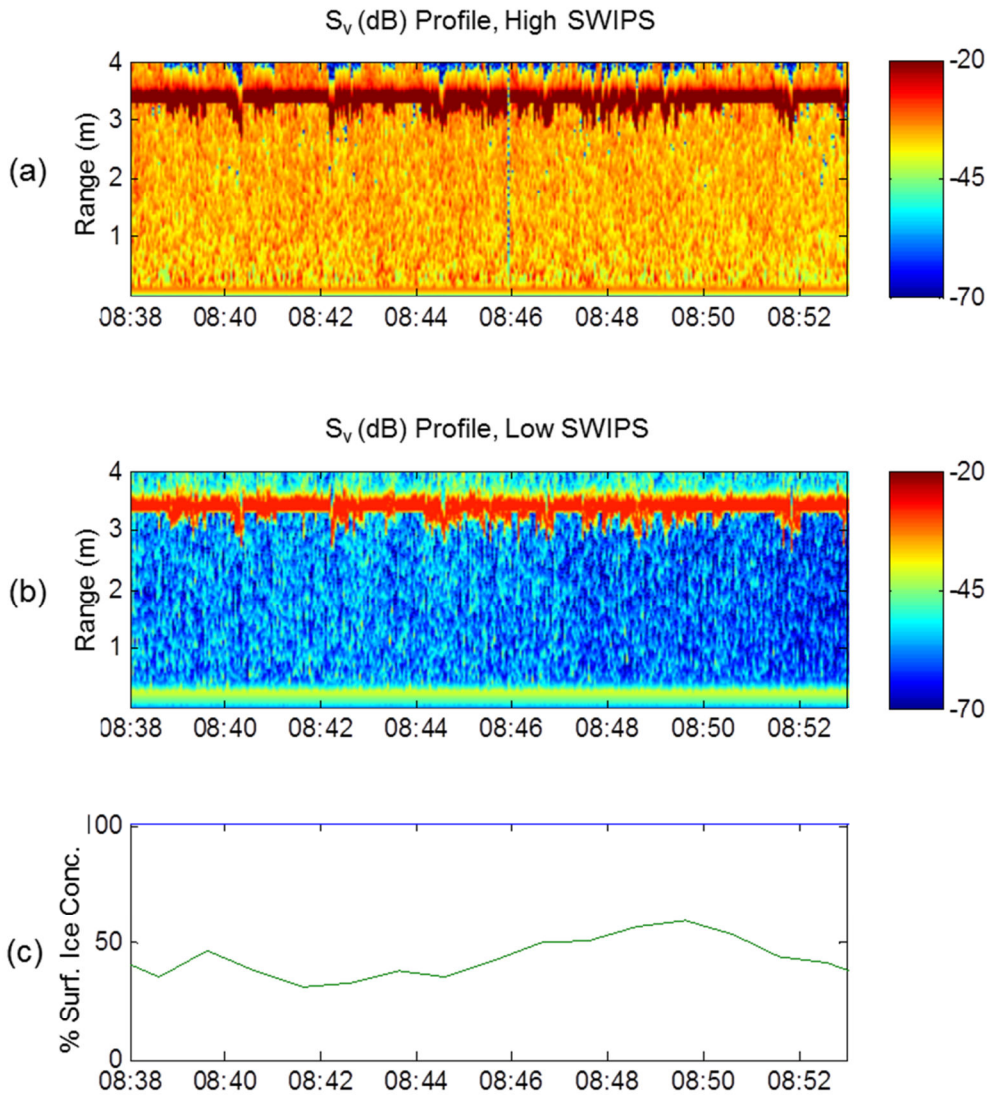

Figure 5-15. 15 minute plot of (a) high and (b) low frequency sonar S_v profiles and (c) calculated high (blue) and low (green) surface ice concentrations from a suspended frazil event on 29-Dec-11.

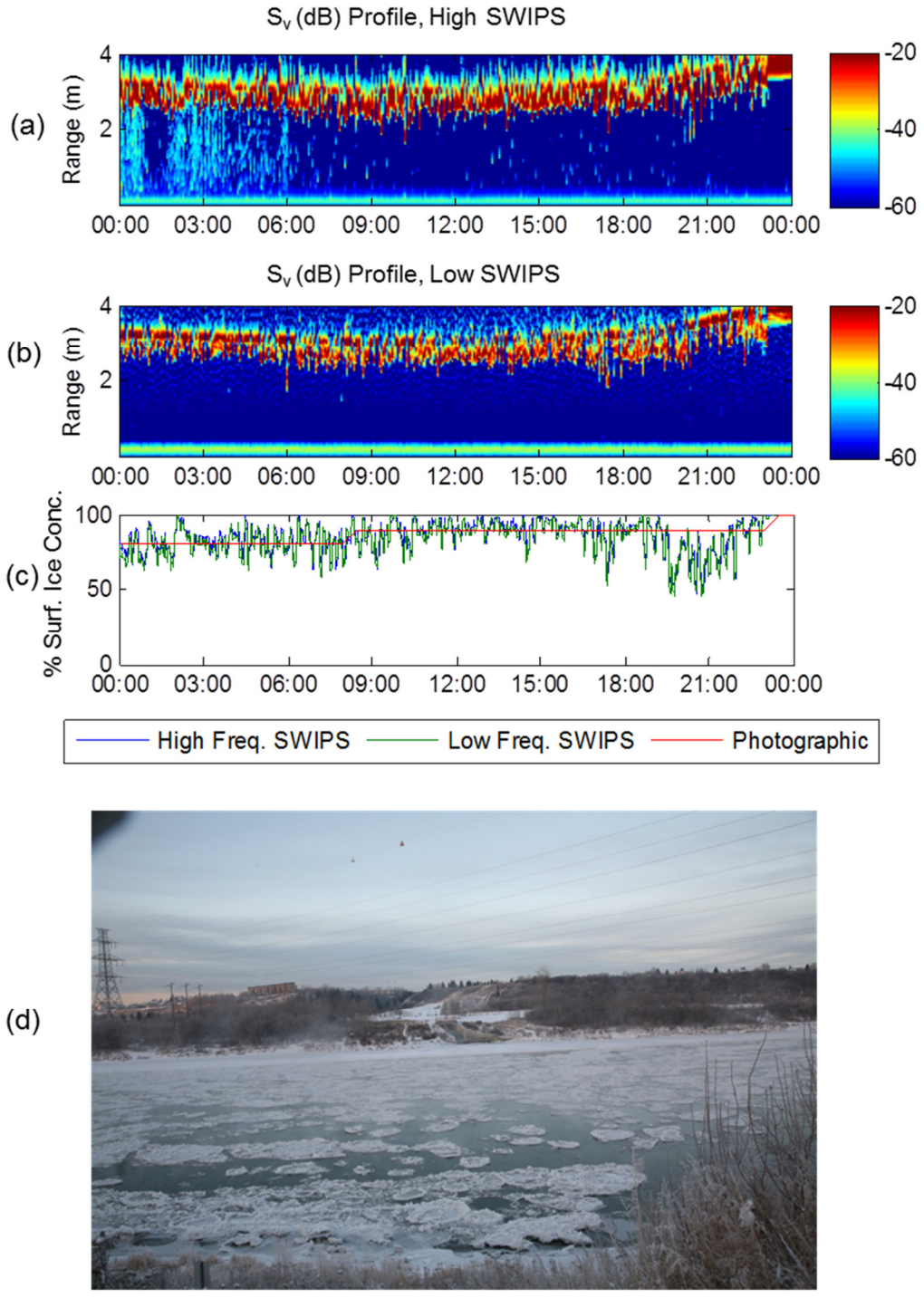

Figure 5-16. (a) High and (b) low frequency sonar S_v profile plots, (c) calculated ice concentrations and (d) Photograph from 19-Nov-10 at 8:30 at station 56.8 km illustrating the excellent visibility of freeze-up pans and rafts.

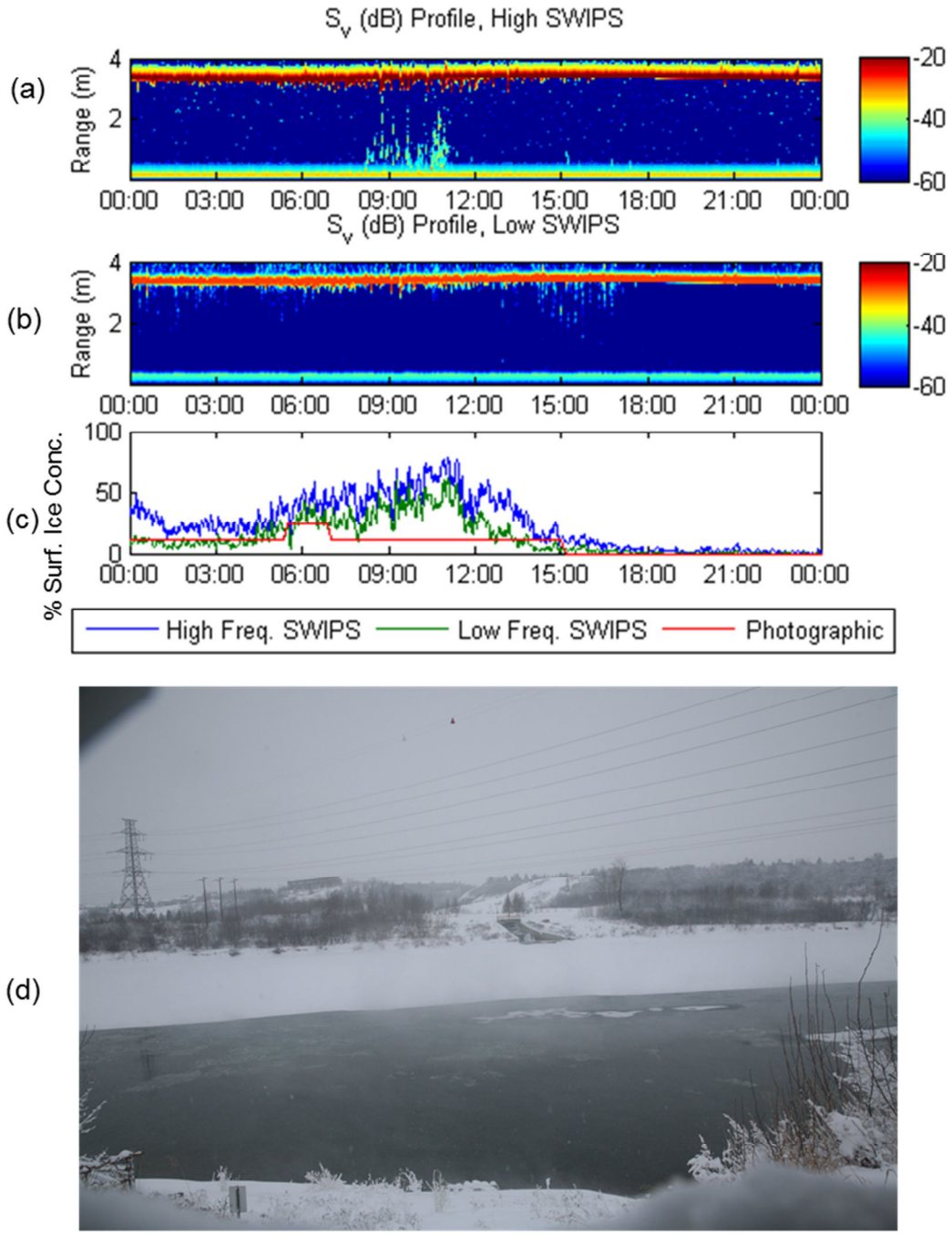

Figure 5-17. (a) High and (b) low frequency sonar S_v profile plots, (c) calculated ice concentrations and (d) Photograph from 15-Jan-10 at 09:49 at station 56.8 km illustrating the translucency and poor visibility of open lead pans and rafts.

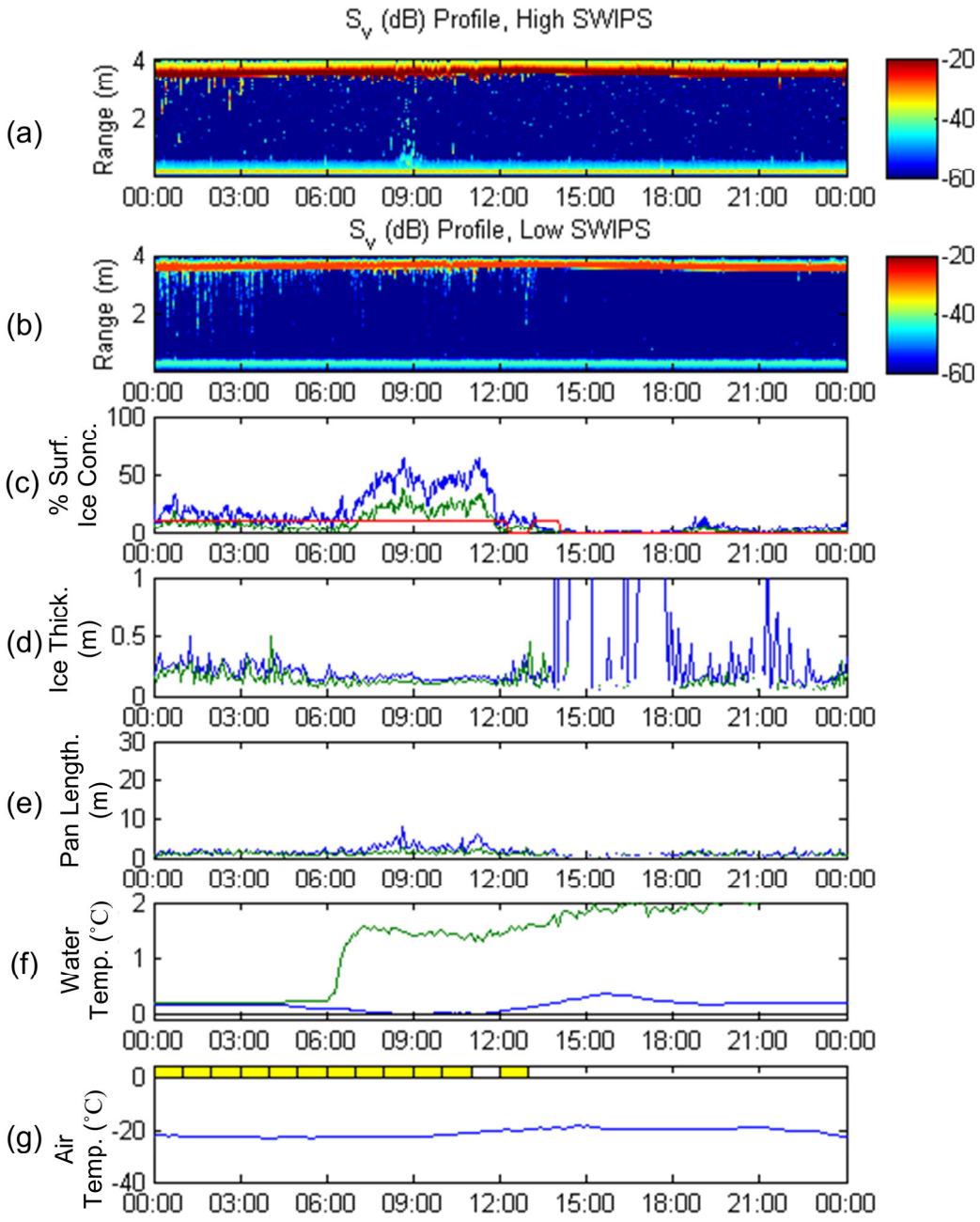

Figure 5-18. Surface ice analysis figure from 17-Jan-11 displaying: (a) high frequency sonar S_v profile, (b) low frequency sonar S_v profile, (c) surface ice concentrations from the SLR camera (red), high (blue), low (green) frequency sonars, (d) High (blue) and low (green) frequency pan thicknesses, (e) High (blue) and low (green) frequency pan lengths, (f) water temperatures 45 m (blue) and 15 m (green) from the right bank and (g) Air temperature (blue) and snowfall presence (yellow).

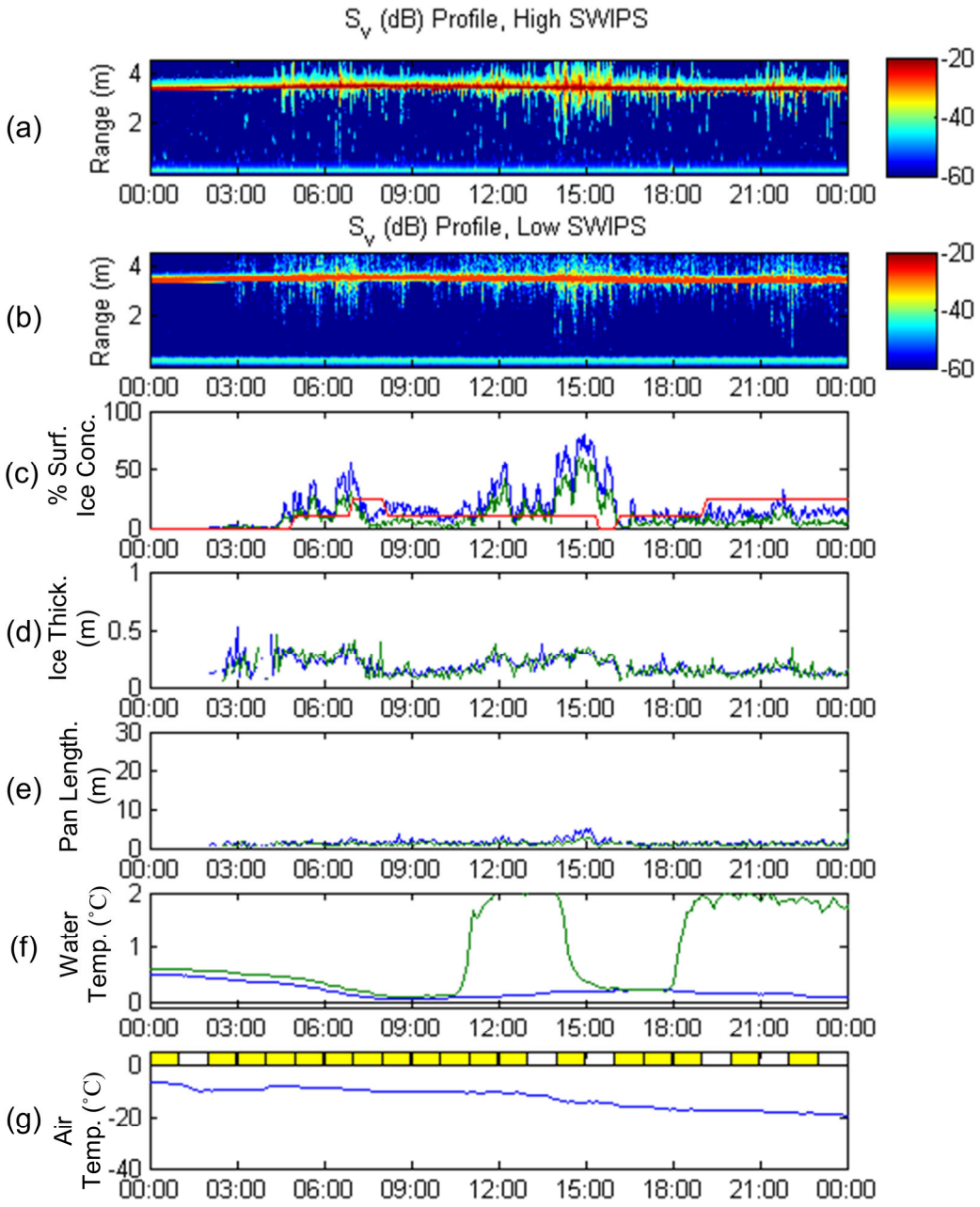

Figure 5-19. Surface ice analysis figure from 27-Feb-11 displaying: (a) high frequency sonar S_v profile, (b) low frequency sonar S_v profile, (c) surface ice concentrations from the SLR camera (red), high (blue), low (green) frequency sonars, (d) High (blue) and low (green) frequency pan thicknesses, (e) High (blue) and low (green) frequency pan lengths, (f) water temperatures 45 m (blue) and 15 m (green) from the right bank and (g) Air temperature (blue) and snowfall presence (yellow).

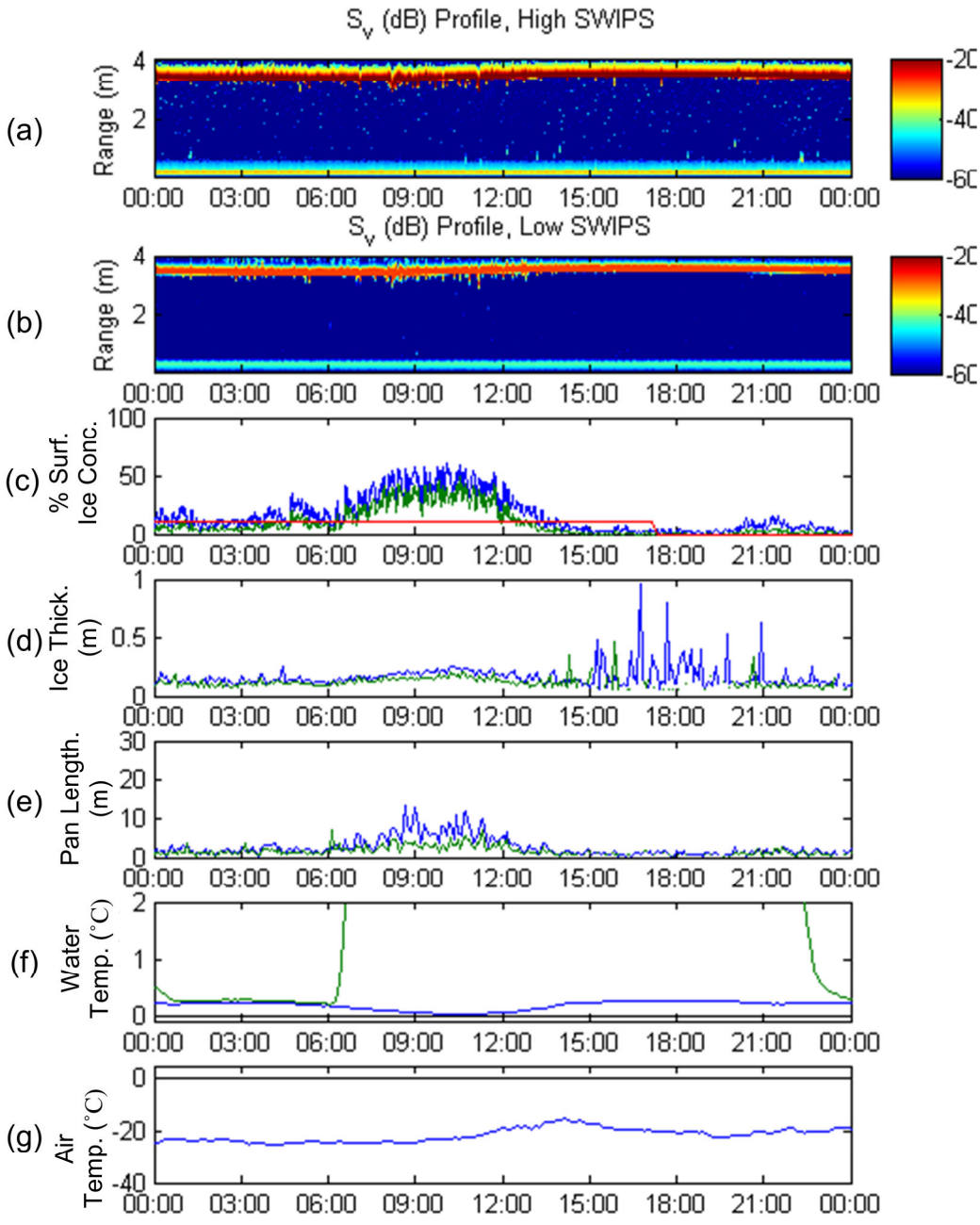

Figure 5-20. Surface ice analysis figure from 22-Dec-10 displaying: (a) (a) high frequency sonar S_v profile, (b) low frequency sonar S_v profile, (c) surface ice concentrations from the SLR camera (red), high (blue), low (green) frequency sonars, (d) High (blue) and low (green) frequency pan thicknesses, (e) High (blue) and low (green) frequency pan lengths, (f) water temperatures 45 m (blue) and 15 m (green) from the right bank and (g) Air temperature (blue) and snowfall presence (yellow).

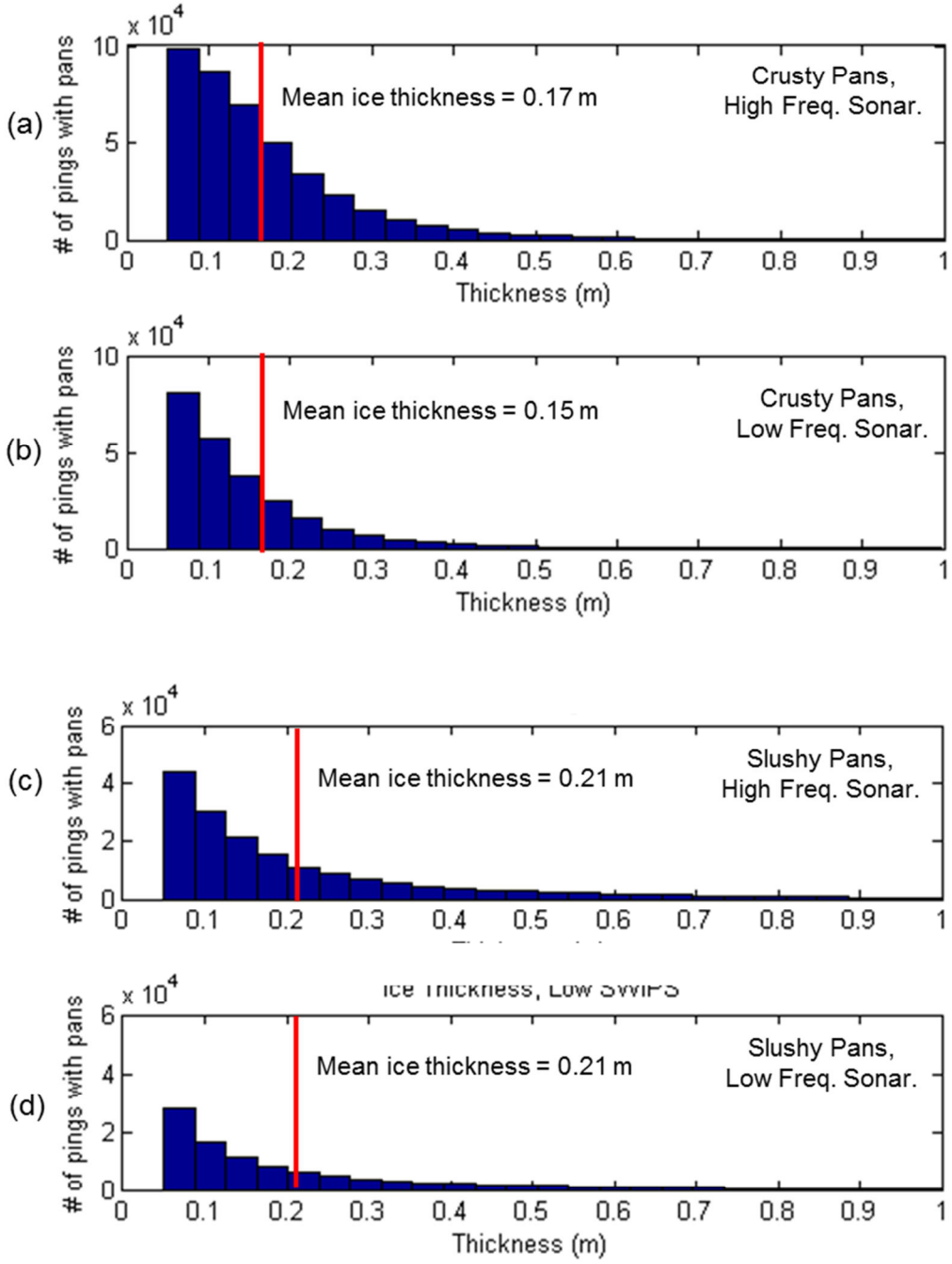

Figure 5-21. Ice thickness histograms displays the quantities and thickness of (a, b) crusty and (c, d) slushy pans detected by the high frequency sonar and low frequency sonar, respectively.

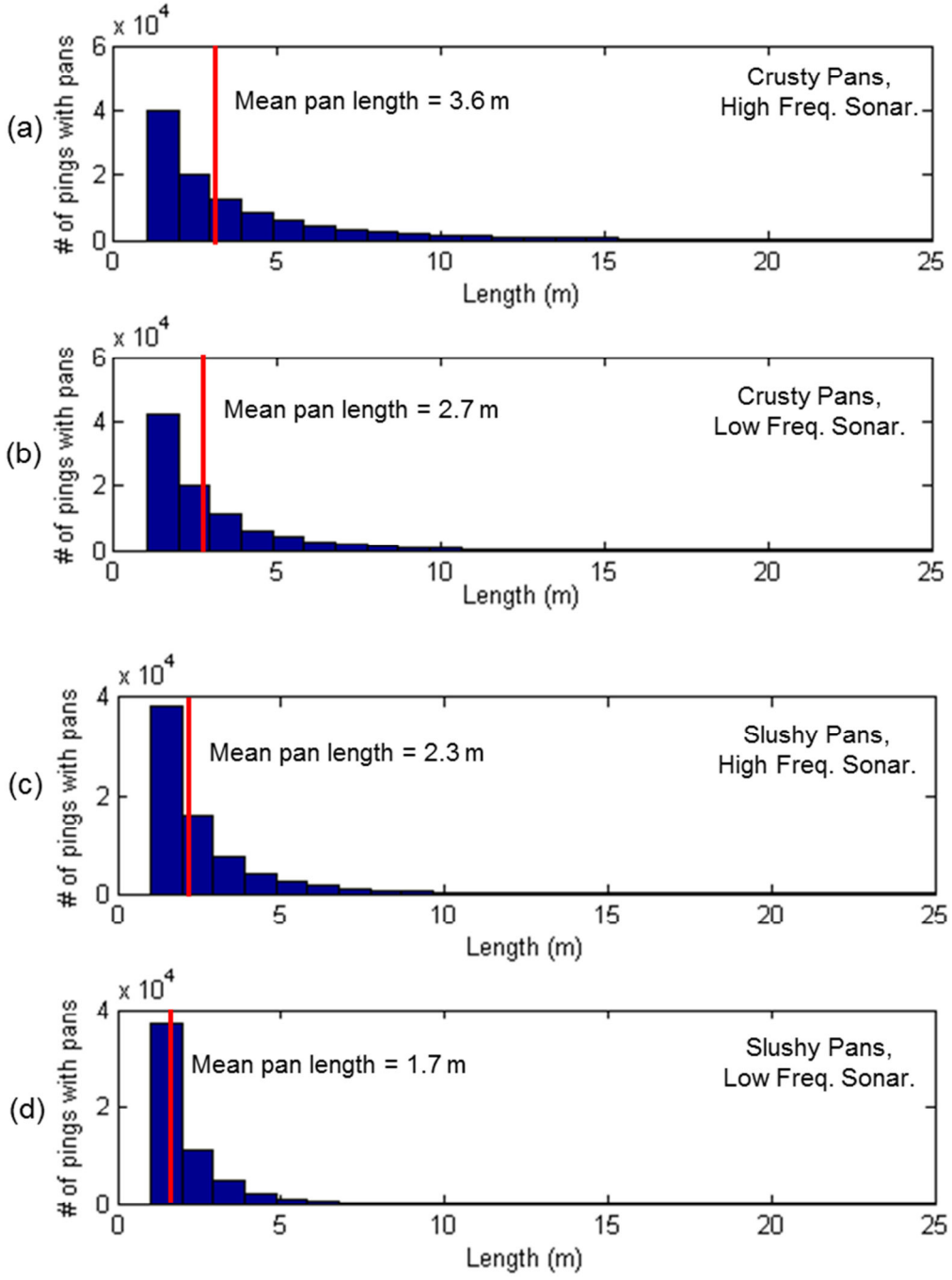

Figure 5-22. Pan length histograms displays the quantities and lengths of (a, b) crusty and (c, d) slushy pans detected by the high frequency sonar and low frequency sonar, respectively.

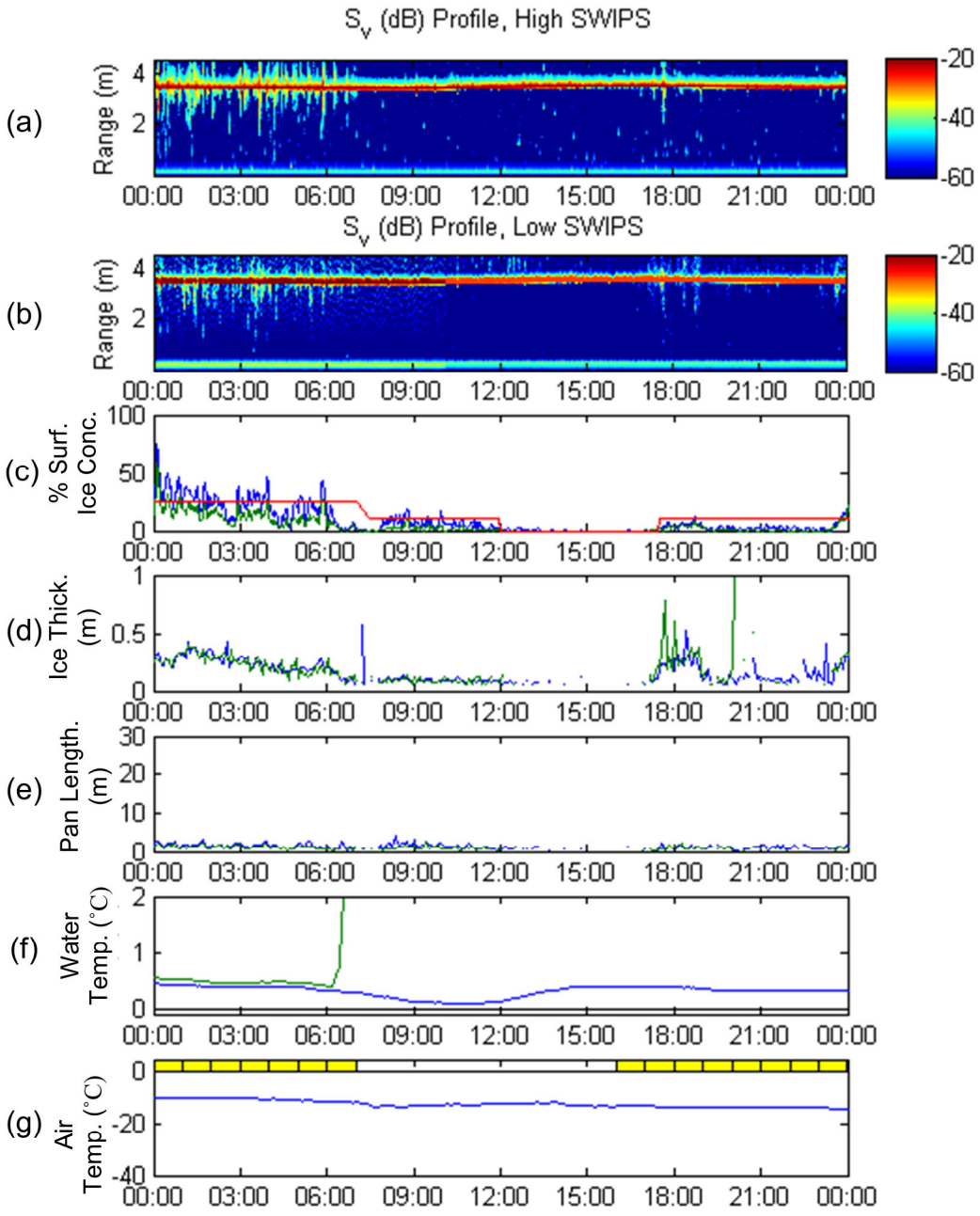

Figure 5-23. Surface ice analysis figure from 09-Dec-10 displaying: (a) high frequency sonar S_v profile, (b) low frequency sonar S_v profile, (c) surface ice concentrations from the SLR camera (red), high (blue), low (green) frequency sonars, (d) High (blue) and low (green) frequency pan thicknesses, (e) High (blue) and low (green) frequency pan lengths, (f) water temperatures 45 m (blue) and 15 m (green) from the right bank and (g) Air temperature (blue) and snowfall presence (yellow).

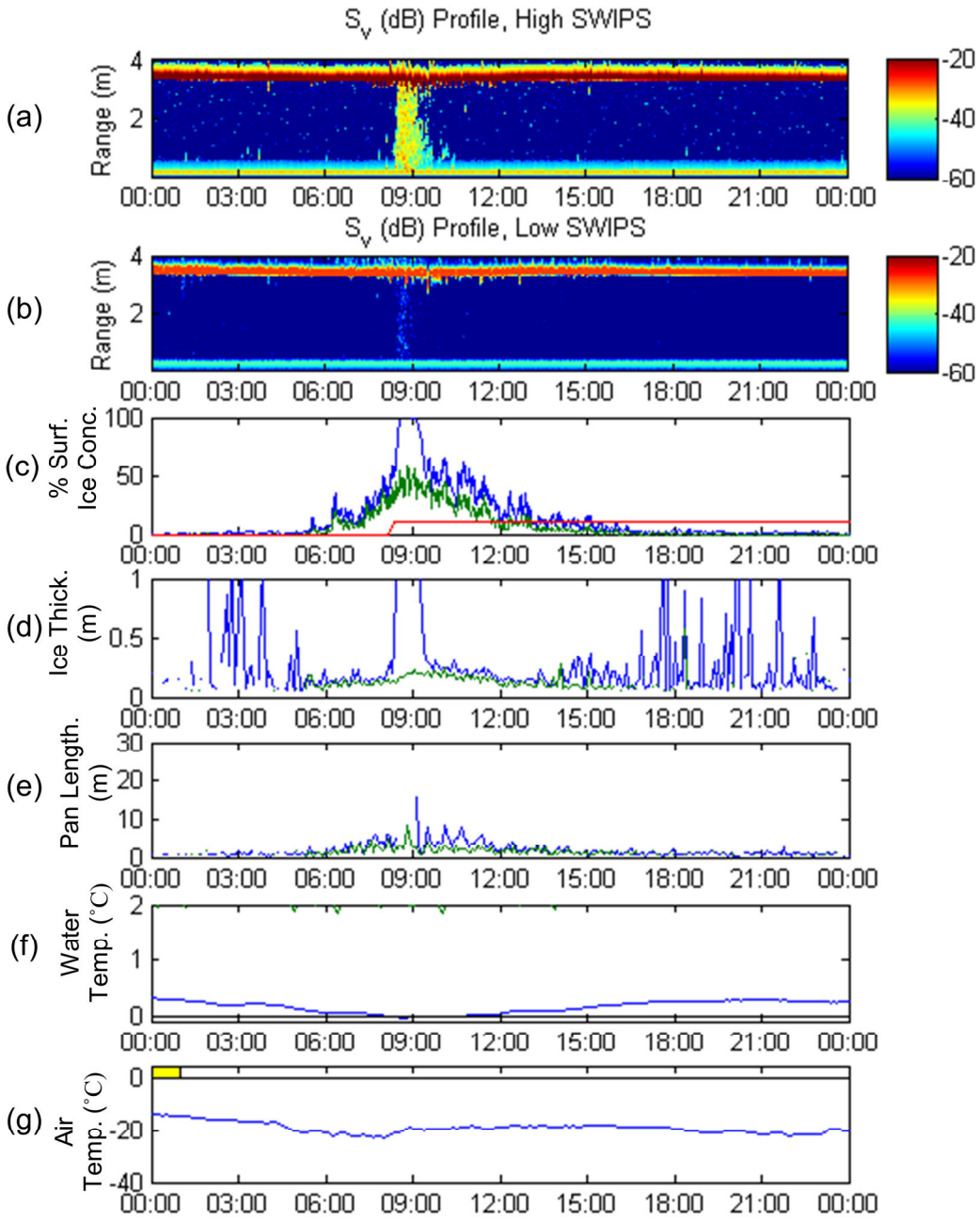

Figure 5-24. Surface ice analysis figure from 29-Dec-10 displaying: (a) high frequency sonar S_v profile, (b) low frequency sonar S_v profile, (c) surface ice concentrations from the SLR camera (red), high (blue), low (green) frequency sonars, (d) High (blue) and low (green) frequency pan thicknesses, (e) High (blue) and low (green) frequency pan lengths, (f) water temperatures 45 m (blue) and 15 m (green) from the right bank and (g) Air temperature (blue) and snowfall presence (yellow).

6. Suspended Frazil Events

In this chapter, the S_v return profiles produced from the high (546 kHz) and low (235 kHz) frequency sonars were used to study suspended frazil events. Depth averaged S_v and s_{v1}/s_{v2} time series were calculated from processed sonar data (Section 3.2.8.3). Utilizing primarily the s_{v1}/s_{v2} time series, the start and end times of frazil events were identified and classified based upon their intensity and vertical distribution in the water column. Combining this frazil data with hydrological and meteorological data, the formation conditions at the time of the onset of frazil events were determined.

6.1. Synopsis of Suspended Frazil Events

Suspended frazil properties were examined by plotting suspended ice analysis figures displaying S_v profile time series from the high and low frequency sonars, depth averaged S_v, s_{v1}/s_{v2}, water temperature, air temperature, precipitation and GBWTP outfall discharge. Figure 6-1 provides an example of these figures with the remainder available in Appendix C.

As discussed in Section 3.2.8.3, strong returns in the S_v profile plots of the high frequency sonar and elevated s_{v1}/s_{v2} values indicate the presence of suspended frazil. Additional evidence that the detected suspended particles are frazil is the presence of super-cooled water, since super cooling is a prerequisite for frazil ice formation (Ashton, 1986). Using these parameters, frazil events were identified in the suspended ice analysis figures.

The first suspended frazil event of the 2010/11 winter season was recorded from 8:00 to 10:00 on 17-Nov-10 (Figure 6-1). At approximately 18:00 on 17-Nov-10, a more intense frazil occurred, which lasted until 09:00 on 18-Nov-10 (Figure 6-2). The final freeze-up frazil event appeared at 16:00 on 18-Nov-10 and lasted until 6:30 on 19-Nov-10 (Figure 6-3). No suspended frazil was observed from 6:30 to 23:00 on 19-Nov-10 when the freeze front passed the instruments.

Every freeze-up frazil event followed a similar pattern, except for an event occurring at 08:00 on 17-Nov-10. The initial vertical distribution in the water column of the frazil was evenly distributed (i.e. well mixed) and the most intense sonar returns occurred in the first 1-6 hours of the event. The event occurring at 08:00 on 17-Nov-10 began concentrated towards the bed. As each event progressed, the intensity (S_v and s_{v1}/s_{v2}) was reduced and the vertical distribution of the targets became concentrated towards the bed. The 08:00 on 17-Nov-10 event began concentrated towards the bed but otherwise followed the same pattern; the most intense returns occurred at approximately 08:30 and as the event subsided, the intensity of the event reduced and the vertical distribution shifted more towards the bed.

Once the GBWTP outfall's thermal plume formed the open lead and exposed the sonar instruments to open water again, suspended frazil events were detected by the sonar instruments throughout the winter. The start and end time of open lead frazil events were identified based upon the time when s_{v1}/s_{v2} values rose above

the ambient background levels (ambient levels are the baseline acoustic returns without suspended targets).

Examples of open lead suspended frazil events are shown in Figure 6-4 through to Figure 6-8. Most open lead frazil events had clearly defined start and end times (In contrast to freeze-up events, which had obvious start times but ambiguous end times). In total, 30 suspended frazil events were detected in the open lead and their start and end times are listed in Table 6-1. Every open lead frazil event began between the hours of 05:30 and 11:00. Average and maximum durations were 2 hours and 4.5 hours, respectively.

The open lead suspended frazil events were classified according to the vertical distribution of frazil in the water column and the intensity of the acoustic signals. Vertical distribution was described as 'well mixed' if the values of S_v did not vary significantly over the depth, which is the case for the event in Figure 6-8. If the S_v values were elevated near the bed and lower near the surface, they were classified as 'bed concentrated', which is the case for the events shown in Figures 6-5, 6-6 and 6-7. Frazil event intensities were quantified using the 15 minute moving average of s_{v1}/s_{v2} at the mid-point of each event. The 15 minute moving average was applied to obtain a more representative estimate of the event intensity during the events that were more oscillatory, such as the event occurring in Figure 6-6. Intensities were divided into three categories: light (s_{v1}/s_{v2}) < 50), medium (50 ≤ $s_{v1}/s_{v2} \geq 100$), heavy ($s_{v1}/s_{v2} > 100$). Examples of light, medium and heavy frazil events are shown in Figure 6-5, Figure 6-6 and Figure 6-8, respectively.

These classification of events based on intensity was affected by changes in the ambient (background values when no suspended particles are present) s_{v1}/s_{v2} values. This ambient level varied as a result of changes in the gain settings and possibly pulse lengths; these settings are listed in Table 3-11. From 9-Dec-10 to 21-Dec-10 and from 17-Feb-11 to 14-Mar-11, the high and low frequency sonars' gains were set to 3 and during these times the ambient s_{v1}/s_{v2} values were ~1. However, when the gain of either unit was reduced to 1, the ambient s_{v1}/s_{v2} increased to ~5. An example of this change is displayed in Figure 6-9, where at 10:00 the low frequency sonar's gain was increased from 1 to 3.

Table 6-1. List of start and end times of suspended frazil events identified in the open lead with vertical distributions and intensities.

Start Time	End Time	Vertical Distribution	Intensity
12/29/10 8:30	12/29/10 9:30	Well Mixed	Medium
12/31/10 9:00	12/31/10 11:00	Well Mixed	Low
1/9/11 11:00	1/9/11 13:00	Well Mixed	Heavy
1/10/11 9:00	1/10/11 11:00	Bed Concentrated	Low
1/11/11 8:30	1/11/11 10:30	Bed Concentrated	Heavy
1/12/11 11:00	1/12/11 11:30	Bed Concentrated	Heavy
1/13/11 9:30	1/13/11 12:00	Bed Concentrated	Low
1/14/11 8:30	1/14/11 12:00	Bed Concentrated	Medium
1/15/11 8:00	1/15/11 11:00	Bed Concentrated	Low
1/16/11 9:30	1/16/11 11:00	Bed Concentrated	Low
1/17/11 8:30	1/17/11 9:30	Bed Concentrated	Low
1/30/11 9:30	1/30/11 11:00	Bed Concentrated	Low
1/31/11 8:30	1/31/11 9:00	Bed Concentrated	Low
2/1/11 7:30	2/1/11 10:30	Well Mixed	Medium
2/16/11 6:30	2/16/11 9:00	Bed Concentrated	Low
2/16/11 9:00	2/16/11 11:30	Well Mixed	Heavy
2/17/11 6:00	2/17/11 10:30	Well Mixed	Heavy
2/18/11 8:00	2/18/11 10:00	Well Mixed	Heavy
2/19/11 8:00	2/19/11 10:00	Well Mixed	Medium
2/20/11 6:00	2/20/11 8:30	Well Mixed	Medium
2/20/11 8:30	2/20/11 10:00	Well Mixed	Low
2/23/11 9:30	2/23/11 11:00	Well Mixed	Medium
2/24/11 6:30	2/24/11 10:30	Well Mixed	Medium
2/25/11 7:00	2/25/11 10:00	Well Mixed	Medium
2/28/11 5:30	2/28/11 9:00	Well Mixed	Heavy
3/1/11 7:30	3/1/11 8:30	Well Mixed	Low
3/2/11 8:30	3/2/11 9:30	Well Mixed	Low
3/4/2011 7:30	3/4/2011 9:00	Well Mixed	Low
3/11/11 8:00	3/11/11 9:30	Well Mixed	Low
3/11/11 8:00	3/11/11 9:30	Well Mixed	Low

6.2. Discussion of Suspended Frazil Features

6.2.1. Suspended Frazil Occurrence

Using the start and end times recorded in Table 6-1, the corresponding available hydrological and meteorological parameters were matched to the events in an expanded table (Available in Appendix D). In this table, the start and end times of the events and the corresponding water temperature, air temperature, GBWTP discharge and temperature, and snowfall presence are listed. These data were used to investigate the conditions that lead to the occurrence of suspended frazil events in the open lead. The following conditions were found to coincide with these events:

- Super-cooled water temperatures (between -0.05˚C and 0˚C)
- Air temperatures between -16˚C and -29˚C
- GBWTP discharges (Q_{GBWTP}) between 0.7 m^3/s and 2.2 m^3/s (1 hour previous to the start time)

Every suspended frazil event occurred below a Q_{GBWTP} of 1.9 m^3/s, except a single event which occurred at a discharge of 2.2 m^3/s. From 1-Dec-10 to 15-Mar-11, Q_{GBWTP} values were below 1.9 m^3/s, 15% of the time. Similarly, air temperatures were below -16˚C for 40% of the time between 1-Dec-10 and 15-Mar-11. It appears that Q_{GBWTP} has the strongest impact upon the production of suspended frazil, while air temperature has a smaller but still significant influence.

The requirement of super cooled water for frazil ice formation is well known to river ice researchers (Ashton, 1986). Super cooling (and subsequent frazil production) in the open lead is a result of sufficient of thermal losses in the open lead upstream of station 56.8 km to dissipate the thermal energy introduced by the GBWTP outfall. An approximate measure of the thermal energy contained in the GBWTP plume is Q_{GBWTP}. A reasonable predictor of the thermal energy lost from the plume as it flows from GBWTP to the measurement site (short of a complete energy budget model) is the air temperature (T_a) minus the water temperature (Hicks *et al.*, 1997). The water temperatures in the open lead ranged between 0 and 1°C for most of the winter and therefore, air temperature alone can be used as a surrogate for the heat loss.

In Figure 6-10 the air temperature (T_a) at the start of each frazil event is plotted versus the GBWTP discharge (Q_{GBWTP}) one hour prior to the event start time, to account for travel time. The 1 hour travel time was found by iteratively testing travel times between 0 and 5 hours. It was found that a travel time of 1 hour produced the strongest correlation between air temperature and discharge. GBWTP water temperature is also likely to affect frazil formation but it only varied by 3°C from (12°C to 15°C) over the winter and this is assumed to be insignificant compared to air temperature variations of 0°C to -35°C. In this figure, the line shown indicates frazil events will not occur at air temperatures above that specified by;

$$T_a = 6.87{Q_{GBWTP}}^2 - 31.4Q_{GBWTP} + 14.3 \qquad [6\text{-}1]$$

A linear form of Equation 6-1 is also shown in Figure 6-10. This equation illustrates that a possible linear relationship exists between the upstream GBWTP discharge (Q_{GBWTP}) and the air temperature (T_a) as expressed by;

$$T_a = -10Q_{GBWTP} \quad [6\text{-}2]$$

Based upon Equation 6-2, every 1 m^3/s of discharge at station 50.3 km requires an additional -10˚C to cool the water to reach super cooling by the time it reaches station 56.8 km. Without additional measurements of suspended frazil events, it is difficult which of Equation 6-1 and Equation 6-2 is the more descriptive of the cooling processes in the GBWTP open lead. However, both equations provide an upper limit for the air temperatures which will allow for suspended frazil formation.

Frazil events that coincided with snow are denoted in Figure 6-10. The events associated with snowfall do not deviate in a notable way from the rest of the observed events, and therefore it can be concluded that the presence of snowfall does not have any effect upon the required air temperatures for frazil formation. However, since only 7 events were observed with snowfall, it is possible that an effect of snowfall on frazil events would be visible with a larger number of samples.

6.2.2. Suspended Frazil Intensity and Vertical Distribution

To determine whether frazil event intensity is also correlated with Q_{GBWTP} and T_a, the same data with frazil event intensity denoted (low, medium, high) were plotted in Figure 6-11. No correlation with intensity is evident in this figure. This is consistent with Morse and Richard (2009), who concluded that frazil event intensities were controlled by the strength of the turbulence rather than meteorological conditions. Morse and Richard (2009) hypothesized that stronger turbulence kept frazil particles entrained longer and that it also re-entrained ice particles deposited on the undersides of pans arriving from upstream. In this study, the effect of turbulence could not be investigated because only water velocity data collected were profiles averaged over a 2 or 5 minute interval.

Of the 30 open lead suspended frazil events observed, 11 were classified as bed concentrated. It is possible that these near bed concentrations are a result of changes in the high frequency sonar instrument's settings. All of these bed-biased frazil events occurred during the period of time in which the high frequency sonar's pulse length was set to 68μs pulse length and the high frequency sonar's gain was set to 1(21-Dec-10 to 17-Feb-11).

Another possible explanation for the bed concentrated frazil events is that although the plume from the Clover Bar Energy Centre outfall ~50 m upstream was not detected by the sonar instrument's water temperature sensors, it is possible that the plume was able to spread over the water surface, melting the

frazil nearer to the surface. All of the near bed frazil events coincided with elevated water temperature by the near shore temperature sensor (15 m from the right bank at station 56.8 km). Figure 6-11(a) displays an example of a near bed frazil event occurring alongside a rise in the near shore water temperature sensor (Figure 6-11(f)).

Bed concentrated frazil distributions were also seen at end of each freeze-up frazil event (Figure 6-1 to Figure 6-3). This could possibly be a result of suspended frazil particles adhering to the underside of frazil pans while the deeper frazil particles remain entrained in the flow. This same mechanism may have affected the open lead pan events.

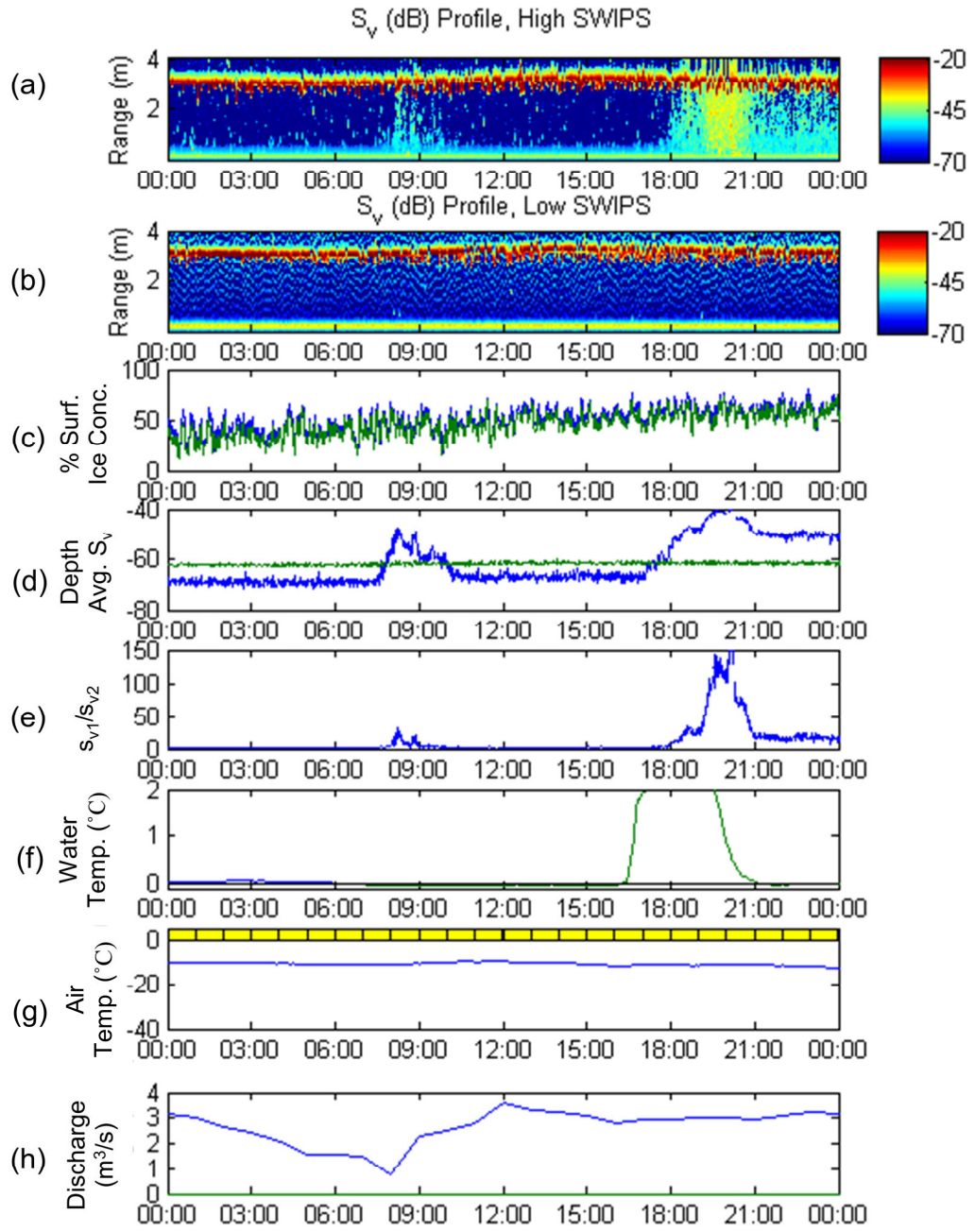

Figure 6-1. Suspended ice analysis figure from 17-Nov-2010 displaying: (a) high frequency sonar S_v profile, (b) low frequency sonar S_v profile, (c) surface ice concentrations from the high (blue) and low (green) frequency sonars, (d) high (blue) and low (green) frequency sonar depth averaged S_v plots, (e) s_{v1}/s_{v2} ratio, (f) water temperatures 45 m (blue) and 15 m (green) from the right bank, (g) air temperature (blue) and snowfall presence (yellow) and (h) discharge from GBWTP outfall (blue) and combined sewer overflow (green).

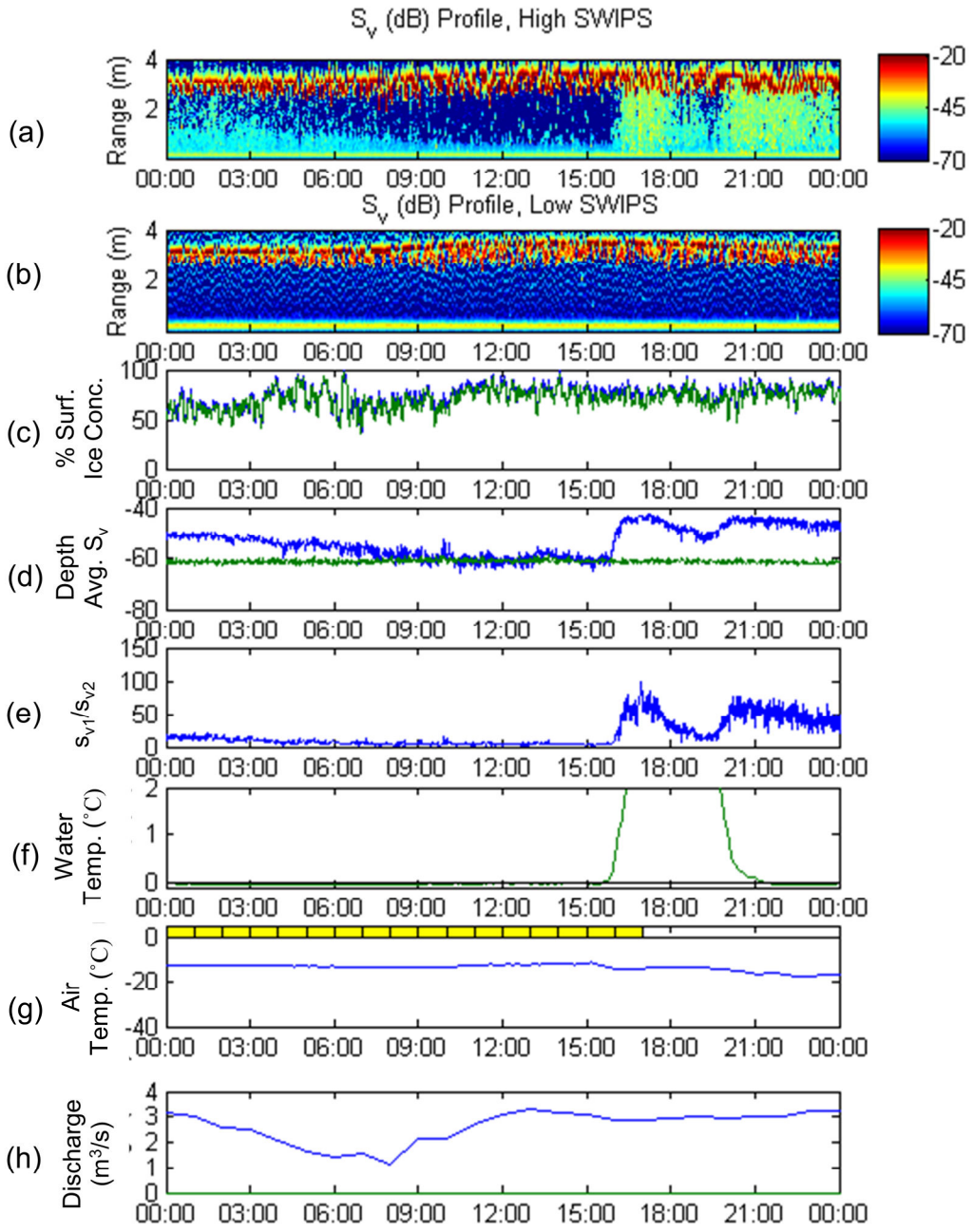

Figure 6-2. Suspended ice analysis figure from 18-Nov-2010 displaying: (a) high frequency sonar S_v profile, (b) low frequency sonar S_v profile, (c) surface ice concentrations from the high (blue) and low (green) frequency sonars, (d) high (blue) and low (green) frequency sonar depth averaged S_v plots, (e) s_{v1}/s_{v2} ratio, (f) water temperatures 45 m (blue) and 15 m (green) from the right bank, (g) air temperature (blue) and snowfall presence (yellow) and (h) discharge from GBWTP outfall (blue) and combined sewer overflow (green).

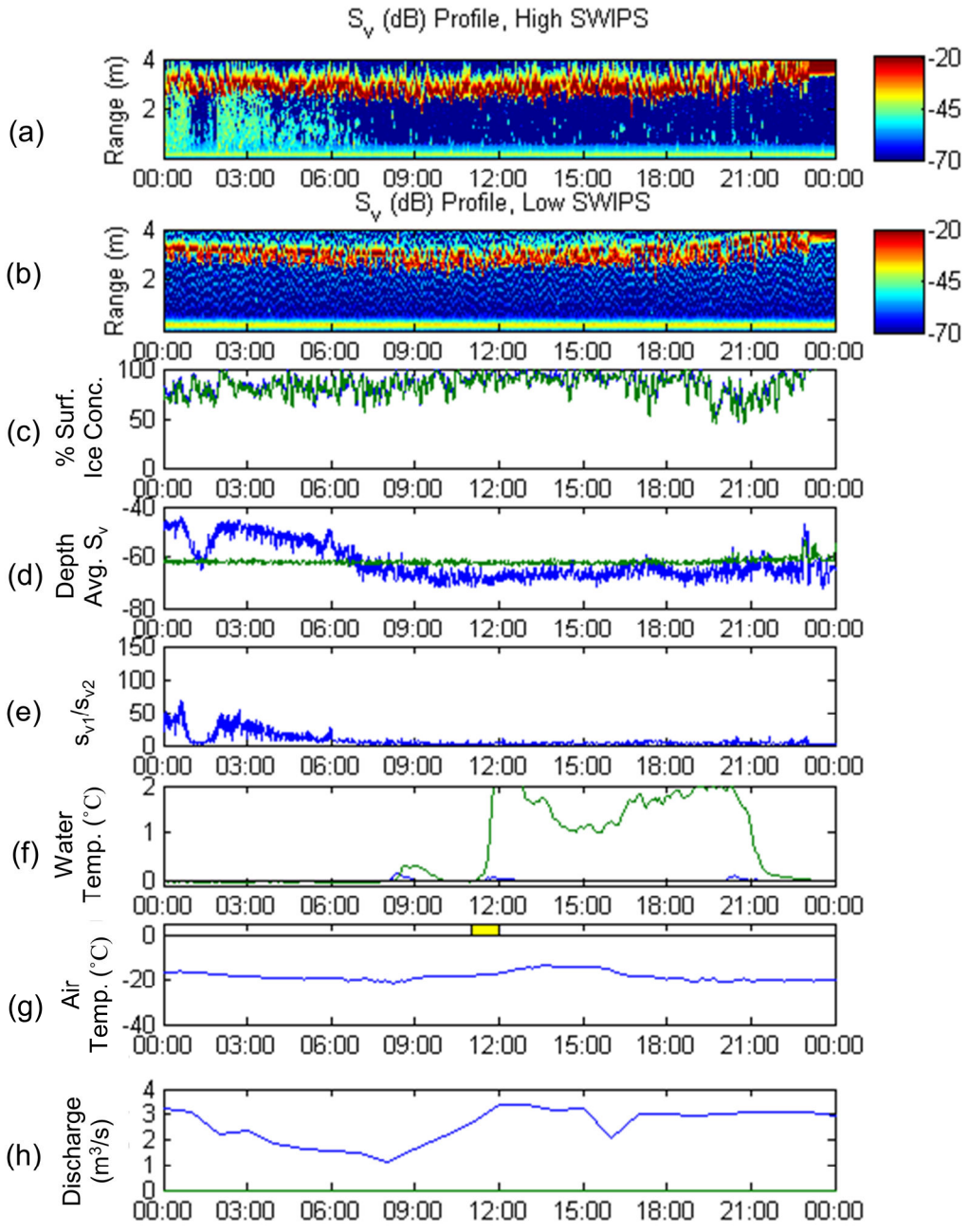

Figure 6-3. Suspended ice analysis figure from 19-Nov-2010 displaying: (a) high frequency sonar S_v profile, (b) low frequency sonar S_v profile, (c) surface ice concentrations from the high (blue) and low (green) frequency sonars, (d) high (blue) and low (green) frequency sonar depth averaged S_v plots, (e) s_{v1}/s_{v2} ratio, (f) water temperatures 45 m (blue) and 15 m (green) from the right bank, (g) air temperature (blue) and snowfall presence (yellow) and (h) discharge from GBWTP outfall (blue) and combined sewer overflow (green).

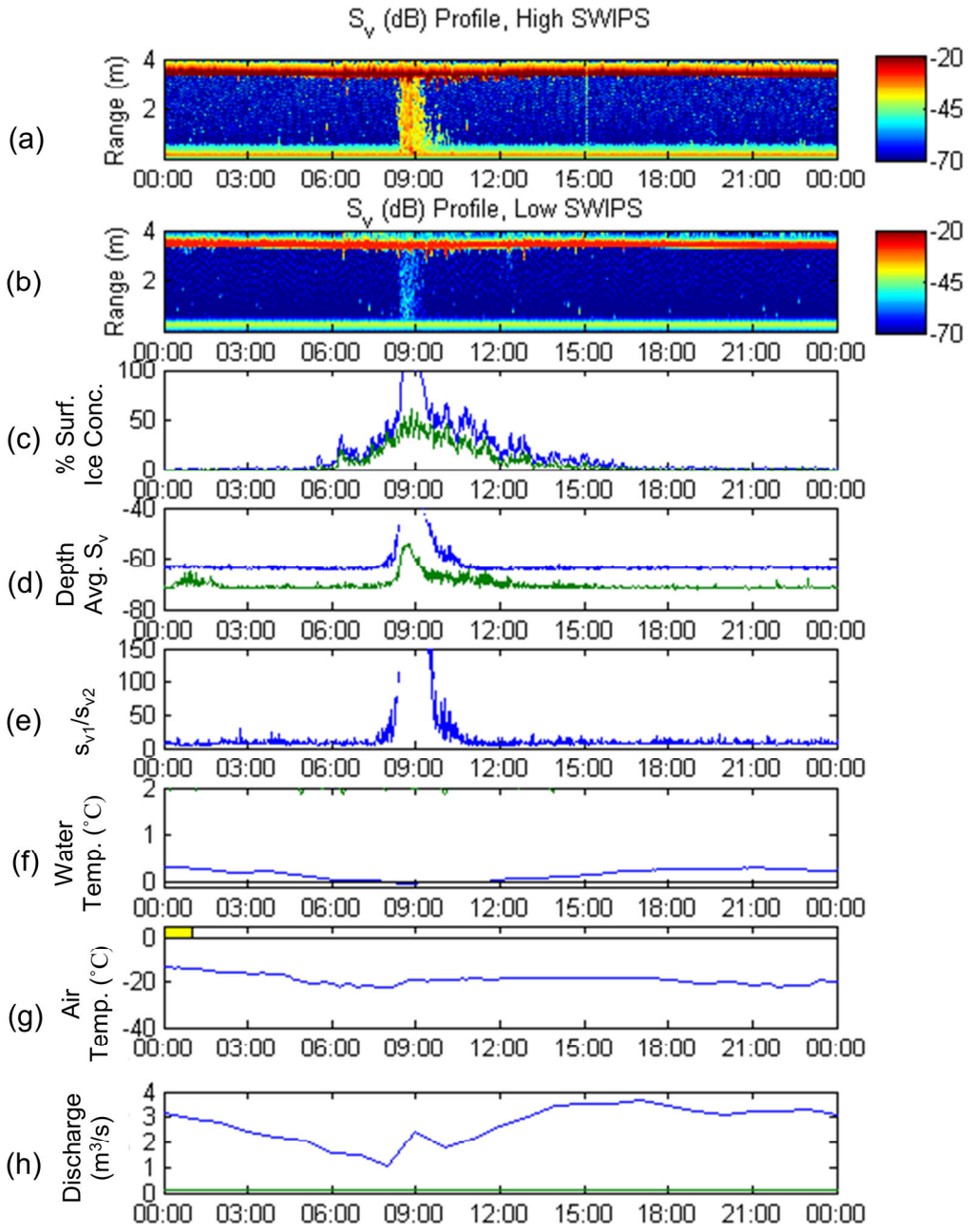

Figure 6-4. Suspended ice analysis figure from 29-Dec-10 displaying (a) high frequency sonar S_v profile, (b) low frequency sonar S_v profile, (c) surface ice concentrations from the high (blue) and low (green) frequency sonars, (d) high (blue) and low (green) frequency sonar depth averaged S_v plots, (e) s_{v1}/s_{v2} ratio, (f) water temperatures 45 m (blue) and 15 m (green) from the right bank, (g) air temperature (blue) and snowfall presence (yellow) and (h) discharge from GBWTP outfall (blue) and combined sewer overflow (green).

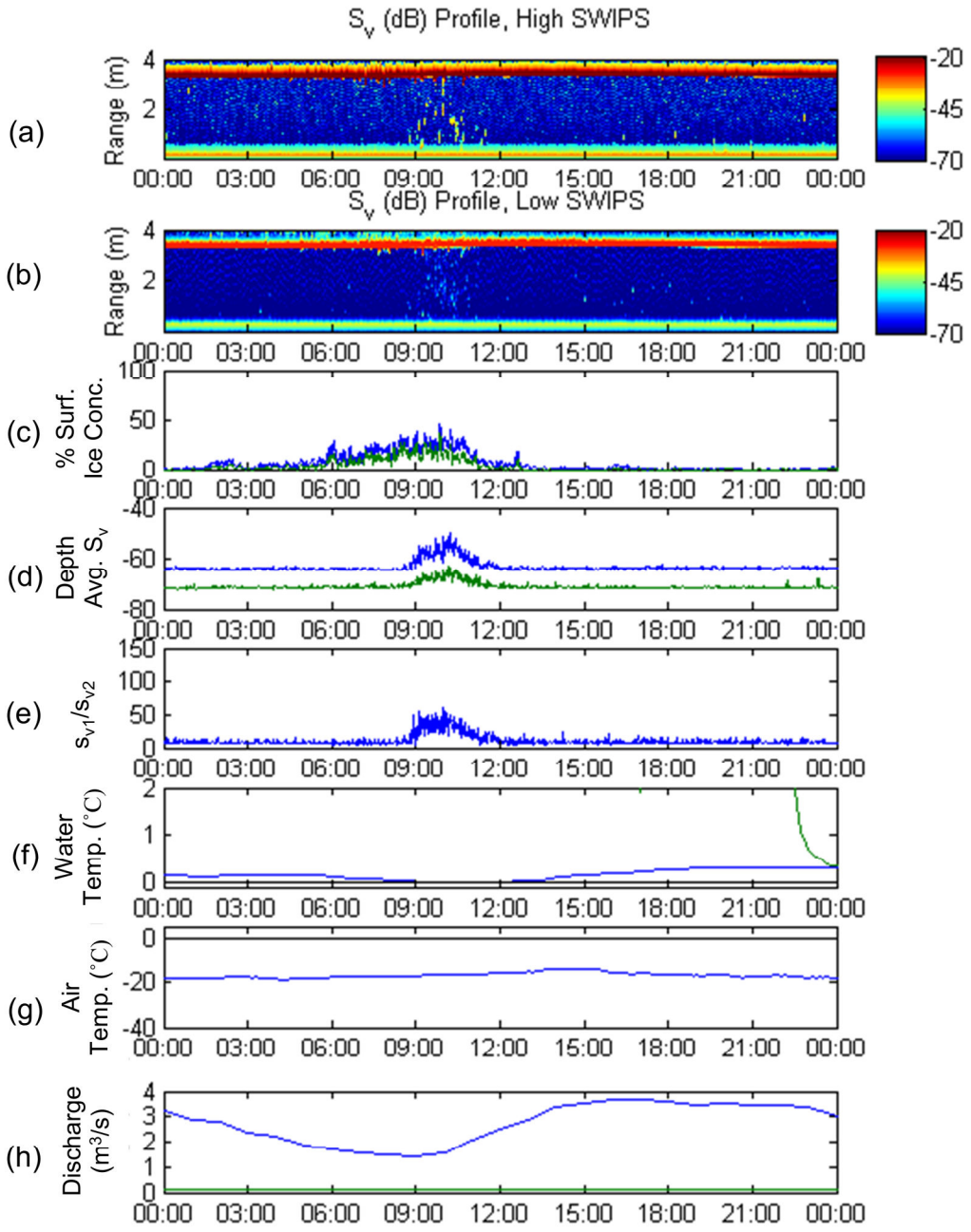

Figure 6-5. Suspended ice analysis figure from 31-Dec-10 displaying: (a) high frequency sonar S_v profile, (b) low frequency sonar S_v profile, (c) surface ice concentrations from the high (blue) and low (green) frequency sonars, (d) high (blue) and low (green) frequency sonar depth averaged S_v plots, (e) s_{v1}/s_{v2} ratio, (f) water temperatures 45 m (blue) and 15 m (green) from the right bank, (g) air temperature (blue) and snowfall presence (yellow) and (h) discharge from GBWTP outfall (blue) and combined sewer overflow (green).

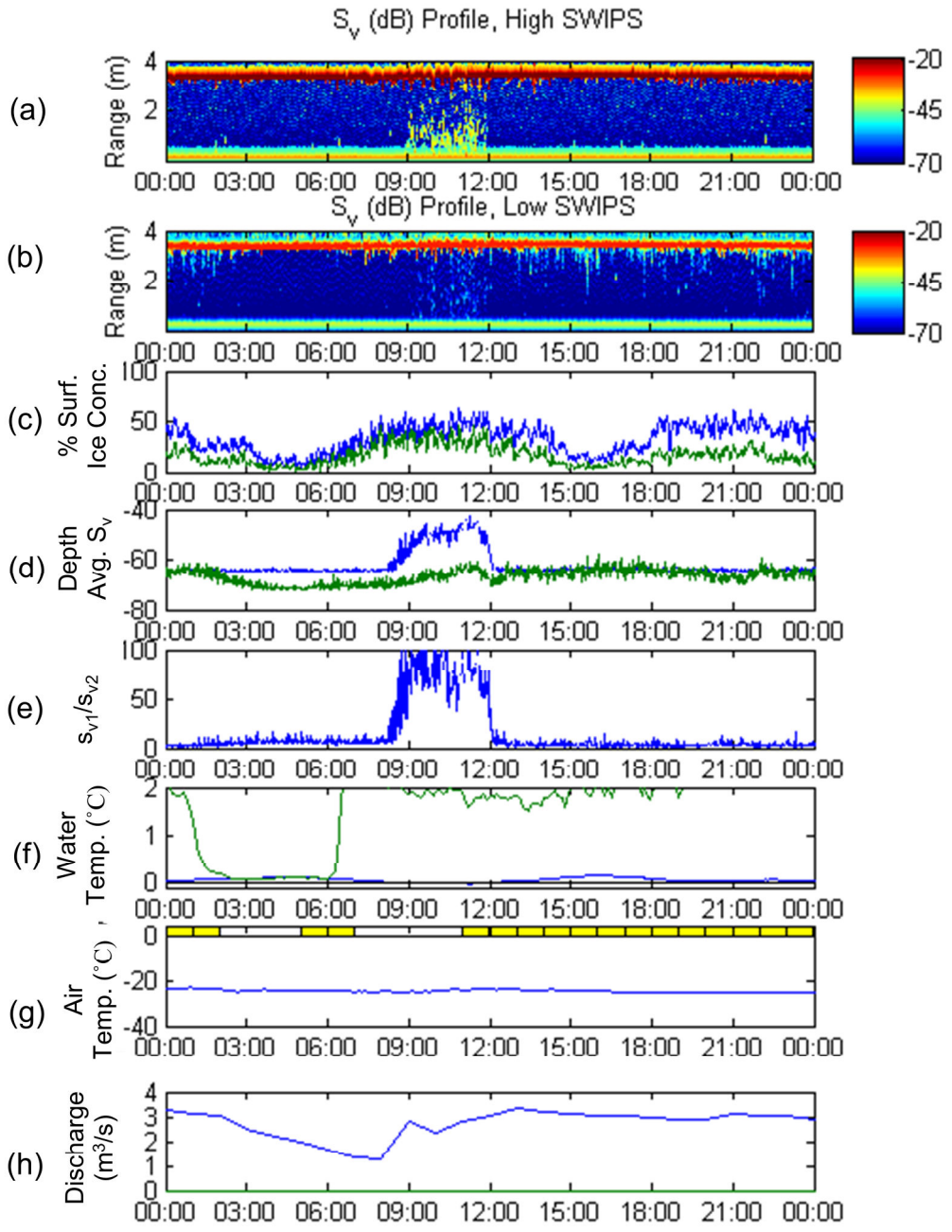

Figure 6-6. Suspended ice analysis figure from 14-Jan-2011 displaying: (a) high frequency sonar S_v profile, (b) low frequency sonar S_v profile, (c) surface ice concentrations from the high (blue) and low (green) frequency sonars, (d) high (blue) and low (green) frequency sonar depth averaged S_v plots, (e) s_{v1}/s_{v2} ratio, (f) water temperatures 45 m (blue) and 15 m (green) from the right bank, (g) air temperature (blue) and snowfall presence (yellow) and (h) discharge from GBWTP outfall (blue) and combined sewer overflow (green).

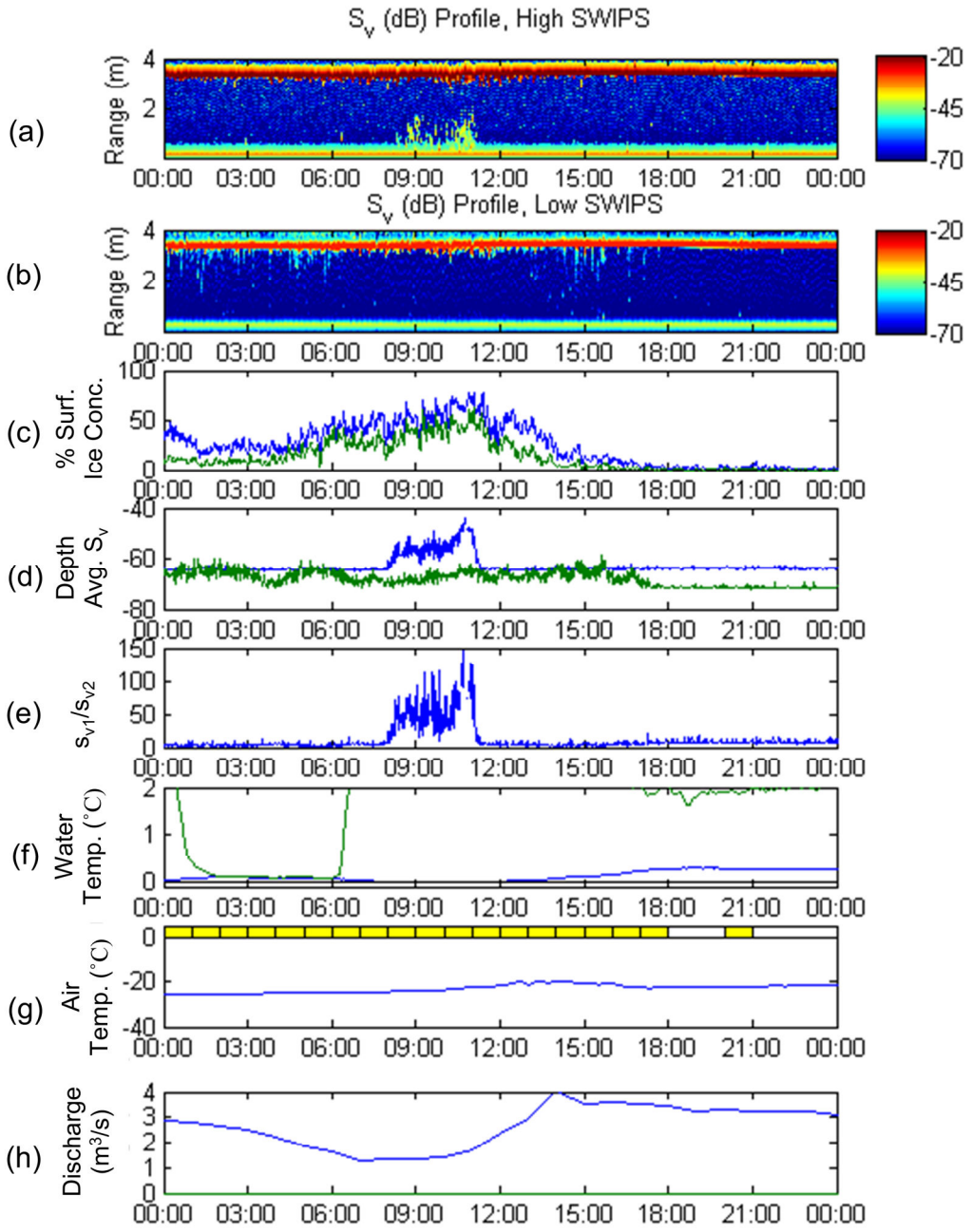

Figure 6-7. Suspended ice analysis figure from 15-Jan-2011 displaying: (a) high frequency sonar S_v profile, (b) low frequency sonar S_v profile, (c) surface ice concentrations from the high (blue) and low (green) frequency sonars, (d) high (blue) and low (green) frequency sonar depth averaged S_v plots, (e) s_{v1}/s_{v2} ratio, (f) water temperatures 45 m (blue) and 15 m (green) from the right bank, (g) air temperature (blue) and snowfall presence (yellow) and (h) discharge from GBWTP outfall (blue) and combined sewer overflow (green).

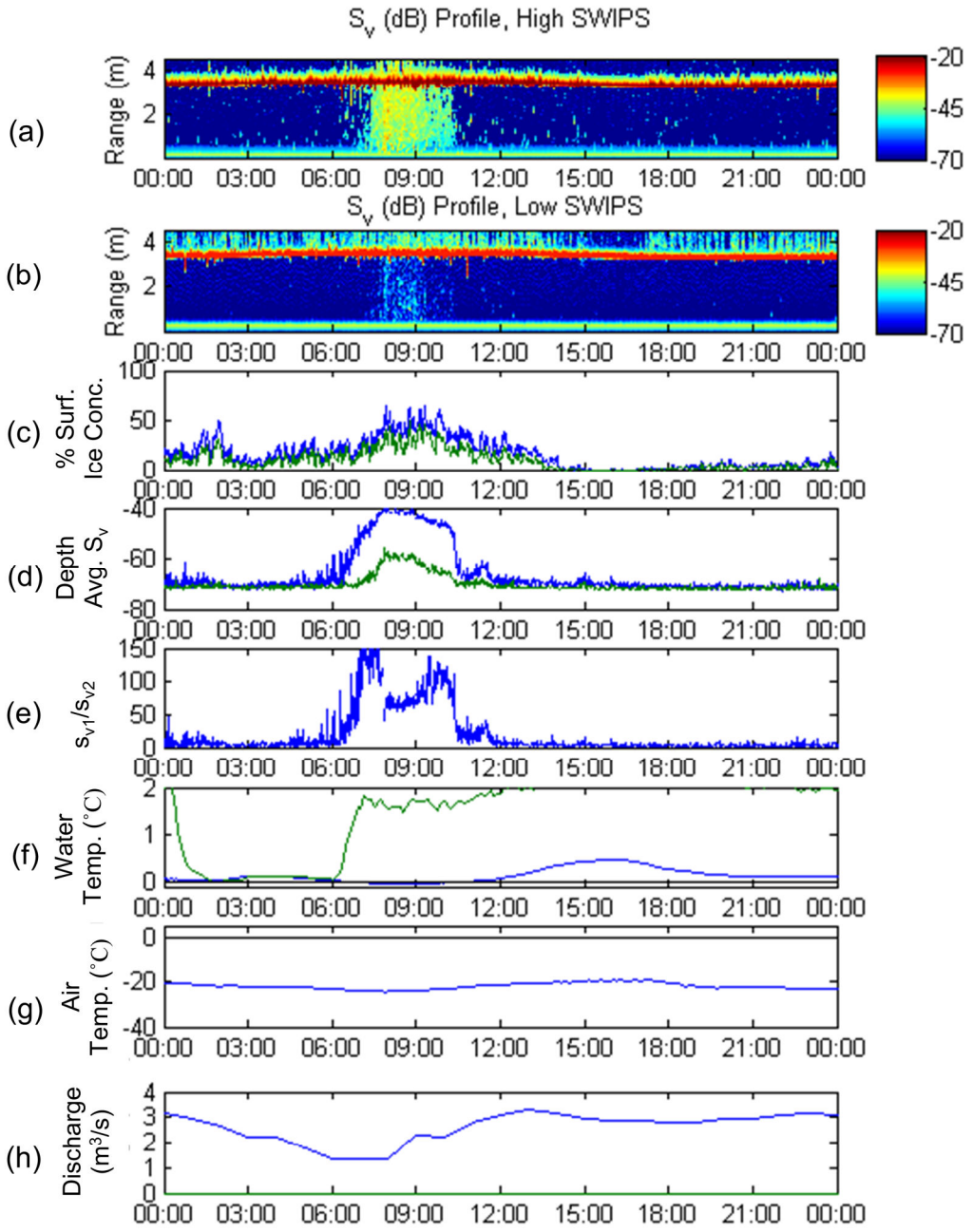

Figure 6-8. Suspended ice analysis figure from 24-Feb-2011 displaying: (a) high frequency sonar S_v profile, (b) low frequency sonar S_v profile, (c) surface ice concentrations from the high (blue) and low (green) frequency sonars, (d) high (blue) and low (green) frequency sonar depth averaged S_v plots, (e) s_{v1}/s_{v2} ratio, (f) water temperatures 45 m (blue) and 15 m (green) from the right bank, (g) air temperature (blue) and snowfall presence (yellow) and (h) discharge from GBWTP outfall (blue) and combined sewer overflow (green).

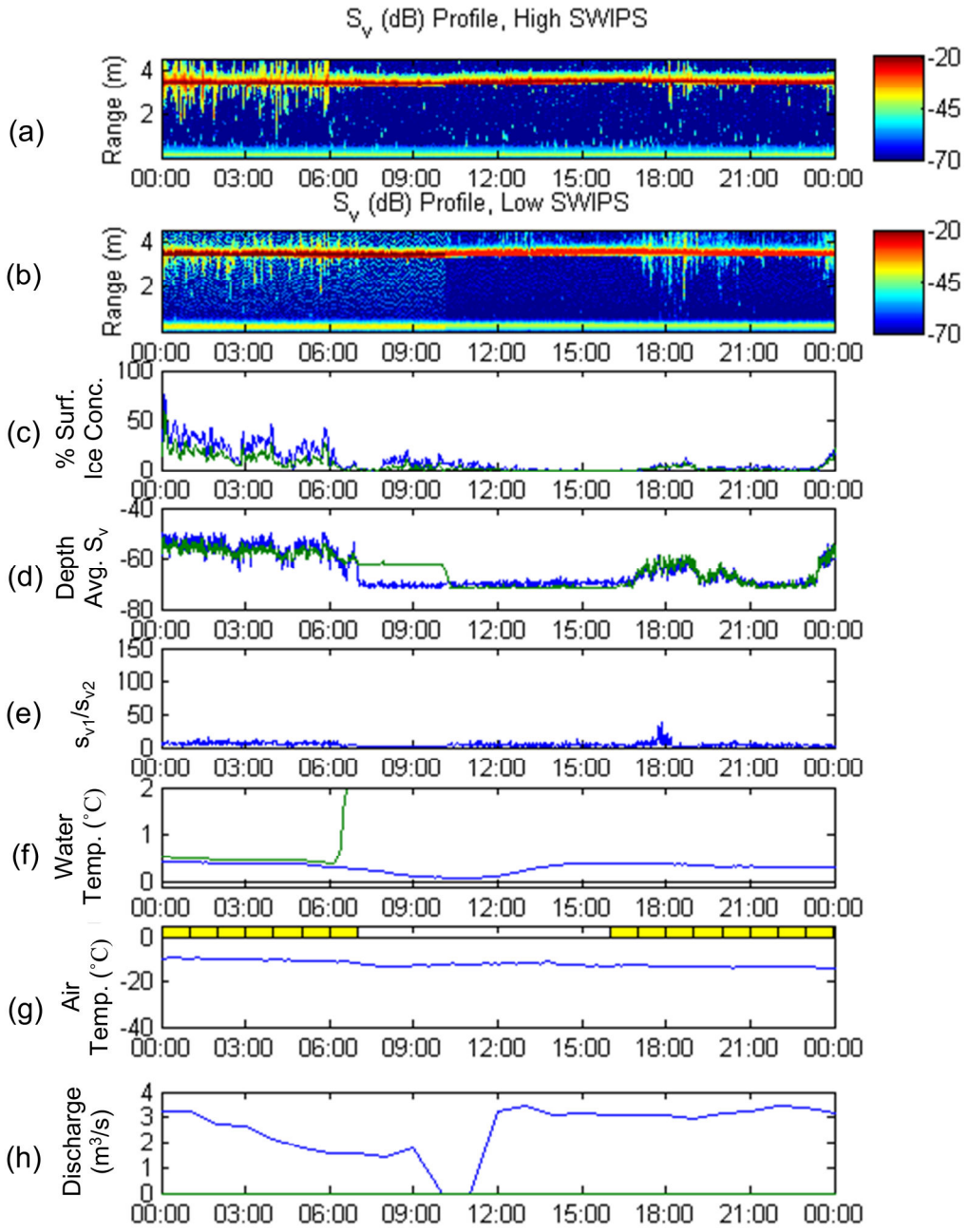

Figure 6-9. Suspended ice analysis figure from 9-Dec-2010 displaying: (a) high frequency sonar S_v profile, (b) low frequency sonar S_v profile, (c) surface ice concentrations from the high (blue) and low (green) frequency sonars, (d) high (blue) and low (green) frequency sonar depth averaged S_v plots, (e) s_{v1}/s_{v2} ratio, (f) water temperatures 45 m (blue) and 15 m (green) from the right bank, (g) air temperature (blue) and snowfall presence (yellow) and (h) discharge from GBWTP outfall (blue) and combined sewer overflow (green).

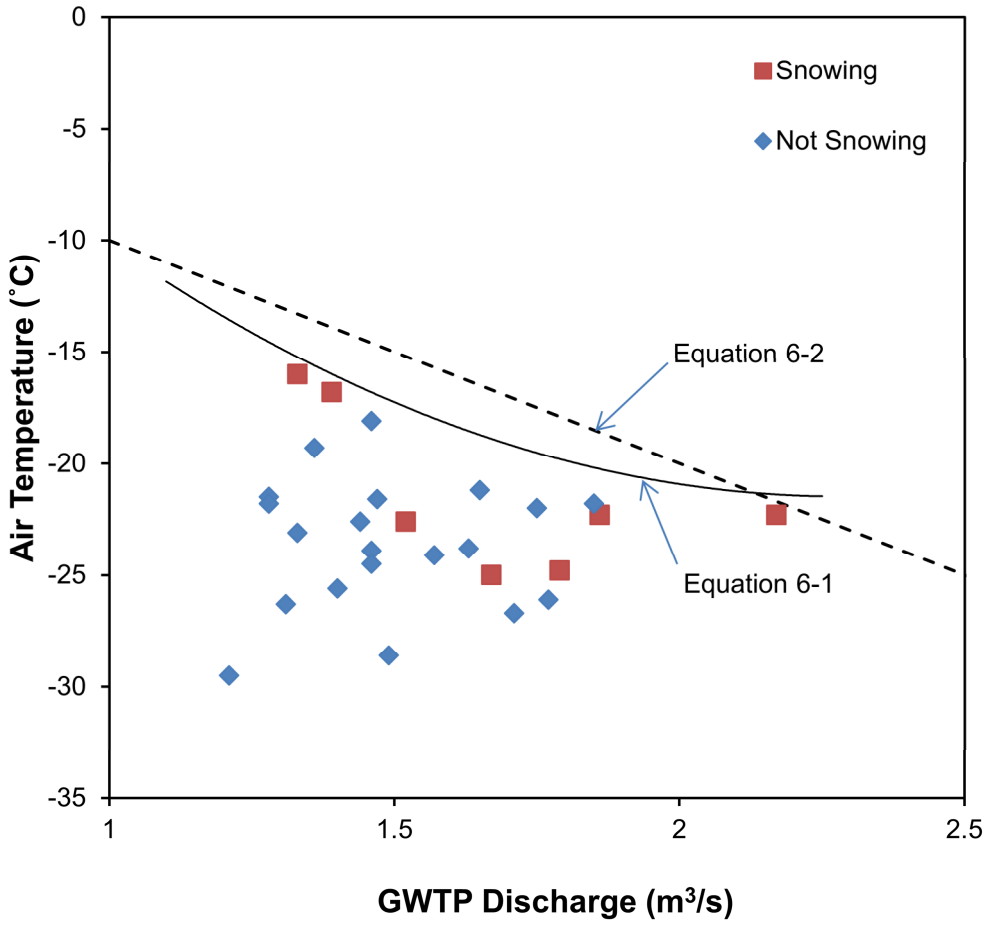

Figure 6-10. Plot of the air temperatures versus GBWTP discharges during each recorded suspended frazil event in the open lead.

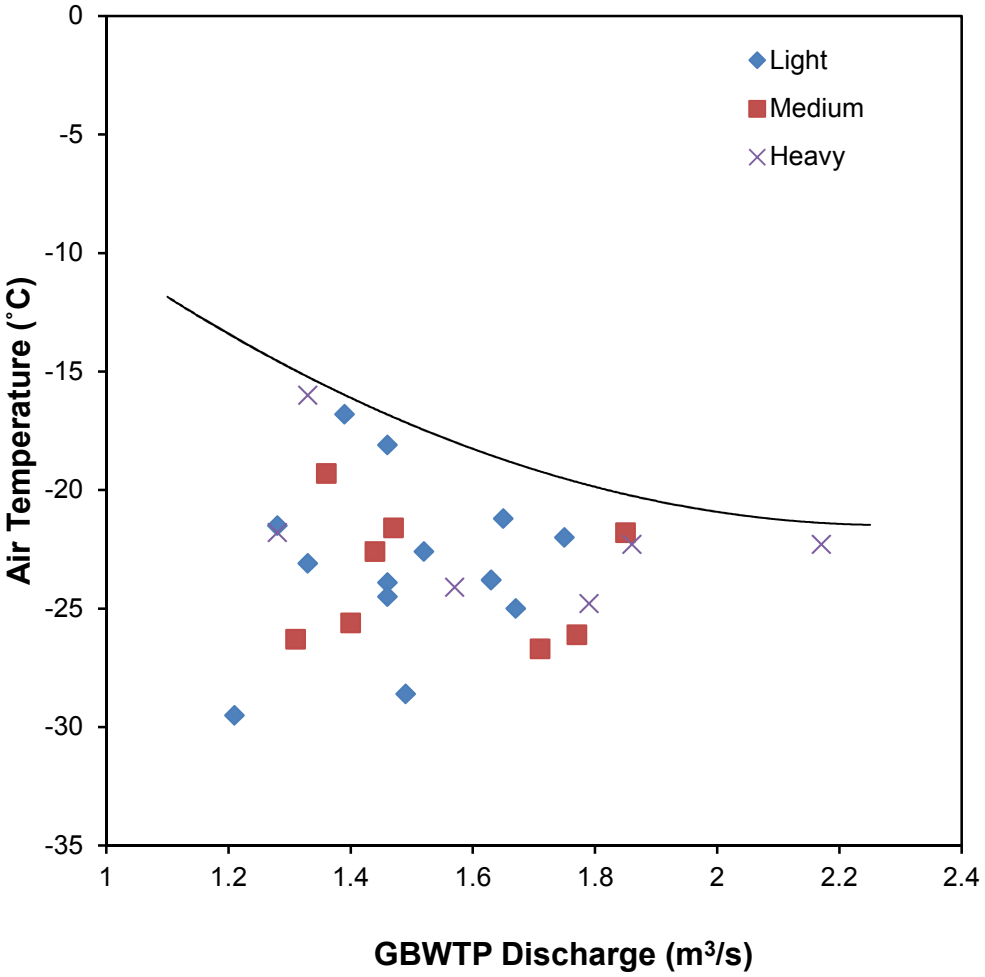

Figure 6-11. Plot of the air temperatures versus GBWTP discharges during each recorded suspended frazil event in the open lead for light, medium and heavy intensity events.

7. Conclusions and Recommendations

This thesis characterized the 2010/11 winter ice regime on the North Saskatchewan within the Edmonton city limits. The progression of freeze-up was also characterized. The locations and sizes of open leads were also documented, focusing upon the open lead created by the Gold Bar Wastewater Treatment Plant (GBWTP) outfall. Mid-winter suspended frazil events occurring within the GBWTP open lead were recorded. Other floating and suspended ice features occurring during freeze-up and in the open lead were also documented and analyzed. Formation criteria were then developed for the occurrence of suspended frazil events as well as the crusty ice pans resulting from suspended frazil.

Using photographic data of surface ice conditions captured by automated time lapse cameras, the progression of freeze-up, the formation of open leads, and the occurrence of surface ice pans in the GBWTP open lead were recorded. It was found that the progression of freeze-up in the Edmonton reach of the North Saskatchewan River could be divided into two reaches, upstream and downstream of Highway 216 (Anthony Henday) Bridge at station 21.4 km. In the downstream reach, freeze-up progressed in a linear fashion with the freeze-up front beginning somewhere downstream of Edmonton and building steadily upstream. In the upstream reach, multiple mid-channel features provided ample locations for the ice cover to bridge prior to the arrival of the downstream freeze-up front. As a result, an ice cover formed in the upstream reach three days prior to when it formed in the downstream reach.

It was found that open lead frazil pans could be divided into two categories: crusty pans and slushy pans. Crusty pans were dominantly a result of upstream suspended frazil events while slushy pans were formed from entrained snowfall. Crusty and slushy were primarily identified based upon the high and low frequency sonars S_v profiles; crusty pans had S_v values near -20 dB while slushy pans were had S_v values near -35dB. Slushy pans only occurred in above zero water temperatures and it is believed that in super-cooled water the entrained snow slush agglomerates with suspended frazil to form crusty pans.

By cross referencing the start and end time of suspended frazil events (measured by the sonars) with the river water temperature, GBWTP discharge and air temperature; the conditions under which each event occurred were determined. It was found that suspended frazil occurred in super-cooled water, with air temperatures below -16˚C and GBWTP discharges below 2.2 m^3/s. A correlation between air temperatures and GBWTP discharges was found (Equation 6-1) which gave a threshold air temperature for the production of suspended frazil as a function GBWTP discharge.

As discussed in Chapter 1, intakes operating in open leads are vulnerable to suspended frazil adhesion and consequent clogging of the water intake. The operators of these intakes generally only become aware of suspended frazil events after the damage has been done. A myriad of mitigation measures are available, but the majority are much more effective prior to the total clogging of the inlet. The suspended frazil formation threshold specified in Equation 6-1 offers a tool to

these operators which will allow the identification of conditions which are likely to cause suspended frazil formation.

While this result is site specific, the process could be repeated at other sites to produce similar results. It is important to note that Equation 6-1 requires that there be communication between the operators of outfalls and intakes along an open lead. In the case of the GBWTP outfall, the discharge is highly periodic and predictions could also be constructed based time of day as opposed to actual discharge. For other outfalls which may not exhibit the same predictable discharge rates, communication between operators becomes extremely important.

This thesis collated and analyzed a large amount of data collected during the 2010/11 winter season. Despite the large volume of available data, the analysis found that river reach spanning from station 53 km to station 56 km requires further study. A shelf against the right bank in this reach is believed to split the open lead into two flows with separate thermal regimes. This separation allows stronger cooling in the shallower right hand flow, resulting in the formation of suspended frazil and crusty pans. At the downstream of this shelf, the flows recombine, resulting in water temperatures between 0˚C and 0.2˚C with crusty pans.

Too properly investigate this formation process, additional data should be collected in future seasons. Detailed bathymetry in this reach is required, as the currently available bathymetry is out dated and coarsely spaced. Water

temperature measurements in the right and left hand flows would also capture this differential cooling. Two dimensional hydraulic and thermal modeling in this reach would also improve the understanding of this process.

While the SWIPS provides an unprecedented level of documentation for suspended and floating ice particles in shallow rivers, it is still not possible to calculate actual particle sizes and concentrations. Further research and development of the SWIPS instrument by its users and the manufacturer may allow these relations to be determined (Ghobrial et al, 2012). Similarly, in-situ observations (underwater photography or direct sampling) of suspended ice particles to determine actual sizes, shapes and concentrations in the field will complement and validate this research. A quantification of particle sizes and concentrations will allow for the investigation of ice production volumes, particle rise velocities and particle growth rates.

8. Cited References

Ashton, G.D., 1986. River and Lake Ice Engineering. Water Resources Publications, Littleton, Colorado.

ASL Environmental Services, 2011. SWIP Brochure. Victoria, B.C. url:http://www.aslenv.com/brochures/SWIP-11.pdf

Buermans, J., Fissel, D., Kanwar, A. 2011. Seven Years of SWIPS Measurements, Applications and Development: Where, How and What Can the Technology Do for Us. 16th Workshop on River Ice. Winnipeg, MB.

Canon Inc., 2007. EOS5D Digital: English Instruction Manual. Canon Marketing Japan Inc., Tokyo, Japan. pp. 174.

Campbell Scientific, 2003. Model 107 and 107B Temperature Probes Instruction Manual. Edmonton, AB., url:http://www.campbellsci.ca/Catalogue/107B.html

Campbell Scientific, 2007. CC640 Digital Camera Instruction Manual. Edmonton, AB. url:http://www.campbellsci.ca/Catalogue/CC640_Man.pdf

Choles, J. 1997. Analysis of the Post-regulation Freeze-up Regime on the North Saskatchewan River. Masters of Science Thesis in Water Resources Engineering. Department of Civil and Environmental Engineering, University of Alberta, pp 17.

Daly, S., 1991. Frazil Blockages of Intake Trash Racks. Cold Regions Technical Digest. No. 91-1.

Daly, S., Haynes, D., Garfield, D., Clark, C., 1992. Field Test of a Surface Heated Trash Rack to Prevent Frazil Ice Blockage. IAHR Symposium. Banff, AB. pp. 71-77.

Environment Canada. 2011a. National Climate Data and Information Archive-Edmonton City Centre AWOS (Climate ID 3012202). Edmonton, AB. website: www.climate.weatheroffice.gc.ca.

Environment Canada. 2011b. Water Survey of Canada-North Saskatchewan River at Edmonton (05DF001). Edmonton, AB. website: http://www.wsc.ec.gc.ca.

Gerard, R. and Andres, D. 1982. Hydraulic roughness of freeze-up ice accumulations: North Saskatchewan River through Edmonton. Proc. 2nd Workshop on the Hydraulics of Ice Covered Rivers, Edmonton, Alberta. pp 62-87.

Ghobrial, T., Loewen, M. and Hicks, F. 2009. SWIPS Field Deployment during Freeze-up 2008. Poster, 15th Workshop on the Hydraulics of Ice Covered Rivers. St. John's, NL.

Ghobrial, T., Loewen, M., Hicks, F. and Maxwell, J. 2010. 2010 Monitoring Frazil Ice Evolution during Freeze-up using the Shallow Water Ice Profiling Sonar. Proc. 20th IAHR International Symposium on Ice, Lahti, Finland.

Ghobrial, T., Loewen, M., Hicks, F., 2011. Laboratory calibration of upward looking sonars for measuring suspended frazil ice concentration. University of Alberta. Edmonton, AB, pp. 19-31.

Ghobrial, T. 2013. Future Thesis Unnamed as of January 2012. Doctorate of Philosophy Thesis in Water Resources Engineering. Department of Civil and Environmental Engineering, University of Alberta.

Hicks, F., Cui, W., Andres, D. 1997. Modeling thermal breakup on the Mackenzie River at the Outlet of Great Slave Lake, N.W.T., Canadian Journal of Civil Engineering, Vol. 24, No. 4, pp. 570-585.

Henderson, F., 1966. Open Channel Flow. Prentice Hall. Upper Saddle River, New Jersey.

Jasek, M., Marko, J., Fissel, D., Clarke, M. and Buermans, J. Instrument for Detecting Freeze-up, Mid-Winter and Break-up Ice Processes in River. 13th Workshop on Hydraulics of Ice Covered Rivers. Hanover, NH.

Kellerhals, R., Neil, C. and Bray, D. 1972. Hydraulic and Geomorphic Characteristics of Rivers in Alberta. Research Council of Alberta. Edmonton, AB, pp 12,13,25.

Nezhikhosky, R.A., 1964. Coefficent of roughness of bottom surface of slush ice cover. Soviet Hydrology, Selected Papers, no. 2, pp. 127-150.

Nortek AS, 2008. Aquadopp Current Profiler: User Guide, January 2008. Vangkroken, Norway. pp. 11.

Northwest Hydraulic Consultants, 2007. North Saskatchewan River Flood Risk Mapping Study, Devon to Fort Saskatchewan (Excluding Edmonton). Edmonton, AB.

Marko, J., Fissel, D., Jasek, M., 2006. Recent Developments in Ice and Water Profilng Technology. Proceedings of the 18th IAHR Symposium on Ice. Sapporo, Japan. pp 37-44.

Maxwell, J., Hicks, F., Loewen, M., 2011. Study of Freeze-up Ice Characteristics on the North Saskatchewan River. 16th Workshop on River Ice. Winnipeg, MB.

Morse, B., Richard, M., 2009. A field study of suspended frazil ice particles. Cold Regions Science and Technology. Quebec, QC. vol. 55, iss. 1. pp 86-102.

Moultrie, 2010. Instructions for I65s GameSpy Digital Camera(Manual). Alabaster, AL.

Ohtake, T., Henmi, T., 1970. Radar Reflectivity of Aggregate Snowflakes. 14th Radar Met. Conf., Tuscon, Arizona.pp 209-210.

Ohmex Instrumentation Ltd., 2005. SonarLite: Portable Echo Sounder (Brochure). Hampshire, U.K.
url:http://www.macartney.de/produkte/Ohmex/015_174_05_05.pdf

Phillips Planning & Engineering Limited, 1994. North Saskatchewan River at Edmonton Flood Risk Mapping Study (Phase 1 – Lower Reach). Mississauga, ON.

Richard, M., Morse, B., Daly, S.F., Emond, J., 2010. Quantifying suspended frazil ice using multi-frequency underwater acoustic devices. River Research and Applications.

Reconyx, 2009. RapidFire and RapidFire Professional Digital Infrared Camera Instruction Manual. Holmen, WI.

Safari, A., Koray, E., 2008. Piezoelectric and acoustic materials for transducer applications. In: Tressler, J.F. (Ed.), Piezoelectric Transducer Designs for Sonar Applications. Springer, Berlin, pp. 217–239.

Schlumberger Water Services, 2011. Mini-Diver Spec Sheet (Letter). Vancouver, B.C. url: http://www.swstechnology.com/groundwater-monitoring/groundwater-dataloggers/mini-diver

Sea-Bird Electronics Inc., 2010. Temperature(&Pressure) Recorder: SBE 39.Bellevue, Washington. url:http://www.seabird.com/pdf_documents/datasheets/39brochureJan10.pdf

Sekhon, R., Srivastava, R., 1 Doppler Radar Observation of Drop-Size Distributions in a Thunderstorm. American Meteorological Society. 28, pp 983-994.

Treebark Cameras, 2011. Mini P41 Camera Speciifcations. Fort Saskatchewan, AB. url:http://www.treebarkcameras.com/cameras.html.

Trimble, 2009. Datasheet – Trimble R8 GNSS – English. Daytona, Ohio. url: http://www.trimble.com/trimbler8gnss_ds.asp

Urick, R.J., 1983. Principles of underwater sound, 3rd Edition. McGraw-Hill Inc.. 423 pp.

Appendix A. Water Temperature Sensor Calibration

Although the water temperature sensors used in this study included manufacturer specifications, a calibration was conducted to verify accuracy. The Mini-Divers, sonars and ADCP were submersed in a 0.80m wide, 1.20m long and 1.50m deep frazil generation tank located in a cold room at the University of Alberta. A high precision SBE 39 temperature sensor [Sea-bird Electronics] was installed in the tank and used as the reference temperature sensor for the calibration. Impellers mounted to the bottom of the tank ensured the water was well mixed. The water in the tank was then cooled from above 5°C to -0.09°C. The water was then warmed to about 2°C and cooled once again to -0.09°C. The calibration was conducted from 5-Sept-11 to 13-Sept-11. The Mini-Diver located at station 57.1 km could not be calibrated as it was lost on an unrelated research trip in May-11.

The temperature recorded by each instrument was compared against the Seabird sensor. It was found that for above zero temperatures, all of the gauges exhibited a highly linear relationship, which was easily corrected with an equation of the y=*slope**(x)+*intercept* form. Table A-1 presents the correction equation and coefficient of determination (R^2) for each sensor. These corrections had R^2 values between 0.9997 and 0.9999.

Table A-1. Corrections for water temperature sensors calibrated from 5-Sept-11 to 13-Sept-11.

Sensor Type	**Deployment Location**	***Slope***	***Intercept***
ADCP	Station 56.8 km	0.9941	0
High Freq. Sonar	Station 56.8 km	1.0269	0.0884
Low Freq. Sonar	Station 56.8 km	1.0331	-0.4613
Campbell 107B Sensor	Station 56.8 km	0.9939	-0.0304
Mini-Diver (SN#G0888)	Station 57.1 km	---	---
Mini-Diver (SN#F1401)	Station 56.3 km (Right Bank)	0.9995	0.0731
Mini-Diver (SN#F1630)	Station 56.3 km (Left Bank)	0.9858	-0.0192
Mini-Diver (SN#D9262)	Station 49.55 km	0.9916	-0.375
Mini-Diver (SN#J2565)	Station 50.75 km	0.9904	-0.0585

Based upon the results in Table A-1, it was found the Mini-Divers were inaccurate relative to the SBE 39 sensor. The *slope* corrections of between 0.9858 and 0.9995 were not a significant issue, since winter studies generally involve water temperatures below 10 degrees Celsius. However, the *intercept* corrections produce considerable inaccuracies. These *intercept* corrections are probably caused by a drifting intercept point. An additional calibration run would have provided some measure of the amount of drift these gauges experience over time, but wasn't possible due limited laboratory availability.

Of all of the temperature sensors calibrated, only the ADCP, the high frequency sonar and the Campbell 107B performed within their manufacturer specifications. The high frequency sonar passing of the calibration is likely to be coincidental as the low frequency sonar contains the same water temperature sensor electronics as the high frequency. As a result, the ADCP was chosen as the reference water temperature sensor for the sonar instruments. During an eight day period (5-Jan-

11 to 13-Jan-11) in which the ADCP was not collecting data, water temperatures from the low frequency sonar were used, with the intercept of the SWIPS unit adjusted by 0.09°C such that water temperatures just prior to 5-Jan-11 matched the ADCP. At end of the 8 day gap, the low frequency sonar was within 0.02°C of the ADCP temperature measurements.

Through this calibration, it was found that none of the temperature sensors used in the field deployment could accurately measure super-cooled water. Both SWIPS units registered super-cooled values but exhibited a considerable amount of scatter, making accurate measurements difficult. The ADCP will not measure values below -0.05°C. Thus, the quantification of the degree of super cooling occurring in the field is limited. However, super cooling presence can still be detected on a binary (true or false) basis by qualifying ADCP temperatures below zero degrees as super-cooled.

Appendix B. Matlab code used for processing dataset.

Available on attached DVD.

Program Title	Function
SWIPSBatchExecutor.m	Calls all of the code necessary to completely process an entire season of data.
SWIPSProcessor.m	Applied signal processing to raw dataset and computes pan targets depths (detailed in Chapter 3)
SWIPSParser.m	Parsing large sonar data into discrete sections and recursively calls SWIPSProcessor.m to process these sections
SWIPSSurfaceIceConc. m	Calculates surface ice concentrations from targets and depths produced by SWIPSProcessor.m
SWIPSThicknessandLength. m	Calculates ice pan thicknesses and lengths from targets and depths produced by SWIPSProcessor.m
SWIPSSurfaceIceFigs.m	Produces the surface ice analysis figures used in this thesis (Appendix C)
SWIPSSuspIceFigs.m	Produces the suspended ice analysis figures used in this thesis (Appendix C)
vertcatter.m	Concatenates time series as called by SWIPSBatchExecutor.m

Appendix C. Surface and Suspended Ice Analysis Figures

Available on attached DVD

Folder	Contents
Surface Ice Figures	Surface Ice Analysis Figures (Numbering is based on Matlab Julian Time)
Suspended Ice Figures	Suspended Ice Analysis Figures (Numbering is based on Matlab Julian Time)

Appendix D. Table of identified pan events

Available on attached DVD.